

# Biomechanics of growth, remodeling, and morphogenesis

Larry A Taber

*Departments of Mechanical Engineering and Pediatrics, University of Rochester, Rochester NY 14627*

This review deals with biomechanical aspects of growth (mass change), remodeling (property change), and morphogenesis (shape change) in living systems. The emphasis is on theoretical models, but relevant experimental results also are discussed. As an aid to the reader, the fundamental biological terms and concepts are defined for the general problem and for each specific topic.

At the outset, the processes involved in growth, remodeling, and morphogenesis are described and placed within the context of the evolution of species. Next, some of the analytical methods used in biomechanical models for these processes are presented. Then, applications of these and other techniques to specific systems are discussed, beginning at the cellular level and proceeding upward to the tissue and organ levels.

At the cellular level, modeling and experimental studies are reviewed for cell division, cell movement, and pattern formation, and then morphogenetic mechanisms for epithelia (cell sheets) are discussed. At the tissue and organ levels, the musculoskeletal and cardiovascular systems are considered. Several models are described for growth, remodeling, and morphogenesis of bone, and mainly experimental results are examined in the cases of skeletal muscle, the heart, and arteries. Specific topics for the cardiovascular system include hypertrophy, residual stress, atherosclerosis, and embryonic development. Finally, some future research directions are suggested.

## CONTENTS

1 INTRODUCTION	488	5 EPITHELIA	503
2 FUNDAMENTAL BIOLOGICAL CONCEPTS	488	5.1 Structure and function	503
2.1 Growth	489	5.2 Morphogenetic mechanisms	504
2.2 Remodeling	489	5.2.1 Global shape changes	504
2.3 Morphogenesis	489	5.2.2 Local shape changes	506
2.3.1 Morphogenetic processes	489	5.2.3 Epithelial models	507
2.3.2 Environmental factors	489	5.3 Cell rearrangement models	507
2.3.3 Morphoregulator hypothesis	489	5.4 Apical constriction model	507
2.4 Evolution	490	5.5 Cortical tractor model	509
3 FUNDAMENTAL ANALYTICAL TECHNIQUES	491	5.6 Shell models	510
3.1 Growth	491	6 MUSCULOSKELETAL SYSTEM	511
3.1.1 Volumetric growth	491	6.1 Bone	511
3.1.2 Surface growth	493	6.1.1 Structure and function	511
3.2 Remodeling	494	6.1.2 Experimental and physical considerations	513
3.3 Morphogenesis	495	6.1.3 Growth	513
4 CELLS	495	6.1.4 Remodeling	516
4.1 Structure and function	495	6.1.5 Morphogenesis	520
4.2 Cell division	496	6.2 Skeletal muscle	523
4.3 Cell movement	497	6.2.1 Structure and function	523
4.4 Pattern formation	499	6.2.2 Growth	523
4.4.1 Biochemical models	500	6.2.3 Remodeling	524
4.4.2 Biomechanical models	500	6.2.4 Morphogenesis	525
4.5 Response to stress	502	7 CARDIOVASCULAR SYSTEM	525
		7.1 The heart	525
		7.1.1 Structure and function	525
		7.1.2 Normal growth	527

7.1.3	Hypertrophy	528
7.1.4	Morphogenesis	529
7.2	Arteries	532
7.2.1	Structure and function	532
7.2.2	Residual stress and strain	532
7.2.3	Hypertrophy	533
7.2.4	Atherogenesis	534
7.2.5	Morphogenesis	536
8	FUTURE RESEARCH DIRECTIONS	536
9	REFERENCES	537

## 1 INTRODUCTION

One of the outstanding problems in developmental biology is how the one-dimensional information contained in the genetic code is translated into three-dimensional form. Biological form is brought about through a combination of genetic and epigenetic (environmental) factors (Edelman, 1988). Genes direct the formation of the basic building blocks, including proteins, extracellular matrix, and adhesion molecules. However, epigenetic factors, including chemical agents and mechanical stress and strain, influence which genes are expressed and how these blocks are assembled into tissues. The dynamic interactions between the genes and the environment are poorly understood.

The generation of biological form involves the processes of **growth** (mass change), **remodeling** (property change), and **morphogenesis** (shape change).<sup>1</sup> While these processes are most dramatic during embryonic development, organisms and their component parts continuously undergo changes in mass, properties, and form. Examples include functional adaptation of bones and muscles, wound healing, hair growth, atherogenesis, and organ regeneration. **Functional adaptation** is a concept that was introduced by Wilhelm Roux in 1880 to describe growth and remodeling in response to a changing environment [see Fung (1990)].

The literature on this subject is vast. It dates back at least to Galileo Galilei (Ascenzi, 1993), who compared the dimensions of bones from animals of different sizes and suggested that their forms are determined by their function and the gravitational environment. To keep our task manageable, we focus primarily on *biomechanical models* of the relevant processes. For the most part, we ignore geometric models and comparative studies involving allometric scaling. Moreover, we do not consider in detail the functional design of organisms. In-depth treatments of these subjects can be found in the classic treatise of D'Arcy Thompson (1942) and the more recent work of Wainwright et al. (1976). In short, we are concerned here not with an analysis of the final form of a biological structure, but with how it acquired that form.

Furthermore, although important, most purely chemical models also are excluded. Ultimately, mechanochemical models are required, and several of the models discussed here have chemical aspects. Finally, we note that all models must undergo experimental validation. Although all relevant data should be considered for this purpose, our discussion of experimental work is limited primarily to engineering-type studies that bear on the modeling efforts.

**Overview.** One purpose of this review is to give the novice reader enough background to begin research in the biomechanics of growth, remodeling, and morphogenesis. In contrast to the hundreds of biologists who have studied these topics, relatively few engineers have become involved. A likely reason for this is that these processes are largely neglected in most basic biology or physiology courses to which a bioengineer may be exposed. Thus, parts of this article are tutorial in nature.

A second purpose is to give researchers already working in one area of the field an overview of other areas. Investigators often get so involved in their own specific topic of interest that they are not exposed to work in separate but related areas, and important information may be overlooked. Reading the literature on bone remodeling, for example, may stimulate ideas that can be applied to the heart.

With these goals in mind, we first present in Sec 2 (and at the outset of the other sections) the fundamental biological concepts and terminology required to understand the relevant literature. Then, Sec 3 discusses generic analytical methods that have been developed to handle continuum formulations of these problems. Next, Sec 4 considers specific models for individual cells, and Sec 5 discusses the motions and shaping of cell sheets. Finally, biomechanical aspects of growth, remodeling, and morphogenesis are discussed for the musculoskeletal and cardiovascular systems in Secs 6 and 7, respectively, and possible directions for future research are presented in Sec 8.

Before beginning, we need to say a few words about notation and the degree of coverage. Since the subject matter involves theories derived from various fields, the standard symbols often overlap. When possible, we try to use standard notations, with symbol definitions kept consistent only within each major section.

Finally, in spite of the length of this review, several important areas have been ignored. Moreover, some specific subjects and researchers have received more attention than others. The author does not claim expertise in all of the fields examined here and apologizes for any oversights or misguided emphasis.

## 2 FUNDAMENTAL BIOLOGICAL CONCEPTS

This section discusses the basic concepts pertaining to growth, remodeling, and morphogenesis and their long-

<sup>1</sup>Remodeling usually is defined as structural adaptation to changing demands, including adaptive growth. In this article, growth is treated generally as a separate phenomenon.

time evolution. Although these processes are linked in general, most investigators have treated them separately, and we generally will do the same.

## 2.1 Growth

Growth, which is defined as added mass, can occur through cell division (**hyperplasia**), cell enlargement (**hypertrophy**), secretion of extracellular matrix (ECM), or accretion at external or internal surfaces. **Atrophy** (negative growth) can occur through cell death, cell shrinkage, or resorption. In most cases, hyperplasia and hypertrophy are mutually exclusive processes. Depending on the age of the organism and the type of tissue, one of these two growth processes dominates (Goss, 1966). The liver, for example, adds mass by cell division, but the *mature* heart hypertrophies. In the embryo, however, the heart grows by hyperplasia. Growth that occurs in response to changing demands on tissues and organs is called **adaptive growth**.

## 2.2 Remodeling

Remodeling involves changes in material properties. These changes, which often are adaptive, may be brought about by alterations in modulus, internal structure, strength, or density. For example, bone and heart muscle may change their internal structures through reorientation of trabeculae and muscle fibers, respectively. Furthermore, in a weightless environment, bone may lose both stiffness and mass density.

## 2.3 Morphogenesis

Morphogenesis is the generation of animal form. Usually, the term refers to embryonic development, but wound healing and organ regeneration are also morphogenetic events. Morphogenesis consists of a complex series of stages, each of which depends on the previous stage. During these stages, as already mentioned, genetic and environmental factors guide the spatial-temporal motions and differentiation (specialization) of cells. Although biological systems contain redundancies, a flaw in any one stage may lead to structural defects.

In the following, we discuss the main processes and environmental factors involved in morphogenesis, and their interactions.

### 2.3.1 Morphogenetic processes

The primary morphogenetic **driving processes** are cell division, cell motion, and cell death (Edelman, 1988). We already have discussed cell division, and selective cell death is no less important. For example, a lack of cell death can produce webbed feet in human babies. In the embryo, cells move either individually (**mesenchyme**) or in sheets (**epithelia**). It is notable that mesenchymal and epithelial cells can transform into one another.

The primary morphogenetic **regulatory processes** are differentiation and cell adhesion. **Differentiation**,

or differential gene expression, dictates the cell type and mechanical properties. (**Expressed genes** are those that are active.) **Cell adhesion**, which also may be gene mediated, determines how cells are linked to each other and to substrates. Cells may possess stronger affinities toward certain types of cells over other types. This differential adhesion can drive **cell sorting**, a likely mechanism for pattern formation in some species (see Sec 4.4).

### 2.3.2 Environmental factors

The integration of the primary morphogenetic processes to produce form is modulated partly by the mechanochemical environment. The mechanical environment, defined by the state of stress and strain, drives passive cell motion and may affect active cell motion, cell division, and cell death. Moreover, mechanical factors may influence gene expression and chemical secretions. Thus, the mechanical environment likely modulates both the driving and the regulatory processes.

The chemical environment is defined primarily by morphogens and morphoregulatory molecules. **Morphogens** include growth factors, hormones, and induction molecules. Growth factors promote cell division, while hormones and induction molecules influence differentiation. **Morphoregulatory molecules** act at cell surfaces to promote cell adhesion (adhesion molecules), epithelial-mesenchymal transformation, and pathways for cell movement.

**Embryonic induction** is an example of a process that involves both mechanical and chemical factors. Cell motion brings certain types of cells into contact with one another. This contact stimulates the release of morphogens, which then induce differentiation into a particular type of cell.

### 2.3.3 Morphoregulator hypothesis

The primary morphogenetic driving processes provide the engine for the generation of biological form, and the environment provides the modulating tools. But how the various mechanisms are integrated to produce a specific structure is poorly understood. The process involves complex motions and interactions of cells that result in cells being in the right place at the right time and differentiating into the right types of cells.

Assuming that adhesion molecules play a central role in morphogenesis, Edelman (1988) proposed the **morphoregulator hypothesis**. This hypothesis contains a genetic and an epigenetic component. The genetic component includes gene signals that determine the appearance and function of morphoregulatory molecules. The epigenetic component consists of the primary driving processes, which function through the mechanochemical environment. According to the hypothesis, the link between these components lies in the actions of the morphoregulatory molecules and the signals from the cell groups formed by their actions back to the genes that

govern their function.

In other words, morphoregulatory genes specify the formation of morphoregulatory molecules, which mediate adhesion and induction of groups of cells. These mechanisms alter the mechanochemical environment, which triggers the driving processes of cell division, cell motion, and cell death to develop form. The formed group of cells then sends signals back to the genes, which adjust the morphoregulatory molecules, and so on. For more details, the reader is referred to the book by Edelman (1988).

## 2.4 Evolution

Each cell of an individual organism contains the same set of genes, which defines the **genotype**, but each cell does not *express* all of the genes. A muscle cell, for example, does not express the same genes as a skin cell. The genes that actually are expressed define the **phenotype**, which depends on the interaction of the genotype and the environment. (The environment of a muscle cell differs from that of a skin cell.) As the environment changes, the genotype remains the same (except for possible mutations), but the phenotype of an individual cell, tissue, organ, or organism may undergo adaptive changes.

Adaptive changes in phenotype characterize **ontogeny**, the development of individual organisms, and **phylogeny**, the evolutionary development of species. **Morphologic evolution** can be defined as changes in developmental (ontogenetic) programs during phylogeny (Oster and Alberch, 1982). Thus, understanding evolution requires an understanding of development.

The extension of Darwin's theory of evolution that is referred to as "neo-Darwinism" is based on two fundamental processes: random genetic mutation and natural selection (Alberch, 1980). According to this theory, genetic mutations produce a range of morphologies within a species, and natural selection favors the survival of those morphologies that can adapt best to their environment. The fittest have the best chances of surviving to maturity and of passing on the advantage to succeeding generations. Thus, natural selection acts on phenotype, which indirectly affects genotype, as the species slowly drifts (evolves) toward a superior gene pool.

Although still a popular theory, neo-Darwinism has difficulty explaining some features of the fossil record (Alberch, 1980, 1982). In particular, evolution is a more ordered process than would be predicted by random mutations. Examining the available data led Alberch (1980) to the following conclusions:

1. Phenotypes cluster around discrete, rather than continuous, morphologies.
2. Variability in each morphological trait is limited and quite resilient to environmental and genetic perturbations. [In some cases, however, relatively large morphological changes occur in relatively short evolutionary times (Edelman, 1988), consistent with neo-Darwinism.]

Although genetic mutations are random, "morphological mutations" are not, i.e., some morphologies are more likely than others.

Any theory of development must be consistent with these observations, which many investigators attribute to **developmental constraints**. These constraints can take the form of **construction rules** that are set by the biomechanics of morphogenesis. Mittenthal (1989), for example, proposed a set of construction rules for general development.

Attempts to integrate development and evolution have not been entirely successful. Some recent efforts have focused on the nonlinear nature of development in conjunction with physical constraints. According to this view, developmental and evolutionary alterations in form are due to organisms passing through a series of morphological bifurcations, with the actual path possibly biased by relatively minor genetic changes. This hypothesis explains the conclusions listed above as follows:

1. Each branch represents a discrete group of morphologies.
2. Away from bifurcations, a given morphological trait is relatively insensitive to perturbations. Near a bifurcation, however, a small perturbation can produce a discontinuous jump to a significantly different morphology.
3. At a bifurcation, the organism is more likely to jump to a stable branch than an unstable branch. Thus, evolution is guided along the morphological branches, and the pattern of change is not random.

It also is possible that development and evolution possess chaotic features, with changes being unpredictable but limited in magnitude (Mittenthal, 1989).

Theories have been proposed based on these ideas. One hypothesis suggests that morphological changes are the product of alterations in the timing of gene action and the rate of development (Gould, 1982). On the other hand, according to the morphoregulator hypothesis (Sec 2.3.3), alteration in the *sequence* of gene expression is the primary determinant of changes in form (Edelman, 1988). In both cases, relatively small changes in the regulatory behavior can produce relatively large morphological changes through a snowball-like effect.

Examples of bifurcations during development include changes in animal coat marking patterns as an animal grows (Murray, 1989) and the branching tubes in the lungs, kidneys, and salivary glands (Goldin, 1980). Models that exhibit bifurcation behavior are discussed in Secs 4.4 and 5.4.



### 3 FUNDAMENTAL ANALYTICAL TECHNIQUES

Growth, remodeling, and morphogenesis are interrelated and overlapping processes. In this article, we generally define growth as a change in volume, remodeling as a change in properties, and morphogenesis as an isovolumic change in shape. Moreover, we distinguish between volumetric and surface growth. In this section, we discuss some of the methods that have been proposed to analyze these processes within the context of continuum mechanics. For generality, the focus here is on theories for finite growth and finite deformation.

#### 3.1 Growth

Mathematical descriptions of growth in plants and animals have been published since the 1940s (Thompson, 1942; McMahon, 1973; Silk and Erickson, 1979; Wilson and Archer, 1979; Cox and Peacock, 1978, 1979). Most of these analyses are purely kinematic, and many borrow from the methods of continuum mechanics to describe, for example, growth rates and velocity fields. During the last quarter century, *mechanical* theories of growth have been formulated, beginning with a study of uniform growth by Hsu (1968) and the *theory of adaptive elasticity* proposed by Cowin and Hegedus (1976) (see Sec 6.1.4). These initial theories laid the foundation for later work.

Skalak and coworkers (1981; 1982) formalized the general kinematic descriptions of finite volumetric and surface growth. In qualitative terms, they also discussed growth discontinuities and the interaction of stress and growth. Moreover, Skalak (1981) pointed out that if the growth strains of each element of an originally unloaded and stress-free body are geometrically compatible, then the body remains stress-free after the growth occurs. If the growth strains are incompatible, however, internal (residual) stresses are generated, i.e., stresses remain when all external loads are removed. In recent years, researchers have come to realize the importance of residual stress in biomechanics.

Residual stresses in biological tissues have been observed for a long time. When skin is cut, the wound opens, and when a segment is cut from an artery, it shortens, indicating residual tension in the intact tissues. Cutting is a common technique used to investigate residual stress. Using this method, Belousov et al. (1975) investigated the patterns of internal stresses in embryos, and Bekesy (1960) found that the basilar membrane of the cochlea is *not* residually stressed and is, therefore, not truly a "membrane" in a mechanical sense.

In a series of papers, Fung and colleagues experimentally demonstrated the existence of residual strains in arteries (Liu and Fung, 1988; Han and Fung, 1991a; Fung and Liu, 1992), veins (Xie et al., 1991; Fung and Liu, 1992), the heart (Omens and Fung, 1990), and the trachea (Han and Fung, 1991b). In addition, they found that the magnitudes of the residual strains in arteries change when the blood pressure is altered (Fung and Liu,

1989, 1991; Liu and Fung, 1989). Fung (1990) suggested that these changes are due to differential growth and remodeling. (See also Secs 7.1.3 and 7.2.2.)

While it is now clear that residual stresses exist and undergo dynamic changes in biological tissues, the purpose of these stresses is not well understood. As discussed by Fung (1991), one possibility is to provide more uniform stresses in the loaded tissue than would occur otherwise, yielding a more efficient load-bearing structure. To investigate this hypothesis, Chuong and Fung (1986b; 1986a) used a nonlinear pseudoelastic analysis to show that the presence of residual strain substantially reduces wall stress gradients in arteries subjected to physiological pressure loads (see Sec 7.2.2 and Fig 51). Their treatment formed the basis for similar analyses of the mature left ventricle (Guccione et al., 1991; Taber, 1991) and the embryonic heart (Taber et al., 1992; Yang et al., 1994) and laid the foundation for later generalizations of the theory. Takamizawa and Matsuda (1990) formalized the general boundary-value problem for including residual strain effects in soft tissues.

These studies accounted for the effects of growth on stress but not the effects of stress on growth. Hsu (1968) and Cowin and Hegedus (1976) proposed general forms for stress-growth constitutive relations, and Fung (1990; 1991) postulated a relatively simple relation between the growth rate and the stress [see Eq (8) below], but these equations await experimental confirmation. Recently, combining and extending the ideas of Skalak, Fung, and coworkers, Rodriguez et al. (1994) formulated a continuum theory that accounts for the coupling between stress and finite growth. Next, we discuss in detail the fundamental aspects of some of these theories. Other theories and applications are discussed in later sections.

##### 3.1.1 Volumetric growth

From a mechanics perspective, as pointed out by Skalak (1981), volumetric growth is analogous to thermal expansion. In linear elastic problems, growth (and thermal) stresses can be superposed on the mechanical stress field, but in nonlinear problems, another approach must be used. The fundamental idea is to refer the strain measures in the constitutive (stress-strain) equations of each material element to its *current* zero-stress configuration, which changes as the element grows. Following Rodriguez et al. (1994), we now formalize this approach mathematically.

Consider an elastic body  $B$  at time  $t_0$  that is unloaded and free of stress (Fig 1). Imagine that the body is cut into infinitesimal elements, each of which then undergoes volumetric growth. The growth of each element may be anisotropic and may consist of either added or subtracted volume. Note that, in this macroscopic description, each element may consist of one or several cells, with hyperplasia and hypertrophy being mechanically equivalent.

After growing, each of the cut elements remains stress-free (the Cauchy stress tensor  $\sigma = 0$ ), but the elements

may no longer be geometrically compatible. The collection of these locally deformed elements makes up the body  $B(t_1)$ , which can be considered a global Riemannian manifold (Takamizawa and Matsuda, 1990). The deformation from  $B(t_0)$  to  $B(t_1)$  is described by the **growth deformation gradient tensor**  $\mathbf{F}_g$  (Fig 1). We assume that  $\mathbf{F}_g$  can be found through experiments, e.g., by cutting, or by solving a boundary-value problem involving a growth-stress constitutive equation, as discussed later in this section.

The elements of  $B(t_1)$  now are reassembled into the body  $B'(t_1)$ . If the elements are not geometrically compatible, they must be deformed to make them fit together. This additional deformation, described by the elastic deformation gradient tensor  $\mathbf{F}_e$  (Fig 1), gives rise to residual elastic stress  $\sigma_0$ . (The applied loads required for this process are removed after the elements are "glued" together.) Finally, external loads are applied to  $B'(t_1)$ , deforming the body through  $\mathbf{F}_\ell$  into  $b(t)$ .

When using the Lagrangian description to solve solid mechanics problems, it is convenient to choose a reference configuration that does not change with time. During growth, the body  $B(t_0)$  serves this purpose. On the other hand, if the growth is completed, then  $B'(t_1)$  may be a useful reference configuration for the loading step. For zero stress to correspond to zero strain, however, the strain measures in the constitutive relations always must be referred to the current zero-stress configuration  $B(t_1)$ , which is time-dependent in general.

If  $B(t_0)$  is chosen as the reference configuration, then the field equations are formulated in terms of the total deformation gradient

$$\mathbf{F} = \mathbf{F}_\ell \cdot \mathbf{F}_e \cdot \mathbf{F}_g. \quad (1)$$

These field equations are the same as those used in classical finite elasticity theory (Green and Zerna, 1968). However,

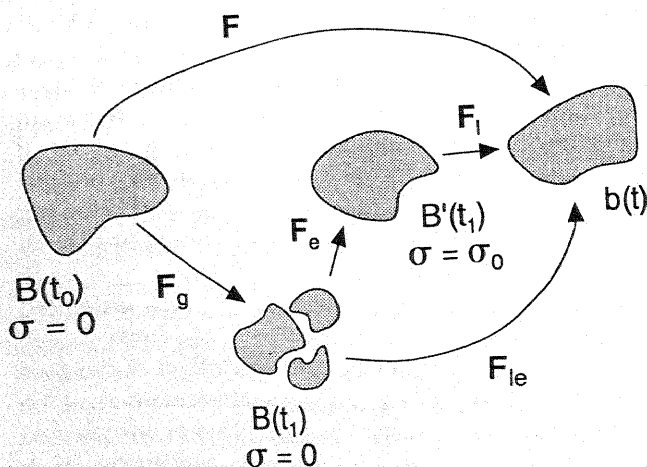


Fig 1. Configurations for a growing body: original zero-stress state  $B(t_0)$ ; locally stress-free state  $B(t_1)$ ; intact and unloaded grown state  $B'(t_1)$ ; and loaded state  $b(t)$ . [Modified from Rodriguez et al. (1994)]

ever, the constitutive relations have the form

$$\sigma = \sigma(\mathbf{C}_{\ell e}) \quad (2)$$

where

$$\mathbf{C}_{\ell e} = \mathbf{F}_{\ell e}^T \cdot \mathbf{F}_{\ell e} \quad (3)$$

is the right Cauchy-Green deformation tensor. Referred to the material coordinates in  $B(t_1)$ ,  $\mathbf{C}_{\ell e}$  is given in terms of

$$\mathbf{F}_{\ell e} = \mathbf{F}_\ell \cdot \mathbf{F}_e, \quad (4)$$

which is the deformation gradient tensor of  $b(t)$  relative to  $B(t_1)$ . If the material properties change during growth, then equation (2) must be modified to read

$$\sigma = \sigma(\mathbf{C}_{\ell e}, \mathbf{C}_g) \quad (5)$$

where  $\mathbf{C}_g = \mathbf{F}_g^T \cdot \mathbf{F}_g$ .

Two sets of stresses are of interest: the residual stress  $\sigma_0$  in  $B'(t_1)$  and the total stress  $\sigma$  in  $b(t)$ . The residual stress can be found by choosing a form for the deformation field that ensures compatibility of  $\mathbf{F} = \mathbf{F}_e \cdot \mathbf{F}_g$  and then solving the boundary-value problem with  $\mathbf{F}_\ell = \mathbf{I}$  and traction-free boundary conditions. The stress  $\sigma$  can be computed similarly, but now  $\mathbf{F}_\ell \neq \mathbf{I}$ ,  $\mathbf{F}$  is given by equation (1), and the boundary conditions are inhomogeneous. If residual stresses are not of interest, then it is not necessary to compute  $\mathbf{F}_e$ ;  $\mathbf{F}_{\ell e}$  can be used as the principal deformation variable. Finally, we note that, since growth is not an isovolumic process, then  $\det \mathbf{F}_g \neq 1$  ( $\det \mathbf{F}_g > 1$  for added volume and  $\det \mathbf{F}_g < 1$  for removed volume). If, however, the material excluding growth is incompressible, then  $\det \mathbf{F}_{\ell e} = 1$ , and the stress-strain relations must contain a hydrostatic pressure term.

Thus far, we have considered how to determine the effects of growth on stress. In general, we also must account for the effects of stress on growth. Actually, it is not yet clear which mechanical quantity, e.g., stress, strain, or strain energy, modulates growth. Experimental data can be found to support each. Moreover, the driving mechanism may be tissue-dependent, and so, unfortunately, a universal mechano-growth law may not exist.

Cowin (1984) argued that strain is probably the mechanical growth factor, since cells can measure strain but not stress with specialized receptors. As pointed out by Rodriguez et al. (1994), however, strain depends on the choice of a reference configuration, whereas the Cauchy (true) stress does not. While the zero-stress state may seem a logical choice for the reference configuration for strain, it may be time-dependent. Moreover, it is likely that tissues never experience the zero-stress state *in vivo*, and so there is no basis for sensing an absolute measure of strain. One example that supports stress as the key factor is the heart, which adapts to changes in blood pressure by growing so as to keep average wall stresses nearly constant (McMahon, 1984) (see Secs 7.1.2 and 7.1.3). On the other hand, stress rate and strain rate also are possibilities that do not have this drawback if defined in an Eulerian sense, and strain may be an appropriate choice for

bone and other hard tissues that undergo small (linear) deformations (Thompson, 1942; Cowin and Van Buskirk, 1979; Cowin and Firoozbakhsh, 1981). Moreover, in muscle the optimal sarcomere length may serve as a reference length for strain. Further discussion of these points for bone and heart muscle can be found in Secs 6.1.1 and 7.1.2-7.1.3, respectively.

Stress-dependent growth can be included in the analysis through a constitutive relation of the form

$$\mathbf{F}_g = \mathbf{F}_g(\sigma) \quad \text{or} \quad \dot{\mathbf{F}}_g = \dot{\mathbf{F}}_g(\sigma) \quad (6)$$

with  $\sigma$  being an implicit function of time. The second form may be more realistic physiologically, since experiments show that the growth rate increases with the magnitude of the applied stress (Curtis and Seechar, 1978). ( $\dot{\mathbf{F}}_g$  can be integrated to obtain  $\mathbf{F}_g$ .) Note that  $\mathbf{F}_g$  contains a rigid-body rotational component, which should not affect the stresses and can be lumped into the deformation given by  $\mathbf{F}_{\ell\ell}$ . Furthermore, if a growth-equilibrium stress state  $\sigma^*$  exists, then we can take (Rodriguez et al., 1994)

$$\mathbf{F}_g = \mathbf{F}_g(\sigma - \mathbf{R} \cdot \sigma^* \cdot \mathbf{R}^T) \quad \text{or} \quad \dot{\mathbf{F}}_g = \dot{\mathbf{F}}_g(\sigma - \mathbf{R} \cdot \sigma^* \cdot \mathbf{R}^T) \quad (7)$$

where  $\mathbf{R}$  is the rotation tensor from the growth equilibrium state to the loaded state.

A specific form of this last equation was proposed by Fung (1990; 1991) in the form

$$\dot{m} = C(s - a)^{k_1}(b - s)^{k_2}(s - c)^{k_3} \quad (8)$$

where  $\dot{m}$  is the mass rate of growth,  $s$  is a suitable measure of stress, and  $C$ ,  $a$ ,  $b$ ,  $c$ ,  $k_1$ ,  $k_2$ , and  $k_3$  are constants to be determined experimentally. This relation contains three growth-equilibrium stresses (Fig 2) for the following reasons. First, point  $a$  represents the normal physiological state. Stresses somewhat lower than  $a$  produce atrophy ( $\dot{m} < 0$ ), while stresses somewhat higher than  $a$  induce hypertrophy ( $\dot{m} > 0$ ). Second, since  $\dot{m} > 0$  in stress-free tissue culture ( $s = 0$ ), the curve must pass through equilibrium point  $c$ . Third, if the stress is too large ( $s > b$ ), resorption may occur, e.g., in a bone. Thus, the third equilibrium point  $b$ , which may represent the state of a bone with a screw inserted, must be present.

Once  $\dot{\mathbf{F}}_g$  and  $\mathbf{F}_g$  are known, then the **growth rate-of-deformation tensor** can be computed from (Rodriguez et al., 1994)

$$\mathbf{D}_g = \frac{1}{2}(\dot{\mathbf{F}}_g \cdot \mathbf{F}_g^{-1} + \mathbf{F}_g^{-T} \cdot \dot{\mathbf{F}}_g^T), \quad (9)$$

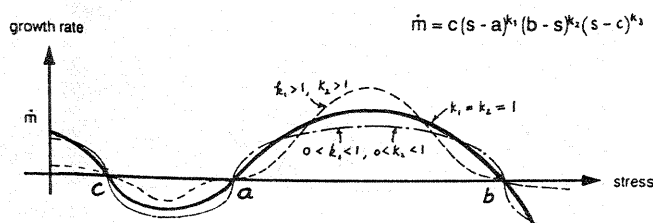


Fig 2. Postulated mass rate of growth versus stress relation. [From Fung (1990)]

where dot denotes partial differentiation with respect to time  $t$ . In addition, the rate of volumetric growth is (Skalak et al., 1982)

$$\frac{1}{V} \frac{dV}{dt} = \text{tr } \mathbf{D}_g \quad (10)$$

where  $V$  is the growth volume.

### 3.1.2 Surface growth

Bones, shells, horns, and branches grow primarily by accretion or resorption at a surface. This type of growth often occurs without generating residual stress. The following discussion is based on the formulation of Skalak (1981) and Skalak et al. (1982).

Consider a surface  $S_0$ , which has material regions  $R_1$  and  $R_2$  on either side (Fig 3a). Each point on  $S_0$  is located by the surface coordinates  $\xi_\alpha$  ( $\alpha = 1, 2$ ). At  $t = 0$ , material grows from both sides of  $S_0$ , forming the new regions  $R_3$  and  $R_4$ , which push  $R_1$  and  $R_2$  outward (Fig 3b), and new surfaces  $S_1$  and  $S_2$  separate  $R_1$  and  $R_2$  from  $R_3$  and  $R_4$ . Of course, volumetric growth may occur in each of these regions, but we ignore this possibility here.

Initially, each point in  $R_1$  and  $R_2$  is located by  $\mathbf{X}$ , which serves as a set of material coordinates, but each point on  $S_0$  gives rise to an infinite number of particles in  $R_3$  and  $R_4$ . To circumvent the redundancy of the material coordinates in these newly formed regions, Skalak (1981) and Skalak et al. (1982) introduced a second time variable  $\tau$ , which gives the time at which each new particle is formed. Then, the spatial position of a new particle is

$$\mathbf{x} = \mathbf{x}(\xi_\alpha, \tau, t) \quad (11)$$

where  $0 \leq \tau \leq t$ . Since the surfaces  $S_1$  and  $S_2$  represent the first of the newly formed material, their points are located by  $\mathbf{x}(\xi_\alpha, 0, t)$ , while the position of  $S_0$  at any time is given by  $\mathbf{x}(\xi_\alpha, t, t) \equiv \mathbf{x}_0(\xi_\alpha, t)$ . The locus of points in each region  $R_3$  and  $R_4$  is located by a separate equation of the form of (11) with  $0 < \tau < t$ .

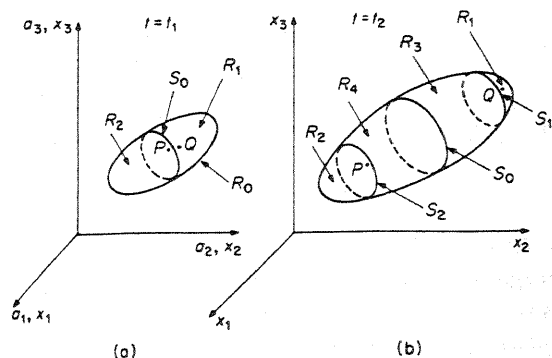


Fig 3. Geometry of surface growth. [From Skalak et al. (1982)]

Now, the velocity of a point on  $S_0$  is

$$\mathbf{v}_0 = \dot{\mathbf{x}}_0(\xi_\alpha, t), \quad (12)$$

and the velocity of a point in  $R_3$  or  $R_4$  is

$$\mathbf{v} = \dot{\mathbf{x}}(\xi_\alpha, \tau, t). \quad (13)$$

Although  $\mathbf{x}$  must be continuous between  $R_3$  (or  $R_4$ ) and  $S_0$ , the material velocity  $\mathbf{v}$  adjacent to  $S_0$  is not necessarily equal to the surface velocity  $\mathbf{v}_0$ , with the relative growth velocity being

$$\mathbf{v}_g = \mathbf{v} - \mathbf{v}_0. \quad (14)$$

The component of  $\mathbf{v}_g$  normal to  $S_0$  may differ on each side of this surface; a positive (negative) component corresponds to accretion (resorption). If the tangential components differ, slippage occurs during growth. Skalak et al. (1982) applied this theory to illustrative examples.

### 3.2 Remodeling

This section considers a theory for remodeling of the internal architecture in general fibrous tissues. Cowin (1986; 1990; 1992) originally developed a form of this theory for cancellous bone, and Tozeren and Skalak (1988) extended it to soft tissue. To date, most studies of adaptive remodeling have focused on bone (see Sec 6.1.4).

Consider a planar tissue that, in the reference configuration, is composed of sets of parallel fibers arranged so as to produce a global orthotropy. The fiber architecture can be quantified by measuring the mean intercept length  $L$  along a line at an angle  $\Theta$  to the horizontal (Fig 4), i.e., the average distance between fibers along the line. As the fiber pattern becomes less discrete, a polar plot of  $L$  versus  $\Theta$  approaches an ellipse, as given by the equation (Harrigan and Mann, 1984; Cowin, 1986)

$$\frac{1}{L^2(\Theta)} = M_{ij} B_i B_j \quad (15)$$

where the  $B_i$  are Cartesian components of the unit vector  $\mathbf{B}$  along  $L(\Theta)$ , and the usual summation convention applies. In cancellous bone, this procedure yields a good approximation for an ellipse (Harrigan and Mann, 1984; Cowin, 1986, 1990).

Extending this construction to three dimensions produces an ellipsoid, and so, to a first approximation, the  $M_{ij}$  are components of a second-order tensor  $\mathbf{M}$ . Based on this result, Cowin (1986) defined the **fabric tensor** as

$$\mathbf{H} = \mathbf{M}^{-1/2} \quad (16)$$

which characterizes the internal structure of an orthotropic material. If all eigenvalues of  $\mathbf{H}$  are distinct, the material is orthotropic; if two eigenvalues are equal, the material is transversely isotropic; and if all eigenvalues are equal, the material is isotropic.

As a tissue remodels, its fabric tensor evolves according to some constitutive law. For bone, Cowin (1990;

1992) proposed a theory based on Wolff's law of trabecular architecture (Wolff, 1986), which states that, in remodeling equilibrium (RE), the principal directions of stress and trabeculation coincide. For finite deformation, this hypothesis implies that the principal directions of  $\mathbf{H}$  coincide with those of the second Piola-Kirchhoff stress tensor  $\mathbf{S}$ , with both tensors referred to a reference configuration.<sup>2</sup> Mathematically, Wolff's law can be written (Cowin, 1986)

$$\mathbf{S}^* \cdot \mathbf{H}^* = \mathbf{H}^* \cdot \mathbf{S}^* \quad (17)$$

where the asterisks indicate RE.

Consider now remodeling that is driven by the state of stress  $\mathbf{S}$ . Depending on experiments,  $\mathbf{S}$  may represent the peak stress, the mean stress, or some other appropriate measure. Let  $\hat{\mathbf{S}}(t)$  represent  $\mathbf{S}(t)$  in principal stress coordinates, which can be defined in terms of a rigid-body rotation  $\mathbf{Q}_{(S)}(t)$  relative to a fixed Cartesian system. In addition, let  $\mathbf{Q}_{(H)}(t)$  be the rotation tensor from the fixed system to the principal directions of  $\mathbf{H}(t)$ . Remodeling equilibrium occurs when (1)  $\hat{\mathbf{S}}$  is equal to a specified equilibrium principal stress tensor  $\hat{\mathbf{S}}^*$  and (2) the eigenvectors of  $\mathbf{S}$  align with those of  $\mathbf{H}$ . In addition, remodeling of fibers may involve a change in fiber volume fraction  $v$ . Under these conditions, the constitutive equations for stress-dependent remodeling can be written in the forms

$$\dot{\mathbf{H}} = \dot{\mathbf{H}}(\mathbf{H}, \hat{\mathbf{S}}, v), \quad \dot{v} = \dot{v}(\mathbf{H}, \hat{\mathbf{S}}, v) \quad (18)$$

where  $\dot{\mathbf{H}} = \dot{v} = 0$  when  $\hat{\mathbf{S}} = \hat{\mathbf{S}}^*$  and  $\mathbf{Q}_{(S)} = \mathbf{Q}_{(H)}$ .

Cowin (1992) called the remodeling theory described by Eqs (17) and (18) an *evolutionary Wolff's law*. He proposed specific remodeling constitutive relations for bone

<sup>2</sup>Here, the term "reference configuration" refers to a given deformation state; within this configuration,  $\mathbf{H}$  can be a function of time as the material remodels.

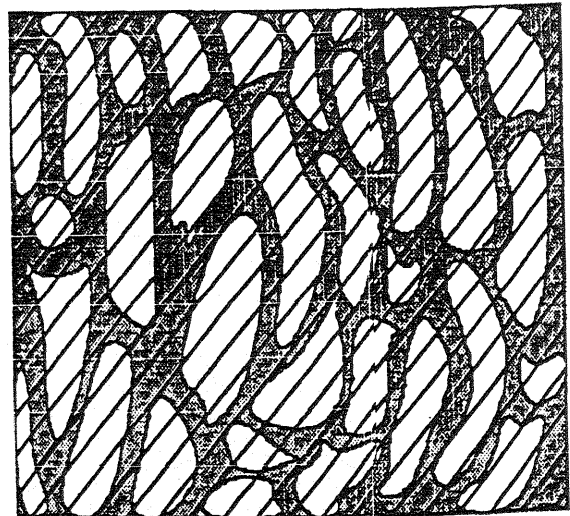


Fig 4. Trabecular geometry. [From Cowin (1990)]

and worked out a numerical solution to the following example.

Consider a trabecular bone element that is in RE under an applied stress for  $t \leq 0$ , such that the principal directions of the stress tensor  $\mathbf{T}^0$ , the strain tensor  $\mathbf{E}^0$ , and the deviatoric part of the fabric tensor,  $\mathbf{K}^0 = \mathbf{H}^0 - \frac{1}{3}\mathbf{I}$ , all coincide (Fig 5a). At time  $t = 0^+$ , the applied stress is changed to  $\mathbf{T}^*$  and held there for  $0 < t < \infty$  (Fig 5b). The problem is to determine how  $\mathbf{E}$  and  $\mathbf{K}$  evolve in time under this new loading condition.

Qualitatively, the bone responds as follows (Cowin, 1990; Cowin et al., 1992). At  $t = 0^+$ ,  $\mathbf{K}(t)$  remains equal to  $\mathbf{K}^0$ , but  $\mathbf{E}(t)$  changes instantaneously due to the new stress system. However, if the material is anisotropic, the principal directions of  $\mathbf{E}$  and  $\mathbf{T}^*$  do not necessarily coincide (Fig 5b). The new stresses trigger the bone to begin remodeling, as the principal directions of  $\mathbf{K}(t)$  and  $\mathbf{E}(t)$  gradually move toward those of  $\mathbf{T}^*$  (Fig 5c). When RE is reached, the principal directions of the three tensors again coincide and remain that way for all time (Fig 5d).

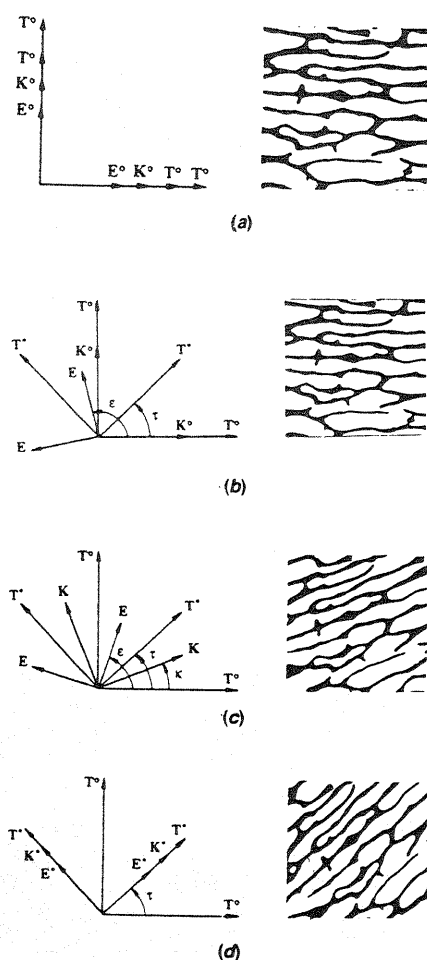


Fig 5. Trabecular remodeling due to step change in applied load. [From Cowin et al. (1992)]

### 3.3 Morphogenesis

Morphogenesis is a complex biomechanical process, involving large deformations of nonlinear, anisotropic materials. Several models have been proposed for epithelial morphogenesis (see Sec 5), but these models generally are restricted to relatively simple geometries. As models become more realistic, more general formulations will be required.

The finite element method offers a natural framework for modeling morphogenetic events. An incremental procedure is useful, with the shape of the structure updated after each time step. The new configuration then serves as the reference configuration for the next step. The driving forces for these motions are both external and internal to the tissue. The external forces are applied by adjacent cells, tissues, and extracellular matrix. (Inertia and gravity loads can be neglected during the relatively slow process of morphogenesis.) Internal forces can be modeled by a changing zero-stress configuration, similar to the method discussed in Sec 3.1.1. Recently, Clausi and Brodland (1993) and Brodland and Clausi (1994) have used finite elements to model three-dimensional invagination, neurulation, contraction wave propagation, and pattern formation in epithelia (see Sec 5 for terminology).

## 4 CELLS

The embryo contains two types of cells: mesenchymal and epithelial. Mesenchymal cells move and deform individually or in three-dimensional groups to construct organs, while epithelial cells move and deform together as sheets to form surfaces. The motions and deformations of both types of cells are driven and guided by external and internal forces. For example, mesenchymal cells can move by extending pseudopods and dragging themselves, or they can be dragged along by the extracellular matrix. Likewise, epithelia can spread actively by aggregate cell shape changes or passively through attachments to adjacent tissues. A knowledge of the forces involved in these motions and deformations is essential to the understanding of morphogenesis. This section considers mesenchymal cells; epithelia are considered in Sec 5.

### 4.1 Structure and function

A cell is composed of organelles and cytoplasm enclosed by a plasma (cell) membrane (Fig 6a). The **organelles** include the nucleus, where the genes reside (on the DNA), and the mitochondria, which supply the energy. The **cytoplasm** is a viscous fluid, and the **plasma membrane** is a protein network that protects the cell contents while allowing the transport of nutrients and waste products.

The shape of eukaryotic (nucleated) cells is maintained by a scaffolding called the **cytoskeleton**, which is a fibrous network of protein filaments. Prokaryotic (non-nucleated) cells apparently do not need this struc-

tural framework. Eukaryotic cell shape is mediated primarily by three types of structural proteins: actin microfilaments, microtubules, and intermediate filaments (Fig 6b).

**Actin microfilaments** link the cytoplasm to the plasma membrane. Acting in concert with myosin, they provide a contractile mechanism similar to that of muscle. This type of activity has been implicated in protrusive cell behavior, e.g., pseudopod formation, the formation of the contractile ring during cell division, and active cell shape change. **Microtubules** are hollow struts that stabilize cell and organelle shape. These elements also appear to have a function during cell shape change, since they orient parallel to the direction of elongation in certain types of cells, but the precise mechanism is not known. Finally, **intermediate filaments** act as struts to reinforce the cytoskeleton. Gordon and Brodland (1987) have estimated the mechanical properties of these various elements.

## 4.2 Cell division

Cell division involves two primary processes: **mitosis**, or the division of the nucleus, and **cytokinesis**, or the division of the cytoplasm and cell membrane. The mechanisms of cell division have been studied for many years, and several biomechanical models have been proposed for cytokinesis since 1977. The pros and cons of these models have been the subject of a relatively recent review

(Akkas, 1987), and so we present only a brief discussion here, omitting many of the details.

Models for cytokinesis fall into one of two categories: fluid mechanical or solid mechanical. In general, these models are based on one of two main hypotheses. First, according to the **equatorial constriction hypothesis**, a circumferential band of actin microfilaments called the **contractile ring (CR)** actively constricts to divide the cell. It is now generally accepted that the CR is essential for cytokinesis (Schroeder, 1987). Second, in the **polar relaxation hypothesis**, the cell cortex develops a global tension just before the onset of cytokinesis, a phenomenon confirmed experimentally (Mitchison and Swann, 1955; Yoneda and Dan, 1972). (The **cortex** is a layer of microfilaments located just below the plasma membrane, Fig 6a.) Then, the poles are stimulated to relax, and the resulting differential surface tension produces equatorial constriction. Even in this case, however, a CR is generally necessary to complete the cleavage. Recently, a critical review of the experimental data led Rappaport (1990) to conclude that equatorial constriction is the stronger of the two hypotheses, but we discuss models based on each.

The specific stimulus for cell cleavage in both hypotheses is thought to be provided by the mitotic apparatus. During mitosis, the pieces of the divided nucleus are propelled to opposite ends of the cell by microtubules that form **asters** (Fig 7), which are thought to trigger cytokinesis by interacting with the plasma membrane. In the equatorial constriction hypothesis, the asters stimulate formation of the CR, while in the polar relaxation hypothesis, the asters stimulate relaxation of the plasma membrane at the poles.

Using both experimental and theoretical methods,

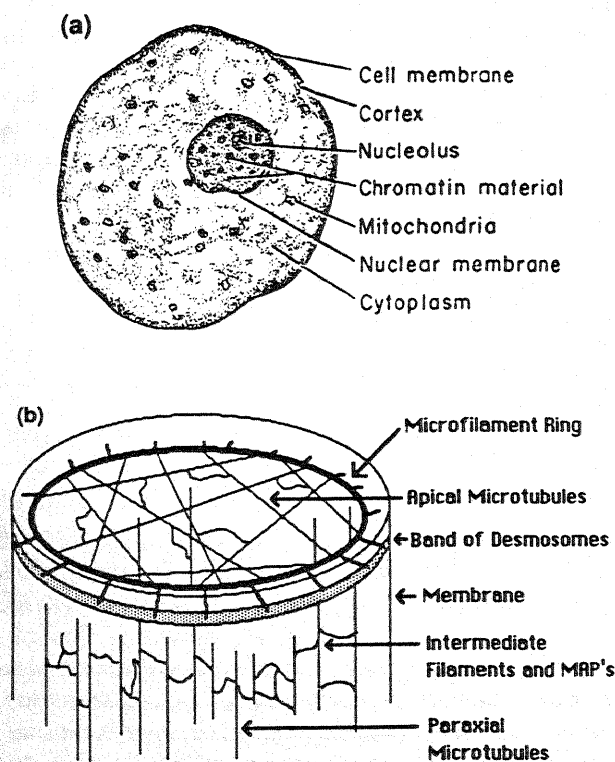


Fig 6. (a) Microstructure of a cell. [From Guyton (1991)] (b) Cytoskeletal components. [From Gordon and Brodland (1987)]

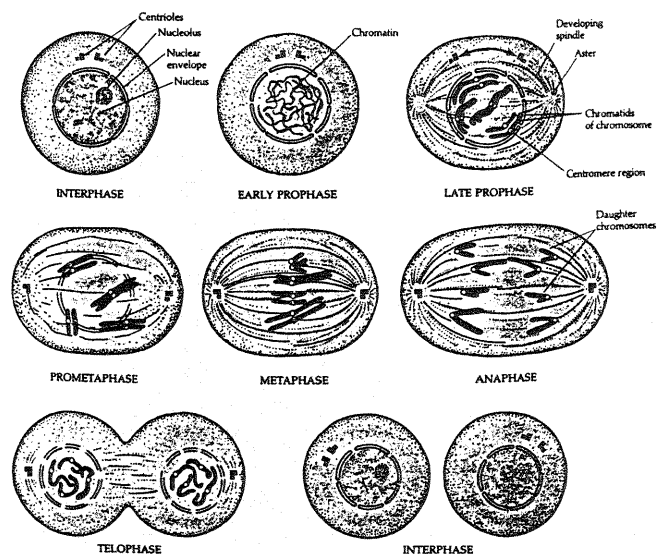


Fig 7. Cell division. [From Gilbert (1991), copyright 1991 Sinauer Associates, Inc.]



Greenspan (1977a; 1977b; 1978) investigated polar relaxation. To demonstrate the feasibility of the hypothesis, he applied surfactant to the poles of oil droplets to locally decrease the surface tension (Greenspan, 1977a, 1978). The equators constricted, eventually dividing the droplets in half. A rigorous fluid-mechanical analysis of the problem (Greenspan, 1977b) suggested that surface flow toward the equator carries filaments to form the CR, which is needed to complete the cleavage if the cell is not entirely fluid.

Extending ideas presented in a computational simulation by White and Borisy (1983), Zinemanas and Nir (1987; 1988) treated a cell as a viscous droplet with a network of actin microfilaments embedded in its surface. In this model, cytokinesis is triggered by a chemical that diffuses from the asters to the cell surface, where it decreases the concentration of filaments. Due to the position of the asters, the poles receive the greatest amount of the chemical, producing polar relaxation. The flow then carries microfilaments toward the equator, where they reorient circumferentially and induce anisotropic contraction to complete the cleavage. In a later paper, Zinemanas and Nir (1990) added elastic and viscoelastic properties to the cell membrane. Local deformations were affected significantly, but otherwise their results changed little.

The solid mechanics models proposed to date have been based on nonlinear membrane theory (Green and Adkins, 1970). Pujara and Lardner (1979) modeled a cell as a spherical elastic membrane filled with an incompressible fluid. The volume was held constant as an inward radial displacement was specified at the equator. The results for Mooney-Rivlin and STZC (Skalak et al., 1973) membranes showed good agreement with experimental profiles during cleavage (Fig 8a). As pointed out by Akkas (1980a), however, their computed monotonically increasing fluid pressure during cytokinesis is not consistent with experimental data (Hiramoto, 1968). Using a similar model, Akkas (1980b; 1981) found that allowing the fluid volume to change or including membrane viscoelasticity does not resolve this discrepancy. Thus, Akkas (1987) concluded that the only way a membrane model can produce the correct pressure variation is if the membrane modulus first increases and then decreases during cytokinesis (Fig 8b). This issue remains unresolved.

### 4.3 Cell movement

During many cellular processes, cell movement is more important than cell division. In the embryo, for example, cell division adds mass, but the molding of this mass into form depends primarily on changes in cell shape and position. Cancer is another example. Abnormal cell division is bad (tumor formation), but abnormal cell motion is often worse (metastasis).

The mechanics of cell movement are not well understood. It is notable, however, that during morphogenesis, cell division and cell movement seem to be antag-

onistic processes (Trinkaus, 1984). Cells usually do not move and divide simultaneously, suggesting that these processes use the same machinery, e.g., microfilaments and microtubules. In addition, different types of cells

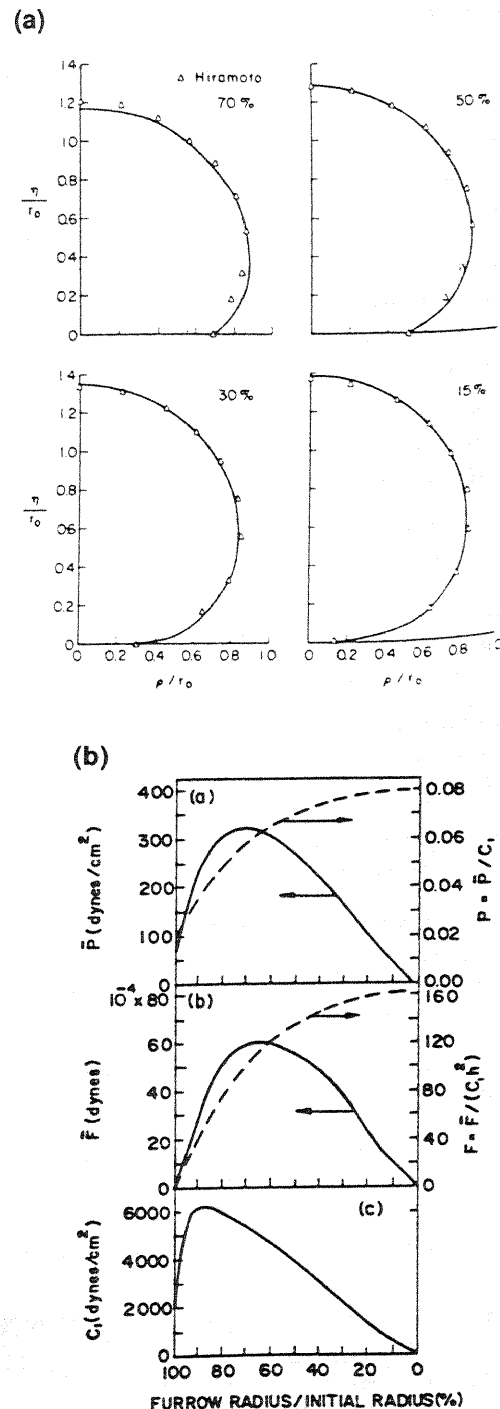


Fig 8. (a) Computed and experimental cellular profiles during cytokinesis. [Reprinted from Pujara P and Lardner TJ (1979), A model for cell division, *J Biomech* 12, 293-299, copyright 1979, with kind permission from Elsevier Science Ltd, The Boulevard, Langford Lane, Kidlington OX5 1GB, UK.] (b) Computed intracellular pressure and CR force versus CR radius and modification in material constant  $C_1$  needed for model to give experimental pressure changes. [From Akkas (1987)]

move in different ways, and the motile behavior of the same cell may depend on the environment. For instance, fibroblasts (connective tissue cells) usually remain relatively stationary *in vivo*. During wound healing or when cultured on a plane substratum, however, they crawl a great deal (Trinkaus, 1984). This section considers the motions of individual cells; shape changes and the movements of cells within epithelia are discussed in Secs 5.2 and 5.3.

In general, cell motion involves four steps (Trinkaus, 1984; Harris, 1990): (1) forward protrusion; (2) adhesion of the protrusion to the external medium; (3) rearward contraction to pull the cell forward relative to the medium; and (4) detachment of the rear of the cell (Fig 9). Several experimental observations must be considered in developing a general model for active cell motion, including:

1. All protrusions except lobopodia (see below) are filled with microfilaments, and all are devoid of organelles (Trinkaus, 1984).
2. The substratum (environment) affects the mode and direction of motion (Trinkaus, 1984).
3. In general, the stronger the traction force a cell exerts on its substratum, the slower the cell moves (Harris et al., 1981; Trinkaus, 1984).
4. Cells often exhibit **contact inhibition**, i.e., they stop moving when they contact other cells (Trinkaus, 1984).
5. Increasing the tension in the plasma membrane reduces protrusive activity (Kolega, 1986).
6. Particles placed on the upper surface of a crawling cell move rearward (Abercrombie et al., 1970; Dembo and Harris, 1981; Trinkaus, 1984).
7. Cytoplasmic strains and strain rates are much larger than those of the plasma membrane, at least in neutrophils (Simon and Schmid-Schonbein, 1990).

To date, models for cell motion have accounted for only certain aspects of these observations, with most models focusing primarily on the biomechanics of cellular protrusions. These protrusions fall into three primary classes (Harris, 1990):

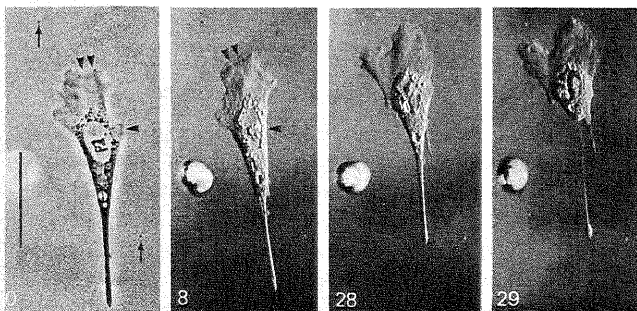
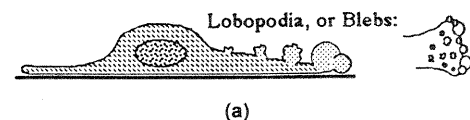


Fig 9. Photomicrographs of crawling cell. [From Chen (1981) with permission, Company of Biologists Ltd.]

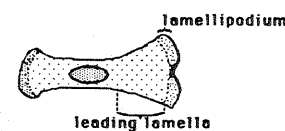
1. **Lobopodia** (blebs) are bubble-like protrusions involving cytoplasmic flow (Fig 10a). In some cases, the lobopodium appears to be analogous to an aneurysm, i.e., a ballooning of a weak part of the plasma membrane due to the internal pressure. Amoebas use this mechanism to crawl.
2. **Lamellipodia** (ruffles) are flattened, relatively stiff protrusions involving little cytoplasmic flow (Fig 10b). These projections characterize fibroblast crawling.
3. **Filopodia** (microspikes) are thin versions of lamellipodia (Fig 10c). They seem to function principally as sensors, waving about like the antennae of an ant. These protrusions guide the direction of motion and may also help pull the cell along.

Actually, other names appear in the literature for these and similar projections. For example, filopodia-like protrusions in leukocytes are called pseudopods, protopods, or uropods (Schmid-Schonbein and Skalak, 1984). Since some recent reviews have addressed models for cell movement in detail (Skalak et al., 1990; Skalak and Zhu, 1990), the following discussion is only qualitative.

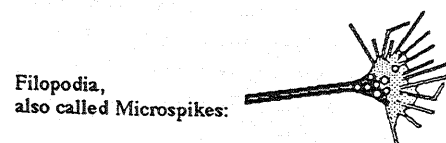
Most models for cellular protrusions involve biochemistry. For example, Odell and Frisch (1975) proposed a reaction-diffusion/flow model for pseudopod (lobopodium) extension in amoebas. They treated a pseudopod as a rigid hollow tube filled with a viscous fluid (cytoplasm) containing contractile fibers that are attached only to the tip of the pseudopod. According to this model, a chemical produced at the tip diffuses toward the cell body, triggering the cytoplasmic fibers to



(a)



(b)



(c)

Fig 10. Types of cellular extensions. [From Harris (1990)]

contract. The shortening fibers then drag fluid toward the tip, creating a pressure build-up that pushes the tip outward. The authors presented only a kinematic analysis of this model.

A qualitative hypothesis for cell crawling was given by Oster (1984), who assumed that lamellipodia are composed mostly of actin gel. Besides external loads, the equilibrium configuration of the gel is determined by a balance of the osmotic pressure, which tends to expand the gel, and elastic fiber stresses, which oppose this expansion. According to Oster's model, a leak at the tip of the protrusion allows calcium to enter. The calcium then breaks up actin fibers near the tip, allowing the gel to swell osmotically and force the tip outward. As calcium is resequenced, the fibers reform and contract, pulling the cell forward. This model can explain several features of cell motion, including contact inhibition as a contacted cell plugs the leak. In his paper, Oster (1984) presented governing equations but no quantitative results. Other models based on osmotic pressure as the driving force have been presented by Oster et al. (1982) and Oster and Perelson (1987).

In a series of papers, Skalak and colleagues presented models for pseudopod protrusion and retraction. Schmid-Schonbein and Skalak (1984) modeled the cell body as a membrane enclosing a viscoelastic solid and the pseudopod as a linear elastic solid composed of polymerized actin. Protrusion is triggered by polymerization, which occurs at the base of the pseudopod and produces an isotropic growth strain that increases the length of the pseudopod by  $\Delta b$ . The position of the base depends on the forces acting on the pseudopod (Fig 11a). Using a one-dimensional analysis, the authors examined a balance of forces due to the cytoplasmic pressure ( $F_i$ ), the external fluid pressure ( $F_2$ ), and the membrane tension ( $F_T$ ). The first force pushes the pseudopod outward, while the other two oppose outward motion. The pseudopod extends when  $F_i$  dominates, and, in agreement with experiments, increasing  $F_T$  inhibits protrusion.

After publication of this theory, new data became available that strongly suggests that actin polymerization occurs at the tip, rather than the base, of the pseudopod. Thus, Zhu and Skalak (1988) proposed a biochemical model in which polymerization at the tip supplies the force that drives the tip outward (Fig 11b). The consequent pressure drop then draws actin-rich cytoplasm from the cell body through a porous pseudopod according to Darcy's law. Comparison of theoretical and experimental results for the time-dependent length of the pseudopod shows good agreement. In addition, Zhu et al. (1989) examined pseudopod retraction with a model based on active contraction of the actin gel.

Finally, we mention the models for amoeboid movement that have been developed by Dembo and coworkers (Dembo, 1989; Evans and Dembo, 1990). In these models, the cytoplasm is a mixture of two viscous fluids, one representing a solvent and the other a network of actin and myosin. The analysis includes biochemical transfor-

mations between the two phases and active contraction of the network phase, as triggered by a diffusing chemical. Dembo (1989) numerically obtained intracellular flow patterns that agree with experimental observations, while Evans and Dembo (1990) examined surface growth at the tip of pseudopods [see also Alt (1990)].

#### 4.4 Pattern formation

During embryonic development, the motions of cells must be coordinated so that the end result is an ordered arrangement called a **pattern**. Globally, the pattern represents the basic body plan. Locally, patterns provide the forms of specific organs, bones, and other structures. Patterns are species-dependent and range from the de-

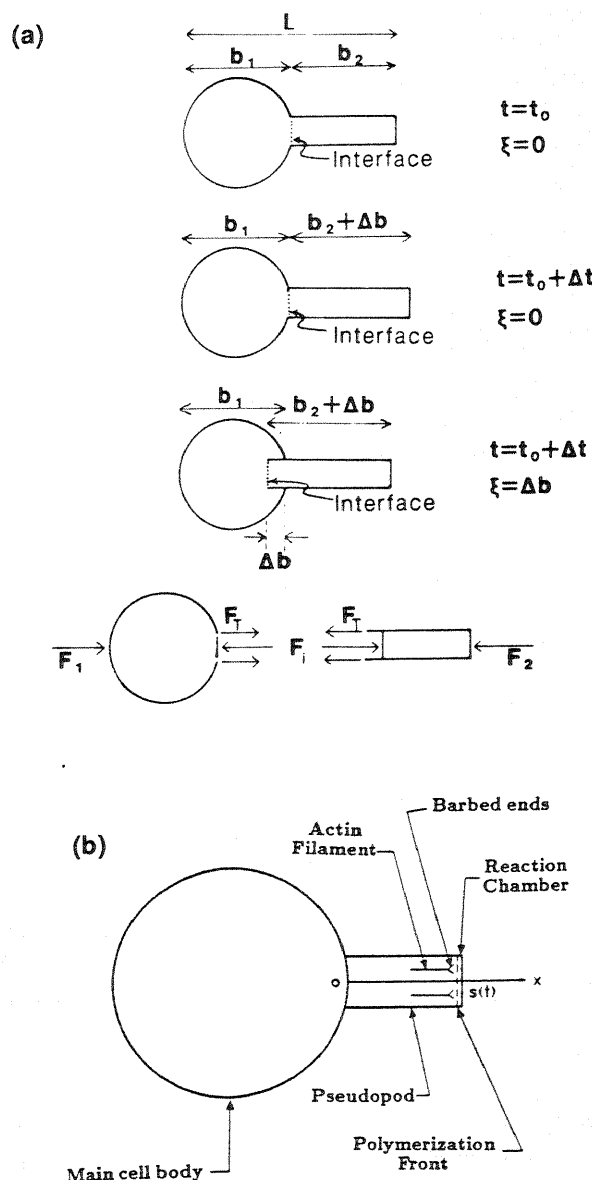


Fig 11. Pseudopod extension models. (a) From Schmid-Schonbein and Skalak (1984). (b) From Zhu and Skalak (1988).

signs of tiger stripes and butterfly wings to the various shapes of bones. The mathematical descriptions of relative (allometric) growth studied by Thompson (1942) are concerned primarily with patterns.

The mechanism of pattern formation is unknown. However, comparison of theoretical results with experimental observations strongly suggests that the process is governed by equations of the form (Murray, 1989)

$$\begin{aligned}\dot{A} &= F(A, B) + D_A \nabla^2 A \\ \dot{B} &= G(A, B) + D_B \nabla^2 B\end{aligned}\quad (19)$$

which define a reaction-diffusion type system. In these relations,  $A$  is an activator,  $B$  is an inhibitor,  $D_A$  and  $D_B$  are diffusion coefficients, and  $F$  and  $G$  are nonlinear functions. As discussed below, patterns arise from these equations through instabilities.

Current models for pattern formation generally fall into one of two categories: biochemical or biomechanical. Although these types of models are fundamentally different in principle, both are governed by equations essentially equivalent to Eqs (19). Since biochemical models hold a prominent place in the study of pattern formation (Harrison, 1987; Wolpert, 1978), we briefly discuss this type of model before examining biomechanical models in greater depth.

#### 4.4.1 Biochemical models

Models for pattern formation based entirely on biochemistry were pioneered by Turing (1952). In these models, diffusion-driven instabilities produce spatially inhomogeneous chemical patterns. Then, according to the **positional information hypothesis** of Wolpert (1969), individual cells "read" the concentration of a pattern-forming morphogen and translate this into a particular differentiation, shape change, or migration.

The physical basis behind the pattern-forming behavior of Eqs (19) is local excitation with lateral inhibition (Oster and Murray, 1989). Initially, the chemical concentrations of activator and inhibitor are uniform in a given domain. If a small disturbance upsets the equilibrium, the concentration of the activator locally increases and diffuses outward. However, if the inhibitor diffuses at a faster rate, it limits the spatial range of the activator and prevents a return to the uniform equilibrium state. The increased concentrations near local disturbances form a pattern in the domain.

The form of a specific pattern depends on the functions  $F$  and  $G$  of Eqs (19), the size and shape of the domain, and other parameters. Many variations of the original model of Turing (1952) have been proposed, with the main differences being the choices of  $F$  and  $G$  (Murray, 1982). These models have been used successfully to predict the effects of measurable parameters on changes in pattern (Murray, 1989). For example, the models predict that relatively small and relatively large animals have more uniform coat markings than medium-sized animals

(Fig 12). As the size of the domain increases, the number of waves (concentration peaks) that can fit within the boundaries increases, i.e., bifurcation boundaries are crossed. This behavior agrees qualitatively with observations. On the other hand, identifying a pattern-forming morphogen has proved elusive.

#### 4.4.2 Biomechanical models

Whereas in biochemical models cells respond in a programmed manner to chemical concentrations, in biomechanical models they participate directly in the dynamics of pattern formation. These latter models are formulated in terms of physically meaningful parameters, and cells react actively and passively to mechanical forces. Morphogens are not necessary.

The basis of most biomechanical models of pattern formation lies largely in experimental observations of the effects of cell traction on artificial substrates. When a fibroblast is cultured on a thin rubber sheet, for example, the sheet wrinkles due to compression under the cell and tension outside the cell (Harris et al., 1980; Harris, 1984), with lines of tension radiating outward for relatively large distances from the cell (Fig 13a). Moreover, when a fibroblast is embedded and cultured in a collagen gel, the collagen fibers near the cell align in a radial pattern (Harris et al., 1984; Stopak and Harris, 1982), apparently also in response to an applied tension. The origin of the forces exerted by the cells is poorly understood, but **stress fibers**, i.e., aligned microfilaments, have been seen in the cytoplasm of these cultured cells (Burridge, 1981). It is notable that stress fibers have been implicated in adhesion of vascular endothelial cells to their substrate (see Sec 7.2.4). (Endothelial cells are epithelial cells that line the lumens of blood vessels and other closed cavities.) However these forces are generated, they apparently serve purposes other than those required for cell motion, since the most mobile cell types exert the weakest tractions (Harris et al., 1981; Trinkaus, 1984).

These and other data suggest that cell-generated tractions play an important role during morphogenesis and

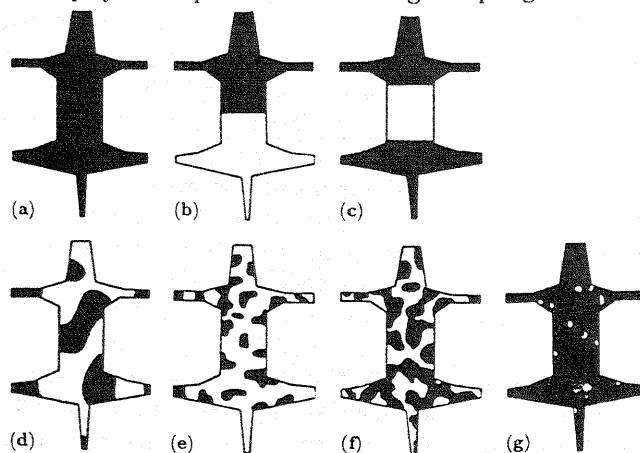


Fig 12. Computed animal coat patterns for animals of increasing size. [From Murray (1989)]

pattern formation. In fact, when several fibroblasts are cultured together in a collagen gel (Harris et al., 1984), a primitive pattern forms of compacted clumps of cells connected by collagen fibers (Fig 13b). Rather than moving actively, the cells are dragged toward the clumps by "convection." In addition, Stopak and Harris (1982) effectively grew a musculoskeletal element in culture. When they embedded chick embryo muscle explants in collagen gel next to a bone, the muscle tissue became attached to the ends of the bone, and the collagen fibers aligned between the explants and stretched them much like tendons would.

Taking these experiments into account, Oster et al. (1983) proposed a biomechanical model for pattern formation based on the following main assumptions:

1. Mesenchymal cells migrate within the fibrous extracellular matrix (ECM).
2. Motile cells generate large tractions that deform the ECM.
3. The direction of cell motion is influenced by the de-

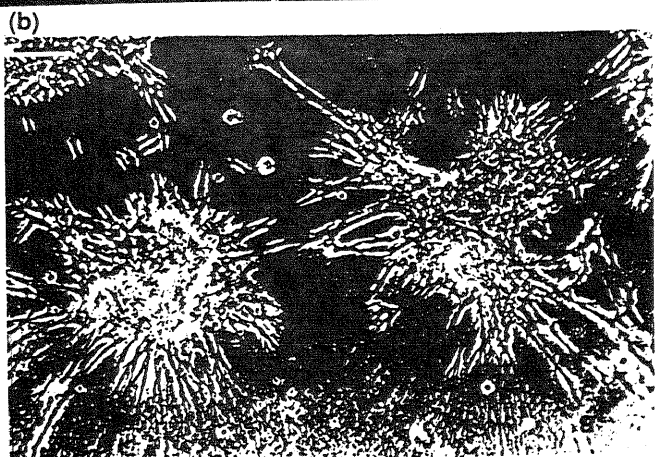
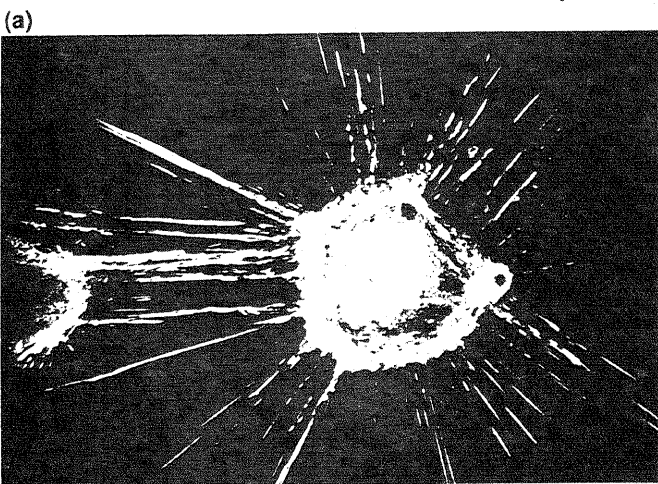


Fig 13. Fibroblast tractions (a) on a rubber sheet [Reprinted with permission from Harris AK, Wild P, and Stopak D (1980), Silicone rubber substrata: a new wrinkle in the study of cell locomotion, *Science* 208, 177-179. Copyright 1980 American Association for the Advancement of Science.] and (b) in a collagen gel [From Harris et al. (1984) with permission, Company of Biologists Ltd.]

formation of the ECM and by adhesion gradients (haptotaxis).

Other assumptions and restrictions will become clear below as we present the governing equations for the model.

First, the mass conservation equations are listed. For the cells, Oster et al. (1983) write

$$\dot{n} = -\nabla \cdot \mathbf{J} + M(n) \quad (20)$$

where  $n(\mathbf{x}, t)$  is the number of cells per unit volume at position  $\mathbf{x}$  and time  $t$ ,  $\mathbf{J}$  is the flux of cells per unit area, and  $M$  is the mitotic rate. The cell flux vector is given by the relation

$$\mathbf{J} = [-D_1 \nabla n + D_2 \nabla (\nabla^2 n)] + [\alpha n \nabla \rho] + [n \dot{\mathbf{u}}] \quad (21)$$

in which  $D_1$  and  $D_2$  are diffusion coefficients,  $\alpha$  is an adhesion coefficient,  $\rho$  is the mass density of the ECM, and  $\mathbf{u}$  is the ECM displacement vector. In this equation, the first bracketed term represents diffusive cell migration, the second term is the flux due to haptotaxis, and the last term is due to convection by ECM deformation. The form of the haptotaxis term is based on the assumption that cells move up an adhesive gradient as determined by the number of adhesive sites, which increase with  $n$  and  $\nabla \rho$ . Furthermore, the  $D_1$  term represents short-range random motion, and the  $D_2$  term represents long-range motion due to pseudopod extension. In general,  $D_1$  and  $D_2$  can depend on the (linear) ECM strain tensor

$$\epsilon = \frac{1}{2} [\nabla \mathbf{u} + (\nabla \mathbf{u})^T]. \quad (22)$$

In addition, the mitotic rate is taken as

$$M = rn(N - n) \quad (23)$$

where  $r$  is the growth rate and  $N$  is the maximum cell density. For the ECM, conservation of mass gives

$$\dot{\rho} = -\nabla \cdot (\rho \dot{\mathbf{u}}) + S \quad (24)$$

where  $S(n, \rho, \mathbf{u})$  is the (neglected) rate of ECM secretion by the cells.

The stress tensor for the composite material is

$$\sigma = \sigma_p + \sigma_a \quad (25)$$

where  $\sigma_p$  and  $\sigma_a$  are passive and active stress tensors, respectively. For a linear viscoelastic material, Oster et al. (1983) used the expression

$$\sigma_p = \frac{E}{1 + \nu} \left( \epsilon + \frac{\nu}{1 - 2\nu} \theta \mathbf{I} \right) + (\mu_1 \dot{\epsilon} + \mu_2 \dot{\theta} \mathbf{I}) \quad (26)$$

in which  $\theta = \nabla \cdot \mathbf{u}$  is the dilatation,  $\mathbf{I}$  is the identity tensor,  $\mu_1$  is the shear viscosity,  $\mu_2$  is the bulk viscosity,  $E$  is Young's modulus, and  $\nu$  is Poisson's ratio. The active stress, due to cell traction, was taken in the form

$$\sigma_a = \frac{\tau \rho}{1 + \lambda n^p} (n + \beta \nabla^2 n) \mathbf{I} \quad (27)$$

where  $\tau$ ,  $\lambda$ ,  $p$ , and  $\beta$  are constants, and the first and second terms in parentheses provide the short-range and long-range contributions, respectively. Moreover,  $\lambda \geq 0$  and  $p \geq 2$  are parameters that define the saturation cell density, i.e., cell motion is restricted by contact inhibition.

Finally, with inertia neglected, the equation of motion is

$$\nabla \cdot \sigma + \rho \mathbf{f} = 0 \quad (28)$$

where  $\mathbf{f}$  is a body force per unit mass. For a substrate of stiffness  $k$ ,  $\mathbf{f} = k\mathbf{u}$  provides a foundation force.

Equations (20) [with (21) and (23)], (22), (24), (25) [with (26) and (27)], and (28) provide five equations to solve for  $n$ ,  $\rho$ ,  $\mathbf{u}$ ,  $\sigma$ , and  $\epsilon$ . Combining these relations results in a reaction-diffusion type system, with cell traction being the primary activator and the elastic forces of the ECM being the primary inhibitor. Physically, patterns form when a local increase in cell density produces a local increase in traction, which drags cells toward the activation focus. In addition, ECM fiber alignment helps guide motile cells toward the focus. These effects are resisted by the ECM viscoelastic stresses, which limit the range of cell convection and the extent of fiber alignment. As other foci develop, pattern emerges.

To gain insight into the behavior of their model, Oster et al. (1983) performed a one-dimensional stability analysis. Unstable linear modes relative to the uniform equilibrium state were used to predict the actual nonlinear pattern. The authors concluded that increasing the domain size leads to a series of bifurcations, i.e., more activation foci, and that different patterns can arise from changes in certain nondimensional combinations of parameters. In addition, they discussed qualitative aspects of two-dimensional pattern formation in, for example, skin-organ primordia and cartilage rudiments in developing limbs. Murray and Oster (1984) analyzed the model in more detail, and Perelson et al. (1986) confirmed the predicted stability behavior with a numerical solution of the one-dimensional nonlinear equations. Belintsev et al. (1987) described a similar but more limited model.

Oster et al. (1985) presented a variation of the aforementioned model that takes into account the swelling behavior of the ECM gel, which is composed primarily of collagen fibers embedded in hyaluronic acid (HA). The cells counteract the swelling by secreting hyaluronidase (HAase), which degrades the HA. In this model, cell traction again provides the activator, but osmotic pressure is the inhibitor. Patterns form as follows. Initially, a domain is in mechanochemical equilibrium with secretions of HA and HAase balanced. A local increase in cell traction, however, drags the cells closer together, increasing the local concentration of HAase. Near this focus, the ECM then deswells, bringing the cells even closer together, and so on.

In their study, Oster et al. (1985) ignored cell motility, cell division, adhesion, and ECM secretion. Thus, Eqs (20), (21), and (24) yield the cell and ECM conser-

vation equations

$$\begin{aligned} \dot{n} &= -\nabla \cdot (n\dot{\mathbf{u}}) \\ \dot{\rho} &= -\nabla \cdot (\rho\dot{\mathbf{u}}). \end{aligned} \quad (29)$$

In addition, since HA does not diffuse but HAase does, conservation of these quantities yields

$$\begin{aligned} \dot{h} &= -\nabla \cdot (h\dot{\mathbf{u}}) + S_h - D_h \\ \dot{a} &= D\nabla^2 a - \nabla \cdot (a\dot{\mathbf{u}}) + S_a - D_a \end{aligned} \quad (30)$$

where  $h(\mathbf{x}, t)$  and  $a(\mathbf{x}, t)$  are the respective densities of HA and HAase,  $D$  is the diffusion coefficient for HAase,  $S_h$  and  $S_a$  are secretion rates, and  $D_h$  and  $D_a$  are degradation rates.

The constitutive law for the total stress tensor was taken in the form of Eq (25) with

$$\sigma_p = E[\epsilon - \alpha \nabla^2 \epsilon] + \mu \dot{\epsilon} - \Pi \mathbf{I} \quad (31)$$

replacing Eq (26), and  $\sigma_a$  was again provided by Eq (27). Here, the  $\alpha$  term is a long-range effect and the osmotic pressure is given by

$$\Pi = \gamma h^2 / (1 + \theta) \quad (32)$$

where  $\theta$  is the dilatation and  $\gamma$  is a constant.

The authors used this formulation specifically to model **chondrogenesis**, the formation of cartilage. A one-dimensional analysis showed that the model can produce patterns similar to those of the previous model. More details of this model related to skeletal development are discussed in Sec 6.1.5.

#### 4.5 Response to stress

Comparative anatomy studies strongly suggest that form depends on mechanical stresses, often including those due to the force of gravity (Thompson, 1942; Wainwright et al., 1976). In addition, direct experimental evidence indicates that stress influences growth, adaptation, and morphogenesis. This section discusses some of this evidence at the cellular level. Other cellular and tissue-level data are considered in later sections.

The effects of stress on growth have been investigated by culturing cells on artificial substrates, which are then stretched. For example, Curtis and Seehar (1978) cultured chick embryo fibroblasts on a fabric mesh. When pulled along one direction, the mesh changed shape with little change in area, thereby shearing the cells. Due to an oscillating deformation, the rate of mitosis increased. Bovine aortic endothelial cells respond similarly (Sumpio et al., 1987). It is not clear, however, whether it is the imposed stress itself or the stress-induced shape change that stimulates cell division. Evidence supporting the latter mechanism was obtained by Folkman and Moscona (1978), who altered substratum adhesiveness to examine more directly the effect of cell shape change. In response to increased adhesion, bovine endothelial cells flattened and divided faster.



When loading conditions change, cells often realign (remodel) to adapt to the altered biomechanical environment. Rotating and transplanting tissue segments in amphibian embryos, Belousov (1980) found that the tissues reorient according to the stress field in the host environment. In addition, Belousov et al. (1988) cultured early embryonic amphibian cells on rubber sheets. When the sheet was not deformed, the cells migrated or remained undifferentiated. When the sheet was stretched for a sufficiently long time, however, the cells developed normally and aligned *perpendicular* to the direction of stretch. Similar experiments with fibroblasts, endothelial cells, and embryonic myocytes produce the same kind of realignment (Buck, 1980; Shirinsky et al., 1989; Dartsch and Betz, 1989; Terracio et al., 1990; Gilbert et al., 1994).

Cells exposed to fluid flow also alter their orientation. For instance, cultured vascular endothelial cells exposed to laminar flow elongate *parallel* to the direction of flow (Nerem, 1990). The degree of elongation depends on the level of fluid shear stress, the duration of exposure, and the character of the substratum. As discussed in Sec 7.2.4, the available data suggest that these shape changes are likely due to active processes.

Explanations have been offered for the seemingly conflicting results given by the stretching and the flow experiments involving endothelial cells. In both types of loading, stress fibers (see Sec 4.4.2) form in the direction of cell alignment (Dewey et al., 1981; Wong et al., 1983; White et al., 1983; Franke et al., 1984; White and Fujiwara, 1986; Shirinsky et al., 1989). These fibers are relatively stiff structures associated with adhesive contacts on substrata (see Sec 7.2.4). Thus, alignment perpendicular to the direction of stretch may be a defense mechanism that allows the cells to avoid being stretched while maintaining contact with the substrate (Buck, 1980; Shirinsky et al., 1989). On the other hand, alignment parallel to the direction of flow would enable the cells to more effectively resist being torn from the substrate by shear stress (Shirinsky et al., 1989).

The signaling mechanism that links the mechanical environment to cell function is unknown. Speculation has centered on, for example, shape change through the actin cytoskeleton (Hay and Svoboda, 1989; Watson, 1991) and stretch-activated ion channels (Sachs, 1986). In addition, according to Hay and Svoboda (1989), shape changes can activate certain genes.

## 5 EPITHELIA

### 5.1 Structure and function

An epithelium is a tightly linked sheet of cells that exhibits apical-basal polarity. The apical surface of the sheet faces the exterior or luminal spaces, and the basal surface faces groups of cells (mesenchyme) or extracellular matrix in vertebrates and fluid in invertebrates. Epithelia line the interior and exterior surfaces of tissues and organs, providing protection from chemicals and other

environmental factors. The component cells are bound together by two sets of circumferentially distributed junctions, which are mediated by adhesion molecules. During morphogenesis, epithelia undergo both passive and active shape changes. In general, these deformations can be grouped into two categories: global and local.

Global epithelial deformations include surface-area changes and constant-area cell rearrangements. During morphogenesis, epithelial spreading (area increase) is much more common than contraction (Fristrom, 1988). Examples of spreading include wound closure and the process of **epiboly**, whereby an epithelium expands to enclose the interior of the early embryo. Cell rearrangement involves an exchange of neighbors without gaps appearing in the sheet or the permeability barrier being disrupted. How this phenomenon occurs among the tightly coupled cells remains largely a mystery.

Local epithelial deformations include invagination, evagination, folding, and placode formation. **Invagination** is a localized inpocketing with the apical surface of the sheet located on the concave side (Fig 14). A classic example is amphibian **gastrulation** (Fig 15a), a process that organizes the early embryo into the primary germ layers from which the various organs eventually derive. The first phase of gastrulation involves an inward dimpling of the outer cell layer of the **blastula**, which is a hollow, fluid-filled ball of cells resulting from the initial series of divisions of the egg. In the second phase, the dimple extends across the embryo to the opposite side, where the mouth forms. Completion of gastrulation yields the primitive gut, with the **archenteron** connecting the dimpled **blastopore** to the mouth. Invagination along a line forms a **furrow**. An example of this latter process is **neurulation** (Fig 15b), i.e., the formation of the hollow neural tube, which later differentiates into the brain and spinal cord.

**Evagination** is a localized outpocketing of an epithelium with the apical surface located on the convex side (Fig 14). This process is relatively rare, with examples including the formation of feathers and scales. Evagination along a line produces a **ridge**.

**Folds** are alternating series of invaginations and evaginations (Fig 14). While single invaginations and evaginations are thought to involve active deformation, folds

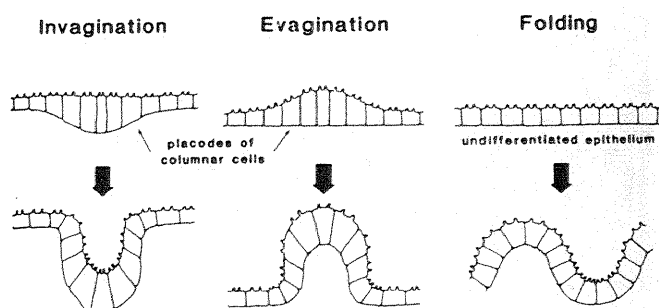


Fig 14. Invagination, evagination, and folding of epithelium. [From Fristrom (1988)]

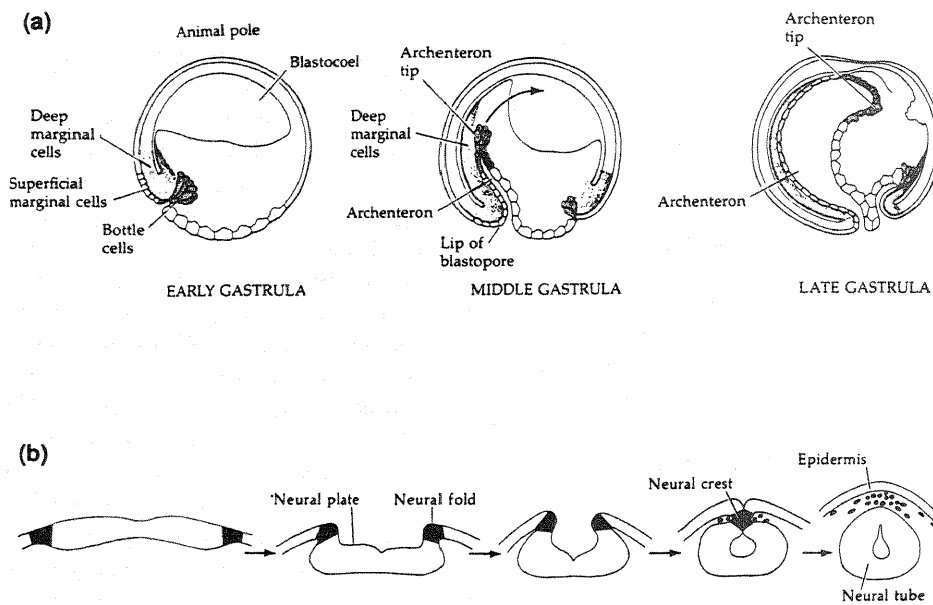


Fig 15. (a) Amphibian gastrulation. (b) Neurulation. [From Gilbert (1991), copyright 1991 Sinauer Associates, Inc.]

are likely a passive response to external forces. Consider, for example, the part of the retinal epithelium called the ciliary body. During avian eye development, this sheet develops radial folds along the edge that is attached to the relatively rigid pupillary ring (Fig 16). This structure can be modeled as a spherical membrane with a rigid circular inclusion and an internal (intraocular) pressure. The folds apparently are due to circumferential buckling of the membrane near the inclusion.

Finally, a **placode** is a columnarization of a local group of cells in an epithelium. Placodes consistently signal the onset of an invagination (Fig 17), the significance of which is discussed in the next section.

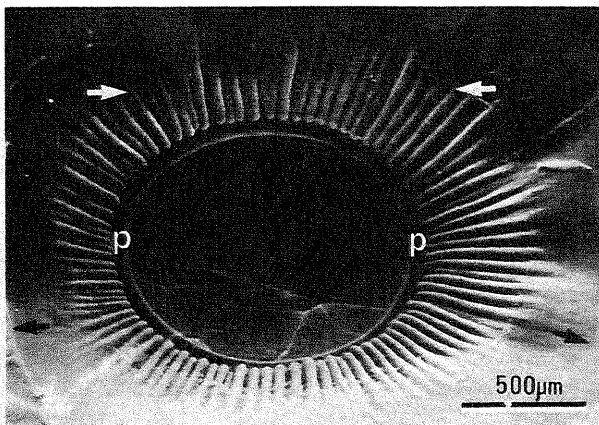


Fig 16. Wrinkling during eye development. [From Bard and Ross (1982)]

## 5.2 Morphogenetic mechanisms

Although epithelial motions and deformations have been studied extensively, the driving mechanisms remain poorly understood in most cases. The available experimental data paint an inconsistent picture. Thus, the proposed mechanisms discussed in this section have not been validated completely, even for the most basic morphogenetic processes.

### 5.2.1 Global shape changes

Dimensional changes of an epithelium can be produced by passive stretching, active cell shape change, addition of cells, or cell rearrangement. A morphogenetic event may involve the simultaneous actions of more than one of these processes.

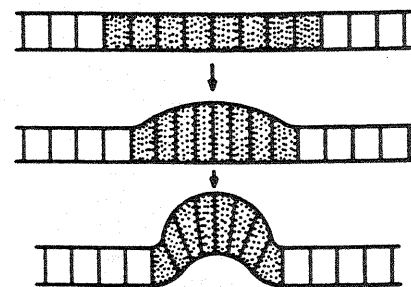


Fig 17. Placode formation at the onset of invagination. [From Ettensohn (1985) with permission from the University of Chicago, copyright 1985 by the Stony Brook Foundation, Inc.]

**Passive stretching.** An epithelium can be stretched passively by tractions applied by adjacent tissues, but in some cases, the cells at the edge of the sheet may supply the tension. Evidence for this latter mechanism comes from experiments with epithelial cells cultured on a plane glass surface. Vaughan and Trinkaus (1966) found that only cells at the outer edges of a sheet adhere to the glass, and these cells actively pull the interior cells outward, stretching the sheet. Note that, if applied forces generate compressive stresses, the sheet may buckle into folds (wrinkles).

Interesting examples of growth and morphogenesis due to passive forces occur during development of the eye. Coulombre (1956) and Coulombre and Coulombre (1958) investigated the role of intraocular pressure in the chick embryo. Both studies involved experimentally reducing the pressure by placing a small glass tube into the gel (vitreous body) inside the eye. They found that intubated eyes grow at a rate slower than normal, indicating that passive stretching due to pressurization drives much of the growth.

Moreover, Coulombre and Coulombre (1958) studied the effects of pressure on morphogenetic aspects of eye development. During normal development, the chick eye remains nearly spherical until the eighth day of a 21-day incubation period, i.e., the radii of curvature of the cornea (the segment in front of the lens) and the sclera (the white of the eye) are approximately equal. After this time, the radius of curvature of the sclera increases more rapidly than that of the cornea (Fig 18). In this study, the authors found the following:

1. Intubated eyes remain essentially spherical (Fig 18).
2. A ring of cartilage begins to differentiate near the edge of the cornea on the eighth day.

These results suggest that normal eye development depends not only on the presence of a normal intraocular pressure, but also on a local change in material properties. After the cartilage stiffens the ring around the cornea, the sclera and cornea grow as separate spherical segments with different radii of curvature.

With similar intubation experiments, Desmond and Jacobson (1977) showed that normal brain development

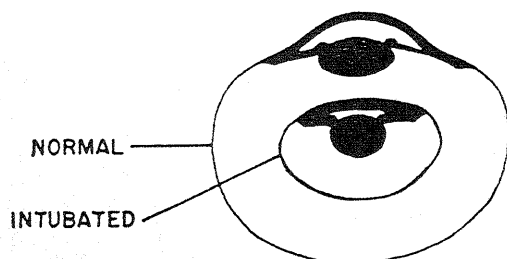


Fig 18. Effect of decreased intraocular pressure during chick eye development. [From Coulombre and Coulombre (1958), copyright 1958 American Medical Association.]

depends on the cerebrospinal fluid pressure. They found that brains subjected to lower pressure grow slower and are abnormally shaped.

**Active cell shape change.** Epithelial cells can undergo active shape changes through microfilament contraction, microtubule elongation, changes in osmotic forces, or changes in intercellular adhesion. Consider first microfilament contraction. The membrane of each epithelial cell contains the contractile proteins actin and myosin, and so a uniform muscle-like contraction theoretically could reduce the surface area. However, two observations argue against this mechanism. First, as already mentioned, global epithelial contractions are relatively rare (Fristrom, 1988). Second, the actin filaments are arranged primarily in a ring around the apex (Burnside, 1973), and so contraction would likely produce a wedge-shaped cell with a constricted apex rather than a uniform diameter change (Fig 19). (This mechanism is important for local bending; see Sec 5.2.2.)

The other listed mechanisms can increase or decrease epithelial surface area. Microtubule elongation perpendicular to the sheet would decrease the surface area, since the incompressible cytoplasm would force the cells to narrow as they columnarize. On the other hand, elongation in the plane of the sheet could produce spreading. In addition, changes in intracellular osmotic pressure can increase or decrease surface area in a form of cell growth. Finally, increased adhesion between cells induces cells to increase their area of contact, with the cells elongating ("zippering up") perpendicular to the sheet. This mechanism would decrease surface area, while decreased adhesion would have the opposite effect (see Fig 20a,c).

**Cell addition.** An epithelium also can spread by adding cells through division or egression, while the opposite effects of cell death or ingression contract the sheet. The transformation of mesenchymal cells into epithelial cells leads to **egression**, the intercalation of cells from the embryo into the sheet, and the transformation of epithelial cells into mesenchymal cells leads to **ingression**, the migration of cells from the sheet into the embryo. Added mass, however, generally contributes little to morphogenesis. In fact, just as cell division stops when cells move (Sec 4.3), cell division usually slows during rapid morphogenetic deformations.

**Cell rearrangement.** Rearrangement of cells can change the shape of an epithelium without a change in surface area. Cell marking experiments clearly show that rearrangement occurs, but it remains one of the least understood morphogenetic processes. Proposed mechanisms for this process include (Fristrom, 1988): (1) cell sorting to maximize adhesion; (2) basal cellular protrusions that draw cells together; (3) cytoplasmic flow similar to that which drives some mesenchymal cell migration; and (4) localized cellular contraction to bring

separated cells into contact. Some of these mechanisms will be discussed in Sec 5.3 in more detail, but none has yet been validated.

### 5.2.2 Local shape changes

Many different mechanisms can bend epithelial sheets. Here, we discuss several that enjoy varying degrees of experimental support. However, none are consistent with all experimental data, and so none are accepted universally.

**Apical constriction.** Each epithelial cell possesses a network of actin microfilaments encircling the apex (Fig 6b). Since myosin also is present in most cells, investigators have postulated that the microfilaments contract, constricting the apex like a "purse string" (Burnside, 1973; Fristrom, 1988). The incompressible cytoplasm then shifts toward the basal end, forcing the cell into a pyramidal shape (Fig 19). If several adjacent cells in a sheet undergo this type of deformation, the sheet bends locally with the apical surface on the concave side (Fig 19), as observed during invagination (Fristrom, 1988).

Even before microfilaments were discovered, Lewis (1947) proposed this mechanism for epithelial bending. He demonstrated its feasibility by constructing a model with brass plates for the cell surfaces and rubber bands for the contractile filaments. For many years, apical constriction gained a large following, based largely on findings that cytochalasin B stops or even reverses local bending processes such as neurulation (Ettensohn, 1985). (Cytochalasin B is a drug that disrupts actin microfilaments.) Recently, however, some researchers have questioned the interpretation of these results, pointing out that cytochalasin B may affect other cell properties (Ettensohn, 1985; Schoenwolf et al., 1988). In fact, Schoenwolf et al. (1988) have found that cytochalasin D, which

affects actin similarly but without the side effects, has a less significant influence on neurulation. This issue is not settled.

**Constrained expansion or contraction.** As discussed in Sec 5.2.1, several mechanisms can cause an epithelium to expand or shrink its surface area. Constraints due to an underlying basal lamina or extracellular matrix may then induce local buckling.

Consider, for example, changes in intercellular adhesion (Fig 20). If the basal lamina is extremely extensible, then decreased and increased adhesion produces epithelial spreading (a) and contraction (c) respectively. However, if the basal lamina is relatively stiff, then increased adhesion induces invagination (b) with cell apices on the concave side, while decreased adhesion induces evagination (d) with cell apices on the convex side. In the limit of zero adhesion, the cells round up, and the maximum possible evagination occurs (e).

As mentioned in Sec 5.1, placode formation usually precedes invagination. Fristrom (1988) pointed out that this is contrary to intuition, since a thickening would increase the resistance of the sheet to bending. However, she speculated that the accompanying alignment of microtubules perpendicular to the sheet likely would make bending easier. Either apical constriction or increased adhesion could produce placode formation in conjunction with invagination.

**Cytoplasmic flow.** Since epithelial and mesenchymal cells often switch roles, they likely possess similar machinery for motion. Thus, Jacobson et al. (1986) speculated that epithelial cells are capable of active movement within a sheet. Their theory for cell crawling, based on cytoplasmic flow, was discussed for mesenchymal cells in Sec 4.3 and will be discussed for epithelial cells in Sec 5.5. Besides accounting for cell rearrangement, the theory accommodates invagination, as cells try to crawl out of the epithelium but are restricted by their junctions to surrounding cells.

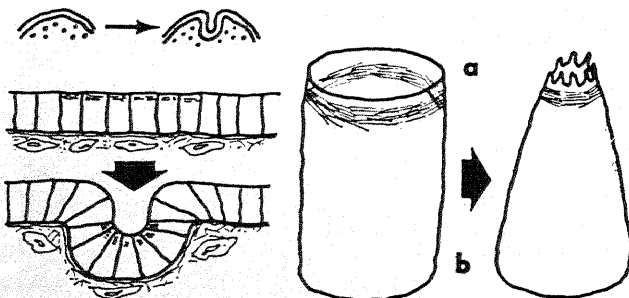


Fig 19. Deformation due to apical microfilament contraction in epithelium (left) and cell (right). [Reprinted with permission from Wessells NK, Spooner BS, Ash JF, Bradley MO, Luduena MA, Taylor EL, Wrenn JT, and Yamada KM (1971), Microfilaments in cellular and developmental processes, *Science* 171, 135-143. Copyright 1971 American Association for the Advancement of Science.]

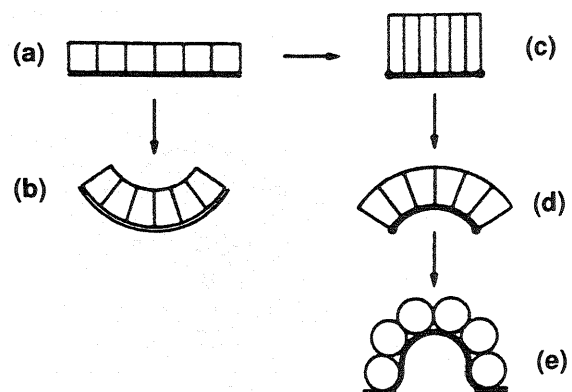


Fig 20. Invagination and evagination due to changes in adhesion. [From Ettensohn (1985) with permission from the University of Chicago, copyright 1985 by the Stony Brook Foundation, Inc.]

### 5.2.3 Epithelial models

In the following sections, we discuss specific models for epithelial morphogenesis. We begin with cell rearrangement models, which are actually computer *simulations* with minimal biomechanical bases. Next, we examine a pair of pseudobiomechanical models, which stand on firm theoretical foundations, but some important physical features are neglected. One model is based on apical constriction, and the other uses cytoplasmic flow as the driving force. All of these models represent an epithelium as a collection of joined cells. Finally, we discuss general continuum (shell) models, which are true biomechanical models, but the ability to focus on individual cells is lost.

### 5.3 Cell rearrangement models

Modeling cell rearrangement within an epithelium is complicated by the need to follow individual cells. Using experiments and a purely geometric analysis, Jacobson and Gordon (1976) and Jacobson (1980) studied cellular motions during neurulation in the newt. Correlating observations with computer-generated morphology showed how the cells must move to give the observed three-dimensional global shape changes. The authors found that the deformation is more complex than a simple rolling into a tube, with the neural plate also elongating in the antero-posterior direction as the neural tube forms. Jacobson (1980) suggested that this elongation may induce buckling of the epithelium, with a furrow forming along the direction of stretch, as occurs when a thin rubber sheet is stretched uniaxially. This furrow eventually forms the neural tube.

Weliky and Oster (1990) developed a simulation for epithelial cell rearrangement that accounts for the effects of changing intra- and intercellular forces. Each cell is represented by a two-dimensional polygon with a variable number of sides and nodes that can slide, appear, and disappear. The motion of each node is determined by the forces acting on the node, and the geometry is updated to maintain compatibility. In this way, the simulation accounts for cell shape change and rearrangement.

In this model, the plasma membrane of each cell contains actomyosin filaments and encloses a filament-rich gel. The forces acting on each node are due to: (1) positive osmotic pressure that expands the gel; (2) a negative elastic pressure due to intracellular filaments opposing gel swelling; (3) tension in the sides due to microfilament bundle contraction; and (4) external loads. During a given time step, each node moves a distance proportional to the magnitude of the total force acting on it and in the direction of the resultant force. Accordingly, internal pressure drives protrusions, while tensile wall stress drives cellular contraction.

The authors used the model to study epiboly (see Sec 5.1) in the teleost fish *Fundulus* (Weliky and Oster, 1990). Initially, a uniform cap of cells was situated on a rigid spherical surface. Epiboly was simulated by specifying

the meridional displacement of the cells at the edge of the sheet. Experiments have shown that the number of cells at the margin decreases continually during epiboly, even as its circumference increases. The simulation was able to reproduce this behavior if the membrane tension of the marginal cells was reduced, so that they could protrude circumferentially to force some cells off the edge (Fig 21).

Weliky et al. (1991) modified this model to include the following general features of cell motility:

1. Persistence of the direction of motion. Probabilities of movement were assigned to each node.
2. Tension-induced inhibition of protrusions. Protrusions were prohibited when the cell was stretched beyond a specified limit.
3. Contact inhibition. Protrusion was stopped when contact with a second cell occurred.

The authors then used the model to examine tissue extension, cell rearrangement, and the interactions of cells with boundaries. They concluded that several rules of cell behavior operate simultaneously during neurulation in the frog.

A similar approach was pursued by Beloussov and Lakirev (1991), who modeled an epithelium as a shell containing movable elements. In this model, the radial displacement of each element depends on the resultant force acting on that element. Using a finite-element formulation, the authors obtained various morphogenetic shapes.

### 5.4 Apical constriction model

Although controversial, apical microfilament contraction likely plays a role in morphogenesis. The epithelial model of Odell et al. (1981) is based primarily on this mechanism. This model contains the following features:

1. The cells in the sheet are tightly bound.

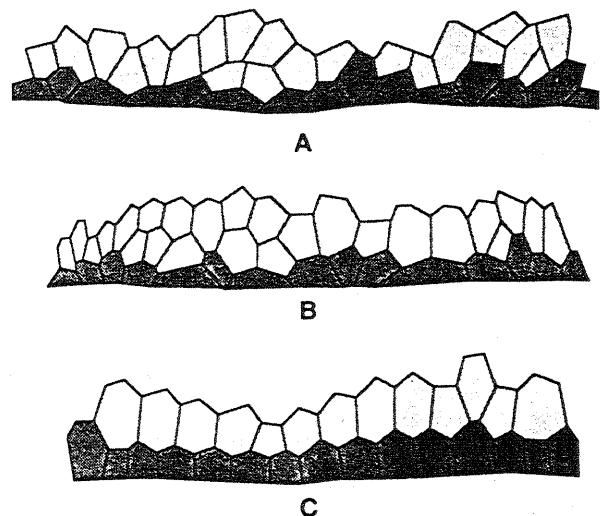


Fig 21. Cell rearrangement in model of epiboly. [From Weliky and Oster (1990), copyright 1990 Company of Biologists Ltd.]

2. The cytoplasm is a viscoelastic solid.
3. The apex of each cell contains a network of microfilaments. When stretched a small amount, the filaments act as a passive viscoelastic material. When stretched beyond a specified threshold value, however, the filaments "fire," developing an active contractile force that remains for all time thereafter.

To represent these features, each cell is modeled by a four-sided, two-dimensional truss element composed of six viscoelastic units (Fig 22), each of which contains a spring ( $k$ ) and a dashpot ( $\mu$ ) in parallel. The diagonal units represent the cytoskeleton, and the others represent the cell membrane. Only the apical unit is capable of active contraction.

The quasi-static response of each one-dimensional viscoelastic unit is governed by the equation

$$F = k(L - L_0) + \mu \dot{L} \quad (33)$$

where  $F$  is the load applied at the ends,  $L(t)$  is the current length, and  $L_0(t)$  is the zero-stress length of the unit. Activation is included by letting  $L_0$  change with time according to a relation of the form

$$\dot{L}_0 = G(L, L_0) \quad (34)$$

where  $G = 0$  for a passive unit. The key to the behavior of the model lies in the choice for  $G$ . For stretch-activated microfilaments,  $L_0$  must have two stable equilibrium values, one being the passive zero-stress length and the other the active zero-stress length. Odell et al. (1981) chose a relatively simple form for  $G$  that contains this feature and allows specification of the activation stretch threshold. Note that microfilament activation is handled in a manner similar to that discussed in Sec 3.1.1 for volumetric growth, i.e., through a changing zero-stress configuration.

Numerically solving these equations for an epithelial model composed of a circle of truss elements, Odell et al. (1981) studied the processes of amphibian gastrulation, *Drosophila* furrow formation, and amphibian neurulation, which are characterized by similar but geometrically different invagination sequences. The force  $F$  is

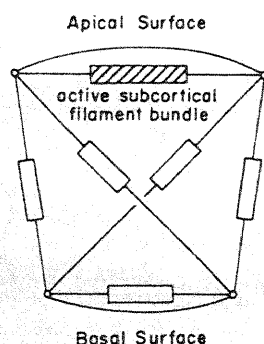


Fig 22. Apical constriction cell model. [From Odell et al. (1981)]

provided by adjacent cells and the cytoplasmic pressure, which is given by a specified function of the cell volume. (Decreasing cell volume squeezes the cytoplasm, increasing the pressure, and vice versa.) Each deformation sequence begins by triggering one cell of a circular ring of cells enclosing a fluid-filled cavity. As the apex of the activated cell shortens, it stretches the apices of the adjacent cells, causing them to fire and so on, generating waves of contraction moving outward from the invaginating cell. The changing cell shapes produce an invagination (Fig 23).

The authors found that experimentally observed morphology could be obtained by adjusting the activation parameters in Eq (34). For example, reproducing the correct geometry during neurulation (Fig 23) requires a low firing threshold. Consequently, most of the cells fire nearly simultaneously, possibly explaining why sections of neural plate continue to roll into tubes after they are isolated from the embryo.

Later, Oster and Alberch (1982) used this model to illustrate epithelial bifurcations during development. For instance, they discussed how Oster et al. (1981) were able to make their gastrulation model buckle outward, rather than inward, by slightly changing the viscoelastic properties of the cells. As Oster and Alberch (1982) pointed out, this behavior may have relevance to skin morphogenesis, since epidermal invagination leads to the formation of hair or skin glands, while evagination leads to the formation of feathers or scales. Thus, consistent with the fossil record, relatively small parameter changes can pro-

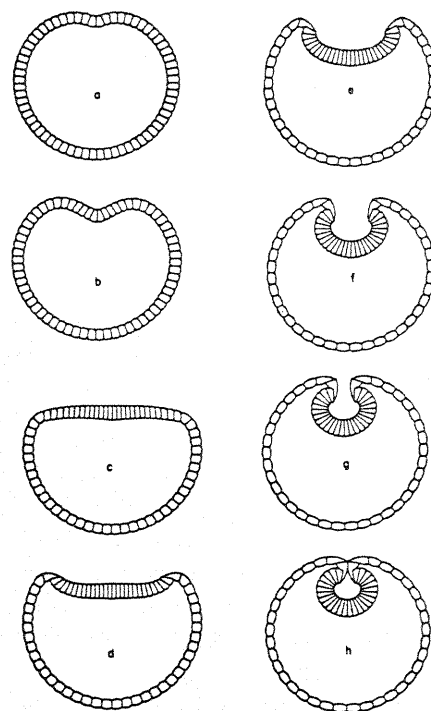


Fig 23. Apical constriction model of amphibian neurulation. [From Odell et al. (1981)]



duce relatively large evolutionary changes (see Sec 2.4).

By extending the model, Oster and Alberch (1982) showed that it also can be used to study pattern formation. For this purpose, they considered a one-dimensional sheet of cells attached to a rigid basal lamina through a bed of springs (Fig 24a). When the cell at the left end is triggered, a wave of contraction spreads across the cells, which begin to undulate, and placodes grow nearly simultaneously over the entire sheet. Eventually, the placodes stabilize at an almost periodic spacing (Fig 24b), giving a pattern. Changing the model properties alters the spacing, and a flexible lamina likely would allow invagination or evagination.

Finally, we note that Clausi and Brodland (1993) used apical constriction as the primary driving force in their finite-element model for neurulation. Assuming that the microfilament force increases with contraction, they obtained quite realistic results.

### 5.5 Cortical tractor model

The primary hypothesis behind the "cortical tractor model" of Jacobson et al. (1986) is that the motile behavior of epithelial cells is similar to that of mesenchymal cells. This model, which is related to the cell-crawling model of Oster (1984), is based on the following assumptions:

1. Cytoplasm flows continuously in a cell from the basal and lateral surfaces to the apex and then back toward the base through the core (Fig 25a). This fountainoid flow pattern is the "cortical tractor."
2. Adhesion molecules enter the flow at the basal end and move with the flow along the fluid-like cell membrane toward the apical end, where they are resorbed unless stabilized by bonding to other cells.
3. The resorption rate for adhesion molecules is slower than their insertion rate into the flow. Adhesion molecules, therefore, accumulate at the apex, keeping the cells bound together at the apical surface (Fig 25a).

The authors argued qualitatively that the cortical tractor model can reproduce placode formation, invagination, folding of the neural tube, and cell rearrangements without breaking the apical seals. The first two processes are driven by differential flow rates between cells. If the flow rates of all cells are equal, they all remain in the plane of the sheet (Fig 25a). However, if the tracting of one cell increases, shear stress against the adjacent cells drives the fast cell basalward. Moreover, if the shear force is large enough to break the apical seals, the cell becomes a mesenchymal cell. Otherwise, the constraint causes the cell to elongate, forming a placode, and the sheet to bend.

According to this model, the key to cell rearrangement lies below the apical surface (Fig 25b). A basal protrusion initiates the process, moving across a junction to a separated cell. The flow then increases the extent of

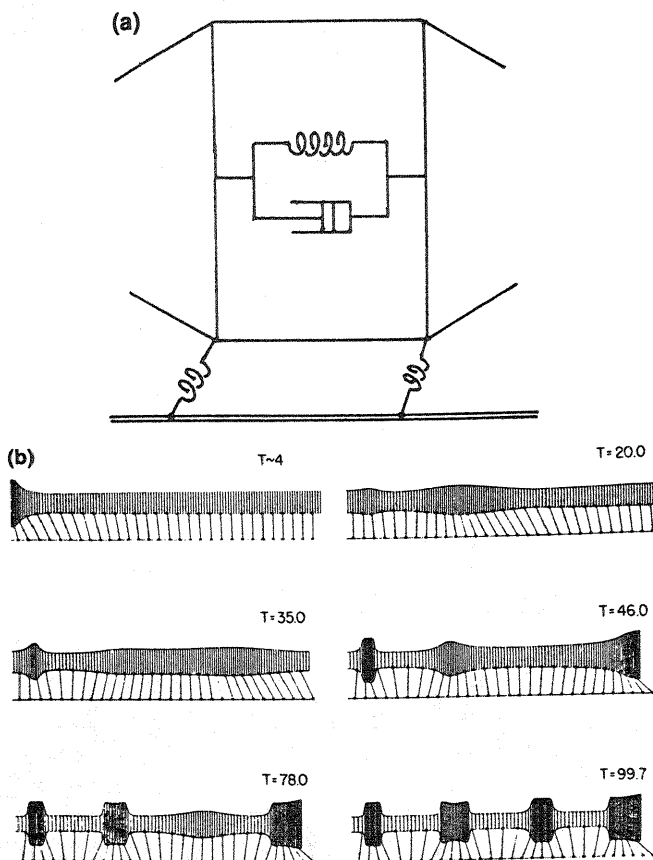


Fig 24. (a) Model of epithelium on substrate. (b) Pattern development given by model. [From Oster and Alberch (1982)]

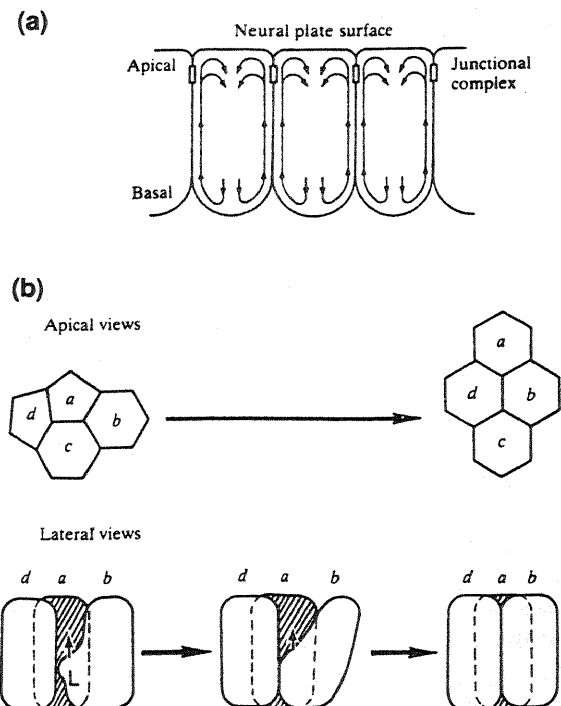


Fig 25. Cortical tractor model. (a) Intracellular flow pattern. (b) Cellular rearrangement mechanism. [From Jacobson et al. (1986) with permission, Company of Biologists Ltd.]

the protrusion, which moves toward the apex along with adhesion molecules. When the protrusion reaches the apex, the cell adheres to its new neighbor, and so rearrangement occurs without breaking the apical seal.

Based on these ideas, Jacobson et al. (1986) modeled an epithelial cell as a quadrilateral filled with a viscous fluid. Their pseudomechanical analysis includes the effects of passive elastic deformation of the cells and active shear due to differences in flow velocity between adjacent cells. In simulating various aspects of amphibian neurulation, the authors found that the model could effectively reproduce many of the observations of Jacobson and Gordon (1976), including elongation of the neural plate and the rolling of cells into the neural tube.

### 5.6 Shell models

Macroscopically, it often is convenient to treat an epithelium as a plate or shell, i.e., as a continuum. Hardin and Cheng (1986), for example, used axisymmetric shell theory and experiments to study sea urchin gastrulation. Their analysis includes the effects of large deformation, but the shell material was taken as linear and isotropic. Gastrulation was simulated by applying forces through the archenteron to opposite sides of a spherical shell representing the blastula (Fig 26).

If the material properties of the entire structure are uniform, the model predicts a flattening of the blastula roof that is inconsistent with their experimental observations. To match the experimental results, the authors found that they had to stiffen the roof or soften the archenteron. Then, however, the blastopore did not close (Fig 26). Thus, they concluded that the characteristic filipodia at the tip of the archenteron merely guide this structure across the embryo, rather than actively pulling it across. On the other hand, this model does not include the internal fluid in the blastula. During deformation, the pressure build-up in this fluid may help close the blastopore.

Another conclusion of the study of Hardin and Cheng (1986) was that cell rearrangement occurs during gastrulation. Within the context of a continuum model, epithelial cell rearrangement can be treated as a fluid-like flow of material. Here, it is relevant that, by applying loads to embryonic cell aggregates, Phillips and Davis (1978) found that the cells behave elastically for short times and as viscous fluids for long times, i.e., they are viscoelastic.

With this in mind, Mitterthal (1987) developed a fluid-elastic thin-shell theory for application to epithelial morphogenesis. The theory is based on the assumption that the shell resists bending and isotropic in-plane stresses elastically, but it cannot support static shear stresses. The kinematic and equilibrium equations are those given by classical large-deformation shell theory. The author derived the constitutive relations from the principle of virtual work with the work due to bending, stretching, and adhesion included.

For axisymmetric deformation of a shell of revolution,

this procedure yields the bending moment resultants

$$\begin{aligned} M_s &= D(\kappa_s + \nu\kappa_\theta) + \frac{1}{2}h(\xi_a - \xi_b) \\ M_\theta &= D(\kappa_\theta + \nu\kappa_s) + \frac{1}{2}h(\xi_a - \xi_b) \end{aligned} \quad (35)$$

and the normal stress resultants

$$\begin{aligned} N_s &= -K + N + \xi_a + \xi_b + T_s \\ N_\theta &= K + N + \xi_a + \xi_b + T_\theta \end{aligned} \quad (36)$$

where  $s$  and  $\theta$  denote the meridional and circumferential directions, respectively. In these equations,  $D$  is the bending rigidity,  $h$  is the deformed shell thickness,  $\nu$  is Poisson's ratio,  $\xi_a$  and  $\xi_b$  are interfacial tensions at the apical and basal surfaces, respectively, and the  $T_i$  are interfacial tensions within the epithelium. In addition, the author stated that, since the shell is fluid-like, the  $\kappa_i$  are curvatures in the deformed configuration. We note, however, that if the shell behaves elastically in bending, these should be curvature *changes*. Moreover, the quantity  $K$  is a bending-stretching coupling term given by

$$K = \frac{1}{2}(\kappa_s^2 - \kappa_\theta^2), \quad (37)$$

and

$$N = -C\lambda_n^2(\lambda_n - 1) \quad (38)$$

is the elastic isotropic in-plane stress resultant in terms of the transverse normal stretch ratio  $\lambda_n$  and a material constant  $C$ . The coupling term  $K$  arises because stretching a shell also can induce curvature change. While this theory should prove useful in theoretical studies of morphogenesis, it apparently has not yet been applied to specific problems.

Mitterthal and Mazo (1983) presented an earlier version of the preceding model that focuses on adhesion-driven epithelial morphogenesis. In this study, the shape of the shell was determined by minimizing the energy due

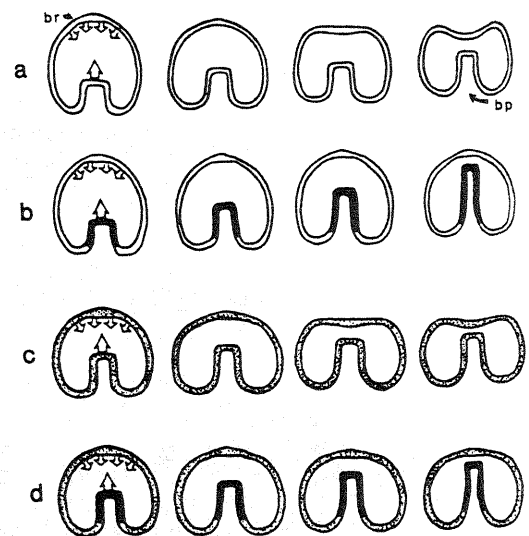


Fig 26. Shell model for gastrulation. [From Hardin and Cheng (1986)]

to bending and adhesive disparities between the component cells. Like cells were assumed to adhere preferentially to each other (less disparity), and both stretching and shear stresses were neglected. For the special case of a cylinder, the authors derived a formula for the equilibrium configuration that predicts the observed geometry of leg segments in *Drosophila*.

A limited number of other shell and membrane epithelial models have been published. A similar shell model, based on adhesive potentials, was presented by Gierer (1977). Also, Zinemanas and Nir (1992) modeled a blastula as a viscous drop of liquid surrounded by a fluid membrane and embedded in an ambient fluid. They controlled the distribution of surface tension in the membrane to simulate exogastrulation.

## 6 MUSCULOSKELETAL SYSTEM

In studies of functional adaptation, the musculoskeletal system has received the most attention. The increase in muscle mass due to elevated loads apparently has been known for millennia, and the relation between loading and bone size has been recognized for centuries (Ascenzi, 1993). Furthermore, more than 100 years ago, Culmann and von Meyer noted a qualitative likeness between the trabecular architecture in the femur and principal stress trajectories in a similarly shaped crane (Fig 27) [see, e.g., Koch (1917), Roesler (1981), Cowin (1986), Fung (1990)]. This observation led around 1870 to Wolff's law, or the **trajectorial hypothesis**, for internal bone remodeling (Wolff, 1986). According to Wolff's law, as discussed in Sec 2.2, the trabeculae of cancellous bone (see below) align with the directions of principal stress (Fig 27), and when the loading environment changes, the trabeculae reorient along the new stress trajectories. The origination of Wolff's law has a somewhat muddled history; for details, see Koch (1917) and Roesler (1981).

Using a stress analysis of the femur based on detailed morphological measurements, Koch (1917) confirmed Wolff's law. He also discussed the possibility of bones being optimized structures, designed for maximum strength with minimum material. The idea of structural optimization has received renewed interest lately (Huiskes and Hollister, 1993; Harrigan and Hamilton, 1994).

Since most engineering studies of growth and remodeling have dealt with bone, the majority of this section focuses on this topic. [See Cowin (1993) and Huiskes and Hollister (1993) for excellent reviews of the current state of the art.] Bone and muscle adaptations, however, are intimately related, since they exert forces on each other. Thus, the behavior of skeletal muscle also is discussed, although relatively briefly.

## 6.1 Bone

### 6.1.1 Structure and function

The skeletal system functions as a support structure against gravity, as a lever system for muscles, and as a protective covering for internal organs (Bouvier, 1989). As a composite material containing both solid and fluid phases, bone accomplishes these tasks while also serving metabolic functions. The solid component is composed of bone cells embedded in an extracellular matrix that includes collagen for elasticity and hydroxyapatite crystals for strength. The fluid component contains blood and extracellular fluid.

Macroscopically, there are two types of bone: compact, or cortical, bone and cancellous, or trabecular, bone. **Compact bone** is a dense material that makes up primarily the shaft, or **diaphysis**, of a long bone (Fig 28a). The inner and outer surfaces of the shaft are called the **endosteum** and the **periosteum**, respectively. **Cancellous bone** is a porous material that makes up the end, or **epiphysis**, of a long bone and is surrounded by a thin shell of compact bone (Fig 28a). Since the trabeculae give cancellous bone a sponge-like appearance, this type of bone also is called "spongy bone."

Microscopically, there are three types of compact bone: woven, lamellar, and haversian (Cowin, 1983). **Woven bone** is a relatively unorganized precursor to lamellar bone in young animals. In the shaft of a mature long bone, **lamellar bone** is made up of a system of concentric laminae separated by vascular networks (Fig 28b). Each lamina, in turn, contains alternating zones of poorly organized and highly organized bone. Some of the lamellar bone eventually converts to **haversian bone**, which consists of cylindrical elements called **osteons**, or haver-

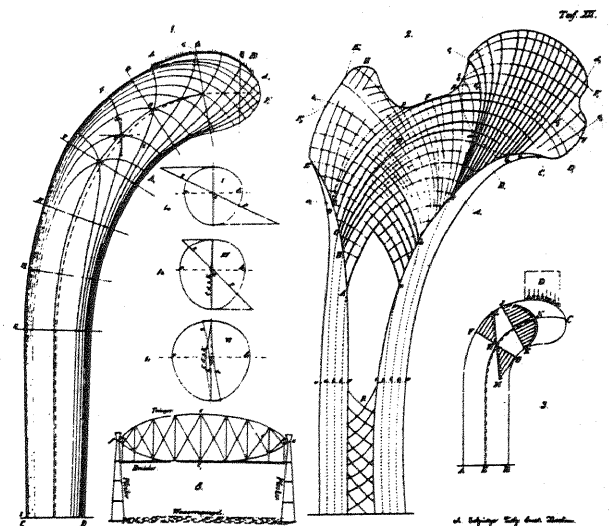


Fig 27. Principal stress trajectories in Culmann's crane and proximal femur as sketched by Wolff J (1870), *Über die innere Architektur der Knochen und ihre Bedeutung für die Frage vom Knochenwachstum, Archiv für pathologische Anatomie und Physiologie und für klinische Medizin, Virchow's Archiv* 50, 389–453.

sian systems (Fig 28b).

One level further down, the osteons have their own substructure. Each osteon is composed of concentric layers, or **lamellae**, surrounding the **haversian canal**, which contains one or more blood vessels. The osteons usually are oriented along the long axis of the bone and are

joined by **cement lines**. The spaces between all of these units are filled with extracellular fluid. For more detail on bone structure, the interested reader is referred to the book by Currey (1984).

Bone contains primarily three types of cells: (1) **osteoblasts**, which create (deposit) bone; (2) **osteoclasts**, which destroy (resorb) bone; and (3) **osteocytes**, which are converted osteoblasts that become trapped in the bone matrix and then serve maintenance functions. Growth and remodeling of bone do not involve cell division. Rather, osteoclasts first resorb old bone, often by tunneling, and then osteoblasts fill in the tunnels with new bone. The newly deposited bone initially has a relatively low modulus, with mineralization and hardening occurring gradually (Frost, 1964; Hart and Davy, 1989). In this way, deposition occurs without introducing residual stress. Bone resorption and deposition are ongoing processes that may be regulated by osteocytes (Cowin et al., 1991). At growth or remodeling equilibrium, osteoclastic and osteoblastic activities balance each other.

Several mechanisms have been proposed for the transduction of mechanical loads to the remodeling response (Treharne, 1981), including: (1) piezoelectric or streaming potentials; (2) mechanical fatigue microdamage; (3) extracellular fluid pressure effects on bone cells; (4) direct loads on cell membranes; and (5) alterations in mineral solubility due to stress. Recently, Weinbaum et al. (1994) used a poroelastic analysis to examine the additional possibility that internal fluid shear stress on osteocytes is the remodeling stimulus. Treharne (1981) favors the fatigue microdamage hypothesis, but experimental data can be found to support each, and there is no consensus. One objective of theoretical modeling is to deduce the actual transduction mechanism.

Biomechanical models have examined stress, strain, and strain-energy density as possible stimuli for bone growth, remodeling, and morphogenesis. Cowin (1984) argued that strain is the most likely candidate, since it can be measured by stretch-activated receptors, whereas stress cannot. On the other hand, as pointed out in Sec 3.1.1, strain depends on the choice of a reference configuration, which may not be well-defined, especially in soft tissues that undergo large deformations. Even in this case, however, a reference state of strain may be some time-averaged configuration that the tissue is "used to." Carter et al. (1987a) favor strain energy or an effective cyclic stress. They hypothesize that the heat energy generated during cyclic loading may trigger chemical reactions. Moreover, they showed for small strains that stress, strain, and strain-energy criteria all have similar mathematical forms. Finally, using a combined theoretical and experimental approach, Brown et al. (1990) examined the effects on bone remodeling of 24 different mechanical parameters. For the turkey ulna, although their results are not conclusive, they found that strain-energy density, longitudinal shear stress, and the largest tensile principal stress/strain are the most likely possibilities.

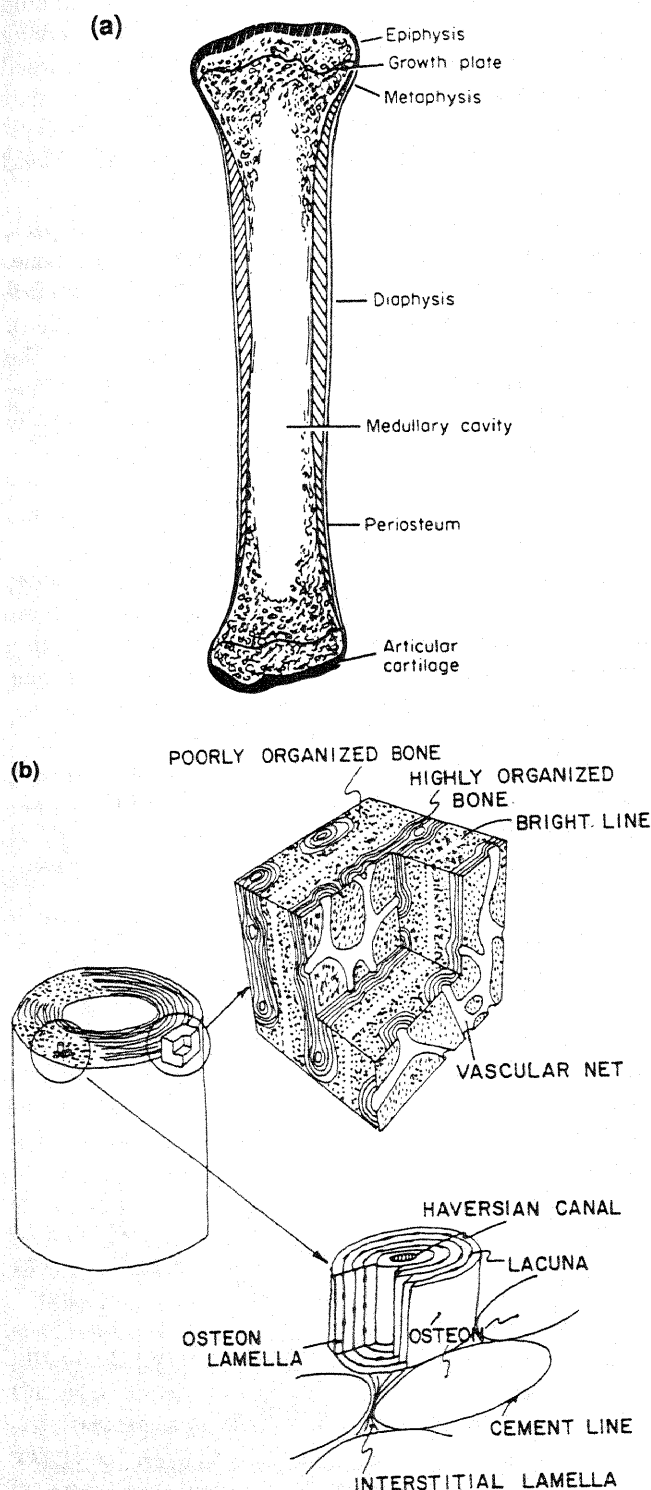


Fig 28. (a) Anatomy of a long bone. [From Rhinelander (1972)] (b) Microstructural organization of compact bone. [From Cowin (1983), reprinted by permission of Blackwell Science, Inc.]

### 6.1.2 Experimental and physical considerations

Experimental measurements and observations must be considered in developing models for bone adaptation. The most instructive experiments are those that carefully perturb loading conditions and measure the patterns of growth, remodeling, or morphogenesis. Methods to decrease loading in bones include internal fixation devices, immobilization, and weightlessness. Techniques to increase stress include exercise and implanted loading devices. The most popular experimental subjects have been femurs and ulnas of dogs and turkeys.

Detailed reviews of specific experiments were given by Carter (1982), Lanyon (1984; 1987), and Meade (1989), while Currey (1968; 1984) and Pauwels (1980) discussed mechanical design principles for bone. Among the more significant factors that should be considered when developing models are the following:

1. Different bones have different functions and are subjected to different loads. Thus, they likely respond differently to the same stress (Meade, 1989).
2. Load-bearing bones likely adapt to minimize bending because (1) bending stresses are higher for a given load than are axial stresses and (2) bending induces tension (Currey, 1968). (Bones are weaker in tension than in compression.)
3. Increased bone mass generally lowers stress but increases the weight that must be borne by the animal. An optimized skeletal system, therefore, must seek a compromise between stress and weight (Currey, 1968).
4. Bone is in remodeling equilibrium over a range of compressive strain levels (Lanyon, 1987; Carter, 1984). Outside this range, decreased compressive stress induces loss of bone mass, and increased compressive stress causes increased mass. For a given change in load magnitude, the rate of atrophy is greater than the rate of hypertrophy. Changes in material properties are secondary (Woo, 1981).
5. Intermittent loads are a more effective remodeling stimulus than are static loads (Chamay and Tschantz, 1972; O'Connor et al., 1982; Lanyon and Rubin, 1984).
6. Cancellous bone trabeculae align along the directions of principal stress, i.e., Wolff's law (Hayes and Snyder, 1981).
7. Trabecular bone density increases in regions of high shear (Hayes and Snyder, 1981) and as the loading rate increases (Goldstein et al., 1991).
8. Bone remodeling can occur if the strain distribution is abnormal, even if the strain magnitudes are normal (Lanyon et al., 1982).

9. Internal microcracks are associated with regions of bone resorption, the first step in the remodeling process (Burr et al., 1985).

### 6.1.3 Growth

All bone growth can be classified as surface growth. Even internal growth is due to deposition on surfaces, such as the surfaces of trabeculae or the walls of canals excavated by osteoclasts. For a couple of reasons, bone growth has received somewhat less attention than bone remodeling, which is described in the next section. First, as Wolff (1986) stated, modification of the external form of a bone often is secondary to internal remodeling. Second, moving boundary-value problems often are more difficult to solve than those with fixed boundaries. In the following, we discuss deposition and resorption of bone at external surfaces.

For decades, investigators have wrestled with defining the biomechanical determinants of bone shape. Frost (1964) proposed a relatively simple conceptual model to explain the response of long bones subjected to bending loads. According to this theory, deposition occurs on surfaces that become more concave under loading, and resorption occurs on surfaces that become more convex. In general, this model predicts physiologically reasonable results unless the bone is loaded in tension. To handle this situation, Currey (1968) modified the theory, with deposition or resorption depending on whether the stress becomes more or less compressive with depth below the surface. Later, Frost (1988) extended these ideas and proposed a semi-quantitative scheme based on the nature of the loading and the local strains. While there is no direct evidence to refute these latter models, their relatively complex recipes make them not very attractive possibilities.

One of the first quantitative models for bone growth is based on piezoelectricity, i.e., electric current produced by mechanical stresses. Experiments have shown that negative charges can induce bone deposition, but positive charges have little effect (Bassett, 1965). Based on these findings, Gjelsvik (1973a; 1973b) proposed a theory in which the surface growth rate depends on a polarization vector, which is determined by the state of stress. There are, however, two problems with this theory. First, it predicts that surface growth depends only on shear stress (in global bone coordinates) rather than normal stress, which is not consistent with experimental findings. Second, recent experiments have indicated that streaming potentials dominate piezoelectric effects (Gross and Williams, 1982). Thus, Demiray (1983), Guzeisu and Saha (1984), and Salzstein et al. (1987) proposed electromechanical models based on mixture theory, with bone considered as a fluid-solid composite.

Most models for surface growth have assumed the existence of one or more growth-equilibrium states of stress or strain. For example, Kummer (1972) postulated a general remodeling law that is expressed essentially by the








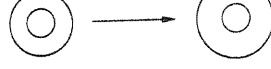

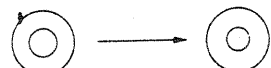
Solution type	Surface movement	Area change	
1	$a_\infty > a_0$	—	
	$b_\infty < b_0$	—	
2	$a_\infty > a_0$	+	
	$b_\infty > b_0$	—	
3	$a_\infty < a_0$	+	
	$b_\infty > b_0$	+	
3 <sup>0</sup>	$a_\infty = 0$	+	
	$b_\infty > b_0$	+	
4	$a_\infty < a_0$	+	
	$b_\infty < b_0$	—	
4 <sup>0</sup>	$a_\infty = 0$	+	
	$b_\infty < b_0$	—	
5	$a_\infty = a_0$	+	
	$b_\infty > b_0$	+	
6	$a_\infty = a_0$	—	
	$b_\infty < b_0$	—	
7	$a_\infty < a_0$	+	
	$b_\infty = b_0$	+	
8	$a_\infty > a_0$	—	
	$b_\infty = b_0$	—	

Fig 29. Types of solution for axial compression of long bones. [Reprinted from Cowin SC and Firoozbakhsh K (1981), Bone remodeling of diaphysal surfaces under constant load: theoretical predictions, *J Biomech* 14, 471–484, copyright 1981, with kind permission from Elsevier Science Ltd, The Boulevard, Langford Lane, Kidlington OX5 1GB, UK.]

part of the curve to the right of point *c* in Fig 2. Near normal equilibrium (point *a*), Cowin and van Buskirk (1979) proposed a linear strain-dependent growth law of the form

$$v(\mathbf{n}, \mathbf{x}_0, t) = C_{ij}(\mathbf{n}, \mathbf{x}_0)[\epsilon_{ij}(\mathbf{x}_0, t) - \epsilon_{ij}^0(\mathbf{x}_0)] \quad (39)$$

where *v* is the surface velocity in the direction of the surface normal *n* at position *x*<sub>0</sub>, the *C*<sub>*ij*</sub> are growth-rate coefficients, the *ε*<sub>*ij*</sub> are Cartesian strain components, and the *ε*<sub>*ij*</sub><sup>0</sup> are growth-equilibrium strains. According to this relation, surface growth depends on the local strain field at the surface, with *v* > 0 for deposition and *v* < 0 for resorption. Tanaka and Adachi (1994) proposed a similar growth law, based on an equestress hypothesis, in which *v* is proportional to the Laplacian of the stress.

Using linear elasticity theory with the evolving positions of the boundaries determined by Eq (39), Cowin and van Buskirk (1979) examined two problems: (1) a bone shaft loaded by a compressive axial force and (2) a bone shaft with an axial load and a force-fitted prosthetic pin. The bone was modeled as a transversely isotropic hollow cylinder, and the pin was taken as an isotropic

solid cylinder. In this theory, applied loads are assumed to be some time average of the actual intermittent loads. The analysis yielded two coupled nonlinear differential equations for the inner and outer bone radii as functions of time.

For small surface displacements, Cowin and van Buskirk (1979) found analytical solutions to these equations. The analysis of the first problem showed that, for a stable solution, both the endosteal and periosteal surfaces must move outward. The solution to the second problem indicated that the endosteal surface moves outward with time, loosening the pin, a result consistent with clinical experience.

As pointed out by Cowin and Firoozbakhsh (1981), experimental investigations have found great variability in the directions of motion of the surfaces of long bones subjected to axial compression. Since these results are inconsistent with the predictions of the linearized solution, Cowin and Firoozbakhsh (1981) examined in detail the behavior of the nonlinear equations. Using a phase-plane technique, they found ten types of solution, eight of which are stable. The stable solutions show that, depend-



ing on the values of three parameters—the periosteal and endosteal growth-rate coefficients and the axial stress—many different growth patterns are possible (Fig 29).

To determine values for the growth-rate coefficients, Cowin et al. (1985) used a modified beam theory to simulate a set of five published animal experiments. In the experiments, the effects of altered compressive and bending loads were studied in long bones of mature and immature animals subjected to immobilization, exercise, and surgical intervention. Using actual cross-sectional geometry and adjusting the growth-rate coefficients of Eq (39), the authors were able to make the computed changes in shape match those found experimentally (Fig 30). To do this, however, they needed to assign different values to the coefficients at the endosteal and periosteal surfaces.

In a subsequent study, Cowin (1987) extended and modified Eq (39) in two ways. First, he made the shear

terms quadratic so growth would not depend on the direction of shear. Second, a finite range of growth-equilibrium strain was incorporated. Let  $\epsilon_{ij}^+$  and  $\epsilon_{ij}^-$  represent the upper and lower bounds of the equilibrium strains such that  $v = 0$  if  $\epsilon_{ij}^- < \epsilon_{ij} < \epsilon_{ij}^+$  for all  $i, j$ , i.e., if the strains fall within a **dead zone** (Beaupre et al., 1990a). (Note that the bone is not actually dead.) Cowin (1987) modified Eq (39) to read

$$v = C_{11}^{\pm}(\epsilon_{11} - \epsilon_{11}^{\pm}) + \cdots + C_{12}^{\pm}(\epsilon_{12} - \epsilon_{12}^{\pm})^2 + \cdots \quad (40)$$

where  $\epsilon_{ij} - \epsilon_{ij}^{\pm}$  denotes the amount that  $\epsilon_{ij}$  exceeds an upper or a lower bound. Using this equation, he analyzed growth of a thin-walled tube due to torsion. For twisting greater than the growth-equilibrium limit, the analysis predicts that the midwall radius increases and the wall thins.

The surface growth theory of Cowin and van Buskirk (1979) has formed the basis of several computational models. For instance, Hart et al. (1984a) developed a three-dimensional finite-element model that accounts for surface growth through Eq (39). In addition, their code includes internal remodeling, with the rate of change in solid volume fraction  $e$  governed by

$$\dot{e} = a_0 + a_1 e + a_2 e^2 + (A_{ij}^0 + A_{ij}^1 e) \epsilon_{ij} \quad (41)$$

where  $a_0$ ,  $a_1$ ,  $a_2$ ,  $A_{ij}^0$ , and  $A_{ij}^1$  are constants. This latter relation was developed by Hegedus and Cowin (1976) and will be discussed in detail in the next section [see Eq (47)]. With  $e$  computed at a given time step, the local apparent bone density was given by

$$\rho = \gamma(e_0 + e) \quad (42)$$

with  $\gamma$  being the true solid density and  $e_0$  a reference solid volume fraction. Then, the elastic moduli for orthotropic bone were updated according to

$$E_i = c_i \rho^3 \quad (43)$$

in which the  $c_i$  were determined from experimental data.

With this model, Hart et al. (1984a) studied cylinders with axial and bending loads. Later, Hart (1990) used a similar finite-element model to study how the maturation of newly deposited bone affects the response of an axially compressed cylinder. Rather than computing the apparent density according to Eq (42), they specified a particular "maturation rule" for  $\rho(t)$ . The results showed that the temporal evolution of the strains, but not the final geometry, depends on the form of  $\rho(t)$ . For a summary of various studies based on this finite-element model, see Hart (1989).

Models for bone growth and remodeling are useful tools for designing prostheses. One difficulty with bone implants is that they alter the normal stress field, with the remodeling response often having detrimental effects. This behavior is due partly to the implant carrying part of the load normally carried by the bone, a phenomenon

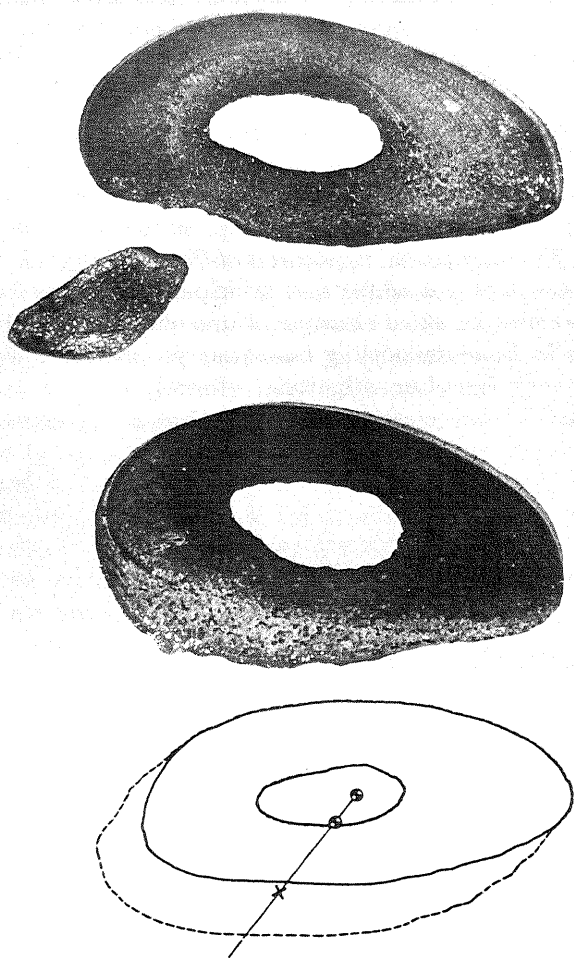


Fig 30. Cross sections of sheep forelimb from chronic experiments with ulna intact (top) and with section of ulna removed (center) to induce abnormal bending stresses. The bottom panel shows control bone surfaces (solid lines) and the theoretical growth prediction (dashed lines). [Reprinted from Cowin SC, Hart RT, Balser JR, and Kohn DH (1985), Functional adaptation in long bones: establishing in vivo values for surface remodeling rate coefficients, *J Biomech* 18, 665–684, copyright 1985, with kind permission from Elsevier Science Ltd, The Boulevard, Langford Lane, Kidlington OX5 1GB, UK.]

called **stress-shielding**. Huiskes et al. (1987) reexamined the prosthetic pin problem with a two-dimensional finite-element model. Rather than strain as the growth stimulus, they used the strain-energy density  $U$ . The surface-growth law included a dead zone and was taken as

$$v = \begin{cases} C[U - (1+s)U_n] & \text{for } U > (1+s)U_n \\ 0 & \text{for } (1-s)U_n \leq U \leq (1+s)U_n \\ C[U - (1-s)U_n] & \text{for } U < (1-s)U_n \end{cases} \quad (44)$$

where  $U_n$  is the nominal growth-equilibrium value of  $U$ ,  $s$  defines the growth threshold, and  $C$  is a constant (Fig 31a). A similar expression was used for an internal remodeling law for  $e$ . Their model consisted of an elastic pin surrounded by a layer of cement inside a cylinder of bone (Fig 31b). For an applied bending moment, the model showed that resorption occurs in the proximal region, with a magnitude depending on the value of  $s$  and the implant diameter (Fig 31b).

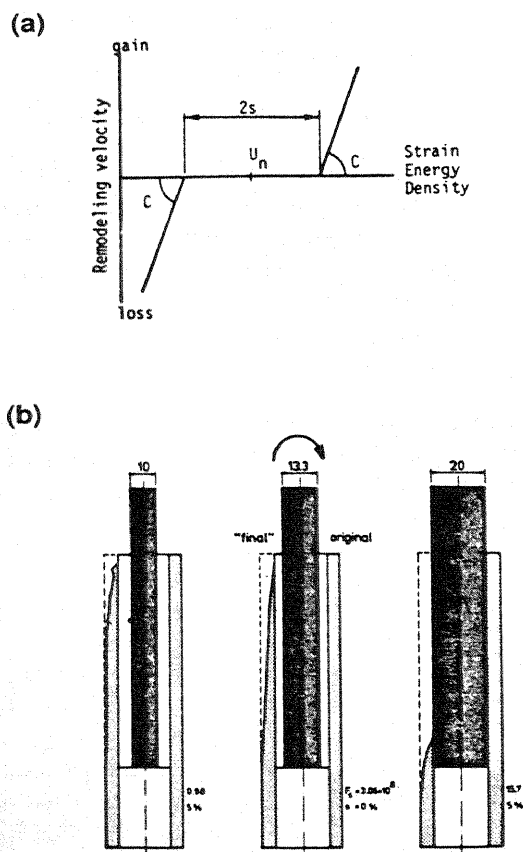


Fig 31. (a) Trilinear adaptive growth rate as a function of the strain-energy density. (b) Predicted remodeling of bone diaphysis due to bending load on prosthetic pin. [Reprinted from Huiskes R, Weinans H, Grootenboer HJ, Dalstra M, Fudala B, and Slooff TJ (1987), Adaptive bone-remodeling theory applied to prosthetic-design analysis, *J Biomech* 20, 1135-1150, copyright 1987, with kind permission from Elsevier Science Ltd, The Boulevard, Langford Lane, Kidlington OX5 1GB, UK.]

Modern implants often are designed with porous surfaces so that bone can grow into the pores, forming a cohesive interface. With this in mind, Sadegh et al. (1993) used a boundary element formulation of the theory based on Eq (39) to study three problems: (1) ingrowth between screw threads of an implant; (2) ingrowth into slots; and (3) remodeling of trabeculae at a bone-implant interface. The results indicate that compression is necessary for ingrowth, and Fig 32 illustrates the trabecular model and the predicted realignment.

All of the models discussed so far are phenomenological, being based on forms of the theory proposed by Cowin and coworkers. An alternative approach, based on the opposing activities of osteoblasts and osteoclasts, was developed by Hart and colleagues (Hart et al., 1984b; Hart and Davy, 1989). This model makes no formal distinction between surface growth and the remodeling of trabeculae, which change in form by growth on internal surfaces. For more details, the reader is referred to the review by Hart and Davy (1989).

#### 6.1.4 Remodeling

Internal bone remodeling involves changes in trabecular architecture, apparent density, or material properties. The trajectorial hypothesis of Wolff (1986), i.e., the alignment of trabeculae and principal stress directions, is the most heralded example of this phenomenon. Theories for bone remodeling have been proposed primarily by two groups of investigators.

Cowin and coworkers have developed a continuum

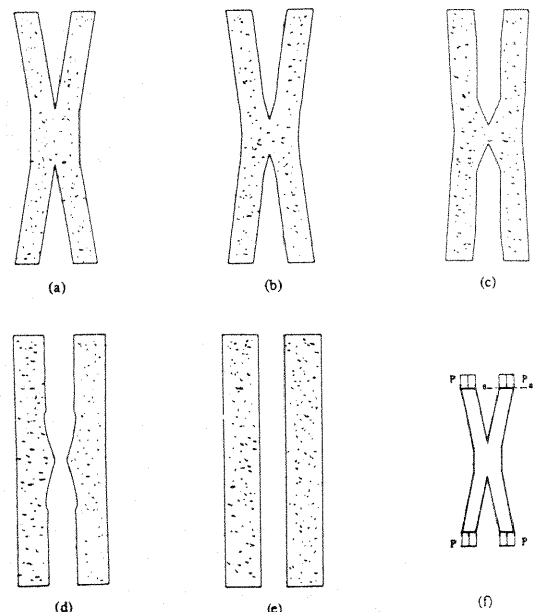


Fig 32. Predicted remodeling of trabecular model at bone/implant interface. [Reprinted from Sadegh AM, Luo GM, and Cowin SC (1993), Bone ingrowth: an application of the boundary element method to bone remodeling at the implant interface, *J Biomech* 26, 167-182, copyright 1993, with kind permission from Elsevier Science Ltd, The Boulevard, Langford Lane, Kidlington OX5 1GB, UK.]

mechanics-based formulation, which they call **adaptive elasticity theory**. The surface-growth theory described in Sec 6.1.3 is a variation of adaptive elasticity, which uses some average strain measure as the remodeling stimulus. Cowin (1986; 1990; 1992) also explored the use of a fabric tensor to describe changes in trabecular orientation. This method was discussed in Sec 3.2 within the context of a general theory for fibrous tissues and will not be considered further here.

The other approach, which we call **bone maintenance theory**, was developed by Carter and colleagues. This theory uses an average measure of the entire stress history for the remodeling stimulus. Variations of bone maintenance theory have been used to study bone development, adaptation, and fracture healing.

In the following, we discuss these theories and their applications. Both Cowin and Carter have published reviews of their work (Cowin, 1981, 1983, 1990; Carter, 1987; Carter et al., 1991), where more details can be found.

**Adaptive elasticity theory.** The theory of adaptive elasticity, presented by Cowin and Hegedus (1976), was the first mathematically rigorous theory for adaptive growth and remodeling. In the view of these investigators, bone is a poroelastic (biphasic) material consisting of solid and fluid phases. The solid phase comprises bone cells and extracellular matrix, and the fluid phase is extracellular fluid. In response to alterations in loading conditions, the porosity (and apparent density) of the bone changes due to chemical reactions that exchange mass between the two phases. These reactions are slow compared to the loading rate and are controlled by the local strain. Using formal arguments of continuum mechanics, Cowin and Hegedus (1976) developed a set of governing equations for their theory. Of particular interest here are the isothermal constitutive equations

$$\Psi = \Psi(\phi, \mathbf{F}), \quad \dot{\rho} = \dot{\rho}(\phi, \mathbf{F}) \quad (45)$$

where  $\Psi$  is the specific free energy,  $\rho$  is the apparent density (solid mass per unit bulk volume),  $\phi$  is the solid volume fraction, and  $\mathbf{F}$  is the deformation gradient tensor.

Hegedus and Cowin (1976) presented a linearized version of adaptive elasticity theory. They introduced the change in solid volume fraction  $e = \phi - \phi_0$  from a reference value  $\phi_0$ , and for small strain, Eqs (45) yield (in Cartesian coordinates)

$$\begin{aligned} \sigma_{ij} &= (\phi_0 + e)C_{ijkl}(e)\epsilon_{kl} \\ \dot{e} &= a(e) + A_{ij}(e)\epsilon_{ij} \end{aligned} \quad (46)$$

where the  $C_{ijkl}$  are elastic coefficients for an anisotropic material, and  $a$  and  $A_{ij}$  are remodeling rate coefficients. To this level of approximation, the authors pointed out that, for orthotropic bone,  $A_{ij} = 0$  if  $i \neq j$ , and so shear due to axial torsion induces no remodeling. As discussed

in Sec 6.1.3, however, this is not true if the shear term is quadratic so that the direction of twist is immaterial (see Eq (40)).

If  $e$  also is small, Eqs (46) can be written in the form (Hegedus and Cowin, 1976)

$$\begin{aligned} \sigma_{ij} &= (\phi_0 C_{ijkl}^0 + e C_{ijkl}^1)\epsilon_{kl} \\ \dot{e} &= a_0 + a_1 e + a_2 e^2 + (A_{ij}^0 + A_{ij}^1 e)\epsilon_{ij} \end{aligned} \quad (47)$$

where  $C_{ijkl}^{0,1}$ ,  $A_{ij}^{0,1}$ ,  $a_0$ ,  $a_1$ , and  $a_2$  are constants. Note that, if  $\phi_0 = 1$  and  $e = 0$ , Eq (47)<sub>1</sub> reduces to Hooke's law. Moreover, although the  $\epsilon_{ij}$  and  $e$  are small, this theory is inherently nonlinear, and so bifurcations are possible. Firoozbakhsh and Cowin (1981) showed that a third-order approximation to Eq (46) is essentially equivalent to the relation proposed by Kummer (1972), i.e., a variation of Eq (8).

Equations (47) or related expressions have formed the basis for many subsequent models of bone remodeling. For instance, Cowin and van Buskirk (1978) used Eqs (47) to examine remodeling in the prosthetic pin problem, i.e., a solid cylinder forced into a hollow cylinder. A stability analysis showed that the pin can induce a local reduction in bone stiffness or a pathological increase or decrease in porosity.

In another study, Firoozbakhsh and Cowin (1980) investigated the remodeling behavior of an initially inhomogeneous, orthotropic cylinder subjected to a constant axial compressive load. At  $t = 0$ , a sinusoidal longitudinal variation in  $e$  and, therefore,  $C_{ijkl}(e)$  was specified. The temporal evolution of  $e$  along the bone (Fig 33) shows that the bone approaches a homogeneous structure as  $t \rightarrow \infty$ . The physical explanation for this behavior is the following: In regions of less dense bone, the moduli are smaller and the strain greater for a given load. The larger strains induce a larger remodeling rate  $\dot{e}$ , stiffen-

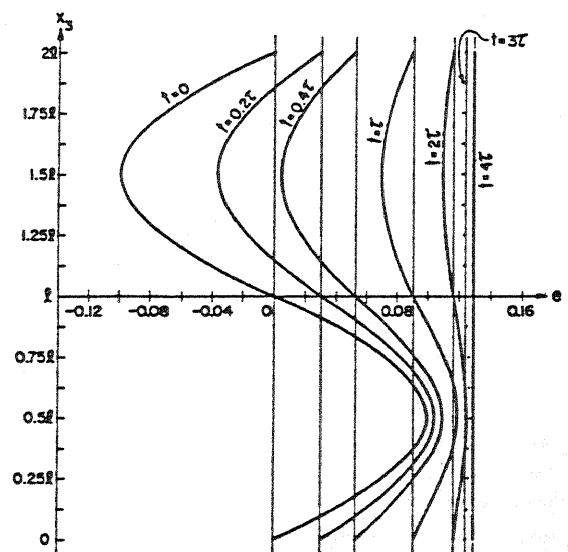


Fig 33. Predicted evolution of solid volume fraction in an initially inhomogeneous bone shaft under constant compression. [From Firoozbakhsh and Cowin (1980)]

ing the bone in these regions. This stiffening then lowers the strains and, therefore,  $\dot{\epsilon}$ . The opposite behavior occurs in regions of more dense bone. Thus, the hills and valleys of  $\epsilon$  gradually level toward a homogeneous equilibrium state ( $\dot{\epsilon} \rightarrow 0$ ). Looking at the inverse problem, Firoozbakhsh and Aleyaasin (1989) showed that inhomogeneous remodeling occurs near an ellipsoidal hole in an initially homogeneous plate subjected to a compressive load.

The work of Cowin and coworkers inspired Buchacek (1990) to develop a related theory. Since remodeling is likely influenced more by recent events than those in the distant past, he proposed a fading memory theory, in which the apparent density and the orientation of material axes depend on convolution integrals.

**Bone maintenance theory.** The work of Carter and colleagues has been influenced by the idea that bone remodeling is a continuous maintenance process that repairs microcracks as they occur [see, e.g., Carter (1984; 1987)]. According to this view, repeated mechanical loads produce microdamage in bones throughout life. If the damage is allowed to accumulate, the bone eventually will fracture in fatigue. Thus, one function of bone remodeling is to prevent failure. Along these lines, Martin and Burr (1982) hypothesized that the lamellar structure of the bone traps microcracks between osteons, preventing their spread (Fig 34). The crack then induces a stress concentration on the Haversian canal wall that stimulates remodeling before a critical crack size is reached.

Several researchers, including Thompson (1942), have alluded to the possibility that mechanical fatigue microdamage plays a role in regulating the functional adaptation of bones. This theory, however, is not universally accepted. One confounding problem is that remodeling has been observed in bones even when the strain level is below that needed to produce microcracks (Meade, 1989). Carter (1984; 1987) realized this fact and suggested that

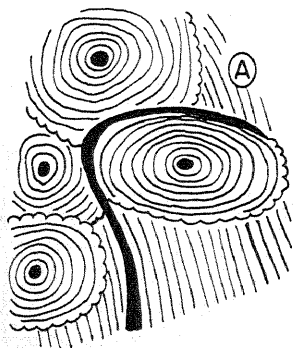


Fig 34. Microcrack trapped by osteons. [Reprinted from Martin RB and Burr DB (1982), A hypothetical mechanism for the stimulation of osteonal remodeling by fatigue damage, *J Biomech* 15, 137-139, copyright 1982, with kind permission from Elsevier Science Ltd, The Boulevard, Langford Lane, Kidlington OX5 1GB, UK.]

other mechanisms also take part, especially at low levels of cyclic strain.

As already discussed, Cowin and coinvestigators generally have treated the adaptations of bone apparent density and trabecular architecture separately. Fyhrie and Carter (1986) proposed a single theory that accounts for both. This theory is based on optimizing a local remodeling objective function  $Q(\rho, \theta, \sigma)$ , where  $\rho$  is the apparent density,  $\theta$  defines the orientation of material axes, and  $\sigma$  is the stress tensor. With the added constraint that  $\rho$  be a minimum, the hypothesis is that bone remodels to maximize its structural integrity with minimal mass.

Fyhrie and Carter (1986) examined two possible candidates for  $Q$ : (1) strain-energy density (stiffness) and (2) strength [ $Q = (\bar{\sigma}/\bar{\sigma}_f)^2$ ;  $\bar{\sigma}$  = effective stress,  $\bar{\sigma}_f$  = effective compressive failure stress]. The optimization analysis showed that both objective functions yield trabecular orientations that align with the principal stress trajectories. Moreover, both predict an apparent density given by

$$\rho = a\bar{\sigma}^b \quad (48)$$

where  $a$  and  $b$  are constants, with  $2/3 \leq b \leq 1$  for stiffness optimization and  $1/2 \leq b \leq 3/5$  for strength optimization.

Expanding these ideas, Carter et al. (1987a) proposed a method to account for the entire stress history of a bone. In the general case, they defined a daily remodeling stimulus by

$$\psi = K \left[ \sum_{\text{day}} n_i \psi_i^m \right] \quad (49)$$

where  $K$  and  $m$  are constants,  $\psi_i$  is the stimulus for loading condition  $i$ , and  $n_i$  is the number of cycles of loading  $i$  per day. A long bone, for example, may undergo  $n_1$  bending cycles and  $n_2$  compressive cycles in a day. Three possibilities for  $\psi_i$  were considered: (1) strength ( $\psi_i = \bar{\sigma}_i/\bar{\sigma}_f$ ); (2) fatigue damage accumulation [ $\psi_i = (\Delta\bar{\sigma}_i/\bar{\sigma}_f)^d$ ;  $d$  = constant,  $\Delta\bar{\sigma}_i$  = cyclic effective stress range]; and (3) strain energy per unit mass of solid bone [ $\psi_i = (U_i/\rho)^k$ ;  $U_i$  = strain-energy density per unit total bone volume,  $k$  = constant]. The authors showed that if  $\psi_i$  is to be uniform throughout the bone, then all of these possibilities lead to the same basic result, with the apparent density given by

$$\rho = K(\sum n_i \bar{\sigma}_i^m)^{1/2m} \quad (50)$$

where  $\bar{\sigma}_i = \Delta\bar{\sigma}_i$  for case (2) and  $\bar{\sigma}_i = (\bar{\sigma}_e)_i$  for case (3), with  $\bar{\sigma}_e^2 = 2\bar{E}U$  being an effective energy stress. ( $\bar{E}$  is an effective modulus.) Note that, if only one loading condition is considered, then Eq (50) reduces to Eq (48).

Based on this theory, Carter et al. (1989) developed a two-dimensional finite-element model to predict the apparent density distribution and trabecular architecture in the proximal femur (Fig 35). Beginning with uniform properties and with three estimated loading conditions,

they computed the solution for each loading case separately. Then, the density of each element was updated according to Eq (50), and a new elastic modulus was computed from  $E = c\rho^3$ , with  $c$  being a constant. Next, a new solution was computed and the process repeated for seven iterations.

To determine the trabecular orientations, Carter et al. (1989) introduced an equivalent cyclic normal stress on a plane with orientation  $\theta$  as

$$\sigma_n^*(\theta) = \left[ \sum_{i=1}^c (n_i/N) |\sigma_{ni}(\theta)|^m \right]^{1/m} \quad (51)$$

where  $\sigma_{ni}$  is the normal stress on the plane for loading condition  $i$ ,  $c$  is the number of loading conditions, and  $N = \sum_{i=1}^c n_i$ . The authors assumed that the trabeculae align with the extrema of  $\sigma_n^*$ . Thus, for  $c = 1$ , they align with the directions of principal stress, i.e., the trajectorial hypothesis. If  $c > 1$ , however, the extrema of  $\sigma_n^*$  are not necessarily orthogonal. In fact, a plot of the distribution of  $\sigma_n^*$  for  $c = 3$  (Fig 35b) shows orientations that, according to Carter et al. (1989), agree more with the drawing of von Meyer than does the sketch of Wolff (1986), in which the trabeculae meet at right angles (see Fig 27).

A key finding of this study was that the solution did not converge to a unique equilibrium state. After three

iterations, the computed density distribution was in reasonable agreement with anatomical observations, but it became unreasonable after seven iterations. Noting this behavior, Carter et al. (1989) suggested that, rather than a remodeling equilibrium state, the existence of an *attractor state* may be more likely in such a complex nonlinear system. Accordingly, a chaotic solution would oscillate about the attractor state, with remodeling occurring continuously throughout the life of the organism, consistent with some physiological data. For a strain-energy stimulus, Harrigan and Hamilton (1992) and Cowin et al. (1994) determined specific conditions for the stability of the governing equations.

In a related study, Fyhrie and Carter (1990) obtained mixed results for the apparent density distribution predicted by a three-dimensional finite-element model. Also, Whalen et al. (1988) used a form of Eq (50) to predict alterations in density due to various physical activities.

Employing the attractor state idea, Beaupre et al. (1990b) extended bone maintenance theory in two ways. First, they included time-dependent remodeling in the manner of Cowin and van Buskirk (1979). (The iterative procedure described above assumes that the material properties, not their rate of change, are proportional to the current remodeling stimulus.) Second, surface growth was added to the theory, with internal remodeling considered as surface growth in internal cavities. In this formulation, the remodeling (surface growth) rate  $\dot{r}$  depends on the difference between the current bone remodeling stimulus  $\psi_b$  [see Eq (49)] and an attractor state stimulus  $\psi_{bAS}$ . The apparent density then is given by

$$\dot{\rho} = \dot{r} S_v \rho_t \quad (52)$$

where  $S_v$  is the bone surface area per unit tissue volume (total trabecular surface area density), and  $\rho_t$  is the true density of the solid part of the bone.

Using this theory in a two-dimensional finite-element model, Beaupre et al. (1990a) examined time-dependent density changes in the proximal femur due to three cyclic loading conditions. The remodeling law they used for  $\dot{r}(\psi_b)$  included a dead zone around  $\psi_{bAS}$  similar to that shown in Fig 31a. Two main findings emerged from this study. First, computations including the dead zone produced more realistic density distributions than those without it. Second, when the load was reduced and then restored to normal levels, the predicted density recovered but to a different distribution. Thus, following immobilization, complete restoration of a bone may never occur, in agreement with some clinical data.

To investigate the long-time consequences of this theory in more detail, Weinans et al. (1992) carried out two-dimensional finite-element computations for various geometries. They found that, as the attractor state is approached, the element apparent density approaches either a maximum (cortical bone) or a minimum (trabecular space) (Fig 36). Thus, *this continuum model produces a discontinuous structure*, in agreement with the actual

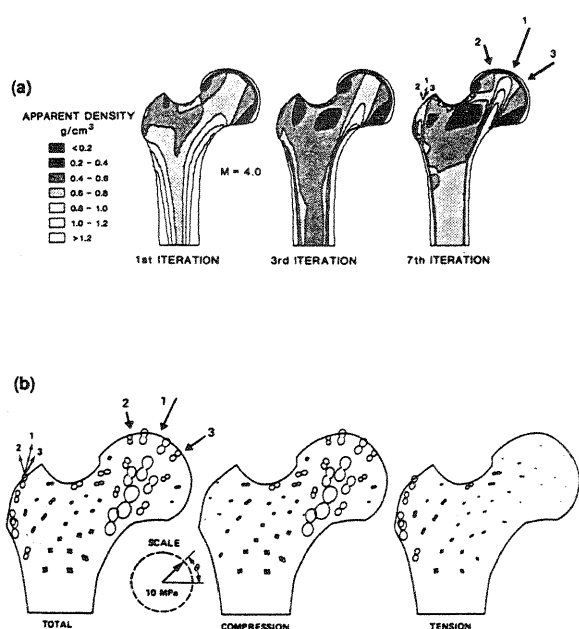


Fig 35. (a) Predicted remodeling of apparent density in femur due to multiple cyclic loadings. (b) Polar plots of equivalent normal stresses. [Reprinted from Carter DR, Orr TE, and Fyhrie DP (1989), Relationships between loading history and femoral cancellous bone architecture, *J Biomech* 22, 231-244, copyright 1989, with kind permission from Elsevier Science Ltd, The Boulevard, Langford Lane, Kidlington OX5 1GB, UK.]

femoral architecture. Moreover, the pattern is fractal-like, consistent with chaotic behavior. Although these results are intriguing, Cowin et al. (1993) showed that this apparent chaos is likely a numerical phenomenon due to the time discretization of the governing equations. Furthermore, the results are not consistent with the continuum assumption on which the model is based. In a recent study, Mullender et al. (1994) have shown that this problem can be overcome by giving the remodeling stimulus a spatial range of influence.

Recently, Prendergast and Taylor (1994) proposed a form of bone maintenance theory that treats remodeling as an ongoing process. At remodeling equilibrium (RE), the rates of microdamage and its repair balance. When these processes are not balanced, changes in geometry and material properties occur. In this theory, the remodeling rate is given by

$$\dot{r} = C \int_0^t (\dot{\omega} - \dot{\omega}_{RE}) dt \quad (53)$$

where  $\dot{\omega}$  is the rate of damage formation, which depends on the stress, and  $C$  is a constant. Application to torsion of a hollow cylinder gave results similar to those for strain-dependent remodeling, but the strains did not re-

turn to their original equilibrium levels.

Finally, we mention an interesting recent application of bone maintenance theory that was used to resolve a confounding problem with total hip prostheses. One option that has been suggested to prevent resorption around a prosthetic pin is to press-fit the implant. Theoretically, the prestress should counteract the stress shielding effect. Experiments with dogs, however, have revealed that while bone resorption is reduced in the short term, the implant eventually loosens. To explore the reasons behind this unfortunate response, van Rietbergen et al. (1993) combined a three-dimensional finite element model with animal experiments. The model predicted that the bone initially grows more dense around the implant, in agreement with their experimental results. But later, the bone stiffens distally of the implant, and this part of the femur then carries a larger fraction of the load. The consequent reduction in load carried in the region around the pin leads to resorption. This study is a clear demonstration of the utility of bone adaptation models.

#### 6.1.5 Morphogenesis

Bone formation begins at about eight weeks in the human embryo. First, undifferentiated mesenchymal cells condense into **anlages**, or **primordia**, forming the basic pattern of the skeleton. Then, depending on the type of bone, the anlages differentiate along one of two paths (Bouvier, 1989). The primordia of cancellous and flat bones, such as the skull, form a fibrous matrix that transforms into bone through a process called **intramembranous ossification**. The primordia of long bones, on the other hand, differentiate first into cartilage through **chondrogenesis**, forming a relatively soft bone-like structure. The cartilage then is converted into bone in a process called **endochondral ossification**.

In long bones, endochondral ossification begins near midshaft, forming a primary ossification center, and then proceeds toward the ends of the bone. Postnatally, a second ossification center usually appears in each epiphysis. The ossification fronts from these two centers approach each other but do not meet, leaving a layer of cartilage called the **growth plate**, which serves as the center of growth until it ossifies in adulthood (Carter and Wong, 1988). In addition, a layer of **articular cartilage** is left at the bone ends to cushion and lubricate the joints (see Fig 38d).

**Pattern formation.** Several models have been proposed for the development of pattern in the skeletal system. Recently, Maini and Solursh (1991) reviewed, compared, and critiqued the various models, as well as the relevant experiments. Of the pattern-forming mechanisms discussed in Sec 4.4, we focus here on the biomechanical model of Oster et al. (1985). Recall that this model is based on the opposing forces of osmotic expansion of the ECM due to hyaluronic acid (HA) production (swelling)

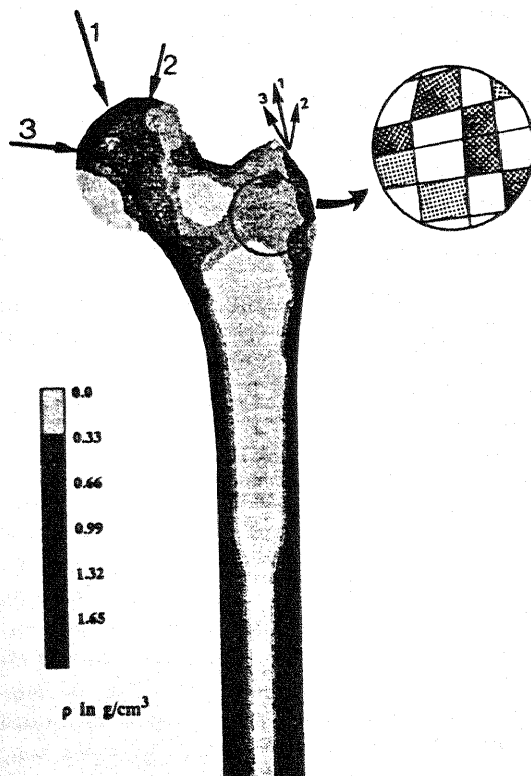


Fig 36. Predicted density distribution in femur. Circle shows discontinuous trabecular structure predicted by originally homogeneous continuum model. [Reprinted from Weinans H, Huiskes R, and Grootenboer HJ (1992), The behavior of adaptive bone-remodeling simulation models, *J Biomech* 25, 1425-1441, copyright 1992, with kind permission from Elsevier Science Ltd, The Boulevard, Langford Lane, Kidlington OX5 1GB, UK.]



on the one hand and contraction due to hyaluronidase (HAase) production (deswelling) on the other.

Qualitatively extending their one-dimensional analysis, Oster et al. (1985) proposed the following model for the developing limb bud, i.e., the limb growing outward from the embryo. Cells multiply in the **progress zone** at the tip of the limb bud and then migrate proximally, secreting HA and inflating the ECM. When the HA concentration reaches a threshold value, HAase is released, deswelling the matrix and leading to localized condensations. Proceeding in a proximodistal direction, these condensations lead to chondrogenesis.

In a cylindrical domain, the model predicts three types of bifurcation, which Oster et al. (1985) call *axial*, *transverse*, and *longitudinal* (Fig 37). A transverse bifurcation, for example, may form the radius and ulna, while a longitudinal bifurcation may produce the bones in the fingers. Trifurcations seldom occur.

**Endochondral ossification.** In the embryo, endochondral ossification begins at about the same time as the first skeletal muscle contractions (Burger et al., 1991). This observation suggests strongly that mechanical forces play a role in this process. Using computational models, Carter and coworkers have published a series of papers on this topic.

First, Carter et al. (1987b) set out to identify the mechanical factor that regulates ossification. For a combination of three loading conditions, they computed strain-energy density distributions in a two-dimensional finite-element model of the proximal human femur at five stages of development. The chosen stages extended from eight weeks of embryonic development, when the femur is entirely cartilage, to eighteen months after birth, when the primary ossification front extends into the epiphysis (Fig 38). At each stage, the internal architecture was

specified, and the (isotropic) material properties of the bone and cartilage were kept constant during development.

The authors found that if high strain-energy density corresponds to ossification, then the model successfully predicts several features of bone morphogenesis, including the primary ossification center (Fig 38a), the tubular diaphysis and marrow cavity (Fig 38a), and the appearance of the secondary ossification center (Fig 38c). Moreover, regions of high hydrostatic compression at 18 months of postnatal development correspond to the location and geometry of the growth plate and the articular cartilage (Fig 38d).

To interpret these results, Carter et al. (1987b) noted that if cartilage is nearly incompressible,<sup>3</sup> then hydrostatic pressure would impart little strain energy, and so the strain-energy density reflects primarily shear stresses. This observation and the results from the model led the

<sup>3</sup>Biomechanical studies have shown that articular cartilage actually is poroelastic and, therefore, compressible in bulk (Mow et al., 1980), although its individual fluid and solid constituents are nearly incompressible.

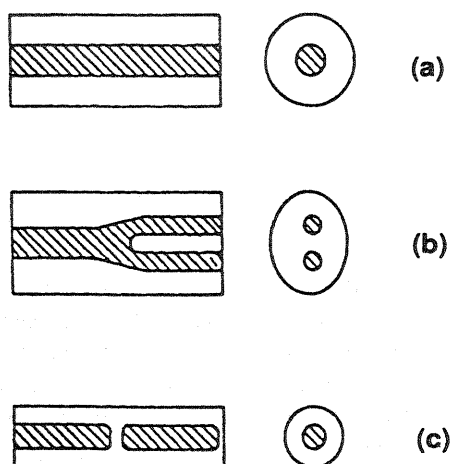


Fig 37. Three types of bifurcation patterns predicted by biomechanical model based on swelling and deswelling of ECM. (a) Axial bifurcation. (b) Transverse bifurcation. (c) Longitudinal bifurcation. [From Oster et al. (1985) with permission, Company of Biologists Ltd.]

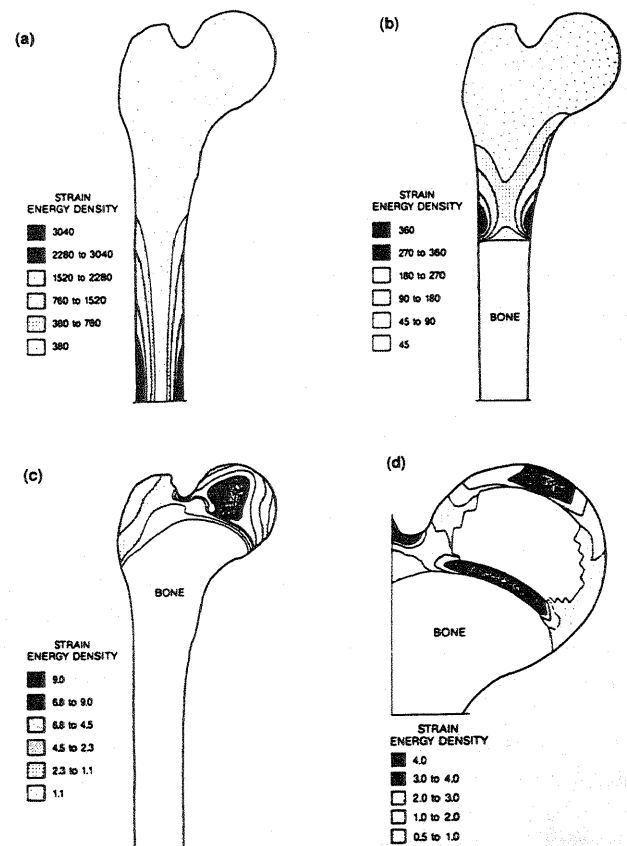


Fig 38. Predicted strain-energy density distributions in proximal human femur at (a) eight weeks of prenatal development; (b) 11 weeks of prenatal development; (c) four months after birth; and (d) 18 months after birth. [From Carter et al. (1987b)]

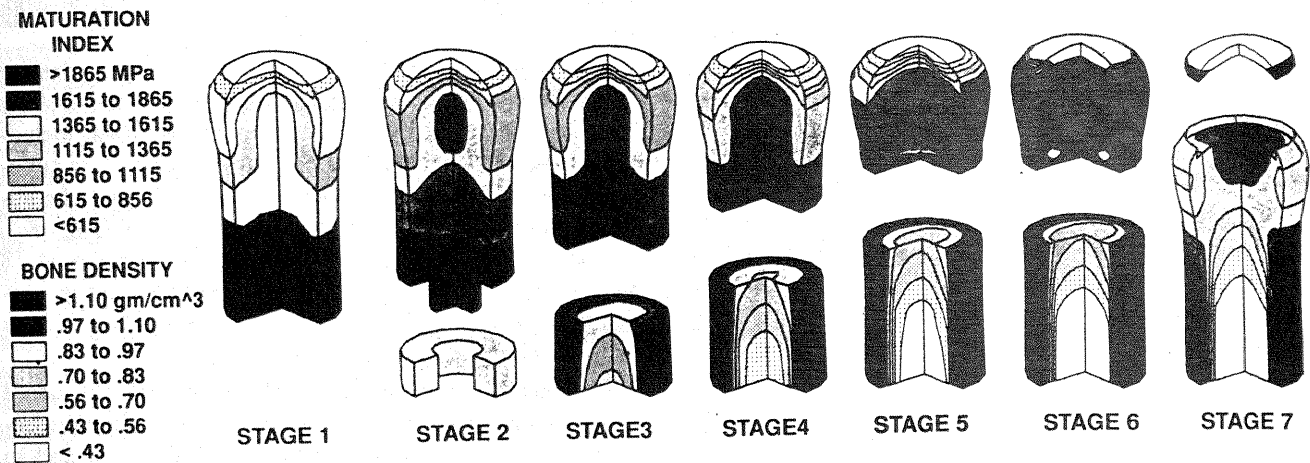


Fig 39. Predicted distribution of maturation index (top) and density (bottom) in cartilage anlage at seven stages of development. [From Wong and Carter (1990b)]

authors to conclude that "the imposition of intermittent shear stresses (or strain energy) into cartilage will accelerate cartilage degeneration and endochondral ossification; and intermittent hydrostatic pressure will retard or prevent cartilage degeneration and ossification." Moreover, they postulated that all cartilage, both developing and mature, undergoes a progressive sequence of *proliferation, maturation, degeneration, and ossification*. These hypotheses have formed the basis for later work by Carter et al. on this topic. Among other things, the theory suggests that degenerative joint disease is due to alteration of the normal hydrostatic pressure in the joint (Carter, 1987).

Next, to quantify this biomechanical theory of bone development, Carter and Wong (1988) introduced the **ossification index**

$$I = \sum_{i=1}^c n_i (S_i + k D_i) \quad (54)$$

where  $n_i$  is the number of cycles for loading case  $i$ ,  $S_i$  is the cyclic octahedral shear stress,  $D_i$  is the cyclic hydrostatic stress, and  $k \geq 0$  is a relative weighting factor to be determined experimentally. Since  $D_i < 0$  for hydrostatic compression, large values of  $I$  (large shear) correspond to accelerated endochondral ossification, while low values of  $I$  (large hydrostatic compression) correspond to inhibited cartilage degeneration.

Using a two-dimensional finite-element model of the convex and concave chondroepiphyses of an embryonic joint, Carter and Wong (1988) found that setting  $k = 0.5$  produced an ossification pattern (distribution of  $I$ ) like that found *in vivo*. In a similar analysis of the development of the sternum, Wong and Carter (1988) obtained realistic results for  $k = 0.7$ . Furthermore, analyzing *in vitro* tissue culture experiments of Klein-Nulend et al. (1986), Wong and Carter (1990a) obtained results that support the basic tenets of the theory discussed above.

Extending their model to include time-dependent morphogenesis, Wong and Carter (1990b) introduced the **maturation index**  $B$ , which is defined to a first approximation by the daily maturation rate

$$\dot{B}_j = \dot{B}_0 + C I_j \quad (55)$$

where  $I_j$  is the ossification index [Eq (54)] for day  $j$ ,  $C$  is a constant, and  $\dot{B}_0$  is the unloaded baseline maturation rate. In addition, they incorporated fading memory by taking the maturation index for day  $n$  in the form

$$B_n = \sum_{j=n-n_0}^n B_j \quad (56)$$

where  $n_0$  is the number of previous days that the tissue "remembers."

Using a three-dimensional finite-element model, Wong and Carter (1990b) studied the development of a cartilage anlage subjected to five superposed loading cases. With the initial distribution of the maturation index specified, the stresses were computed, and the density and maturation index were updated according to Eqs (50) and (54)–(56). When  $B_n$  reached a specified threshold value in an element, the properties of the element were changed to those of bone. This process was continued, and the time-evolution of  $B_n$  predicted the progression of the primary ossification front toward the epiphysis, the formation of the secondary ossification center, and the articular cartilage remaining at the end of the bone. Furthermore, the apparent density distribution predicted the resorption that leads to the marrow cavity (Fig 39).

The good agreement between theory and experiment in these investigations supports the formulas of Carter et al. as construction rules for the developing skeletal system. Moreover, the evidence suggests that these rules

hold from early embryonic development through maturation in the adult to possible degeneration later in life. Even fracture healing seems to obey a form of these rules (Carter et al., 1988; Blenman et al., 1989). On the other hand, these models have not yet been validated experimentally under carefully controlled loading conditions.

## 6.2 Skeletal muscle

### 6.2.1 Structure and function

Skeletal muscle connects bones and joints, enabling an organism to move and perform work. A muscle is organized into a hierarchy of structural elements (Fig 40), with the primary element being the **muscle fiber**. Each fiber is a single cell that is about 10-60  $\mu$  in diameter and several centimeters long, and contains hundreds of nuclei. Bundles of fibers, or **fasciculi**, are bound together by connective tissue to form a muscle (Fung, 1993).

The cytoplasm of each muscle fiber is filled with **myofibrils**, which are about 1  $\mu$  in diameter and extend the length of the cell. A myofibril, in turn, is composed of arrays of **myofilaments**, which are arranged into **sarcomeres**, the main functional units. Each 2  $\mu$ -long sarcomere is made up of interdigitating thick (myosin) and thin (actin) myofilaments.

The total tension exerted by a skeletal muscle contains a passive and an active component. The passive tension, which is due to the elasticity of the fibers and connective tissue, increases exponentially with stretch (Fung, 1993). Passive muscle also exhibits the viscoelastic effects of creep and stress relaxation (Fung, 1993).

The active tension derives from a transduction of electrochemical energy into mechanical energy. According to the *sliding filament theory* of muscle contraction, **cross bridges** pull the myofilaments past each other without changing their lengths. In response to a single electrical stimulus, a muscle held isometrically **twitches** as it generates a force that increases to a peak and then falls off. As the frequency of a train of stimuli increases, the contractile force builds up until a critical frequency is reached, and then the muscle exerts a constant force in a state of **tetanus** (Fig 41a). The magnitude of this developed force depends on the stretch, with a peak occurring at a sarcomere length of about 2.2  $\mu$  (Fig 41b). If one end of the tetanized muscle is then released against a constant load, the muscle contracts with an initial velocity that decreases as the load magnitude increases (Fig 41c).

Skeletal muscle fibers can be classified into two general categories: fast-twitch and slow-twitch. Compared to fast-twitch fibers, slow-twitch fibers are thinner, have a lower maximum velocity, generate a smaller peak force, and have a higher aerobic capacity (Phillips and Petrofsky, 1983). Most skeletal muscles contain some of both of these fiber types.

### 6.2.2 Growth

Skeletal muscle growth has been studied extensively with both *in vivo* and *in vitro* experimental techniques (Stew-

art, 1972; Goldberg et al., 1975; Salmons and Henriksson, 1981; Booth, 1982; Vandenberg et al., 1991). Engineering-type investigations, however, are virtually nonexistent. The methods discussed in Sec 3.1.1 can be used to model growth of skeletal muscle, but this has not yet been done. Noting again that all findings have not been consistent, we list some of the features of skeletal muscle growth that should be considered in developing models:

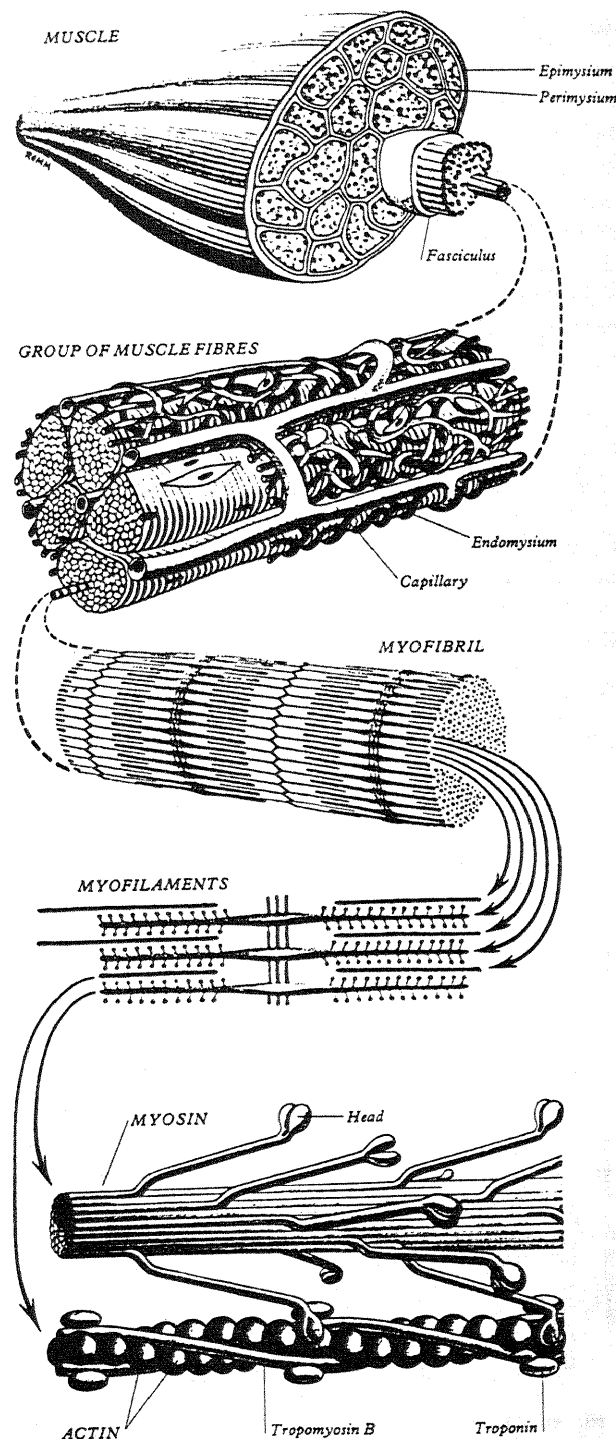


Fig 40. Organization of skeletal muscle. [From Gray's Anatomy, 36th edn., edited by P.L. Williams and R. Warwick, W.B. Saunders, Philadelphia]

1. As the bones lengthen during normal postnatal growth, the muscles keep pace as individual fibers grow longer by adding sarcomeres in series at their ends (Williams and Goldspink, 1971; Goldspink, 1972).
2. Mature skeletal muscle fibers normally stop dividing shortly after birth (Goldspink, 1972), but non-

muscle cells and collagen continue to proliferate (Goldberg et al., 1975). In extreme cases of hypertrophy, however, myofibrils split along their length when a critical diameter is reached (Goldspink, 1972; Goldberg et al., 1975). Moreover, skeletal muscle regenerates fibers when injured (Zak, 1973).

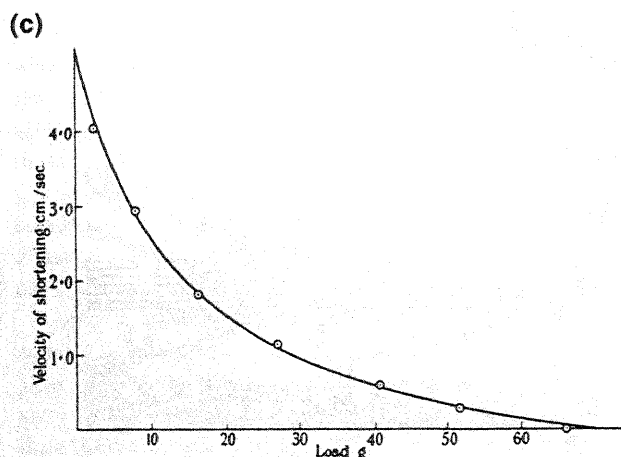
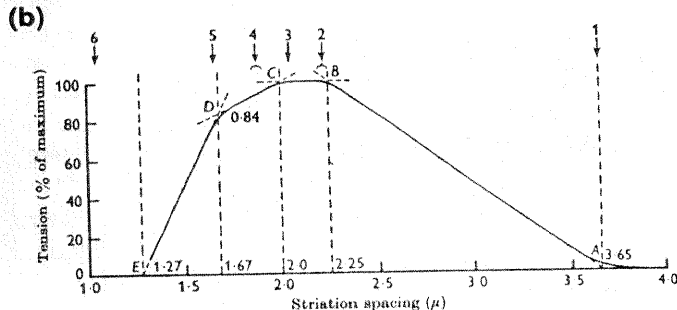
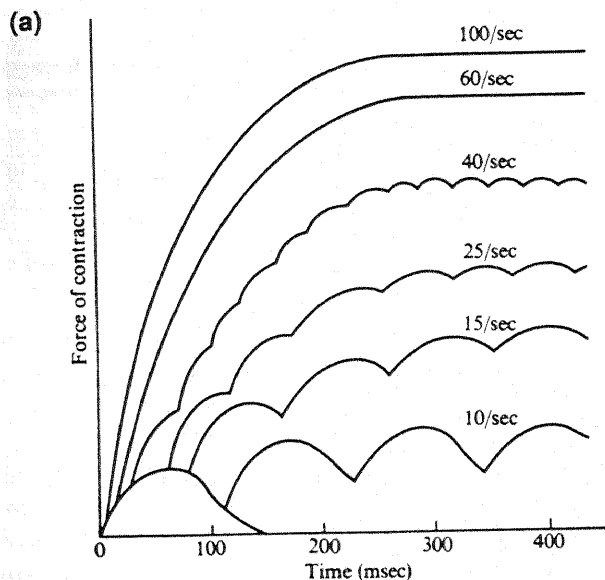


Fig 41. Skeletal muscle mechanical characteristics. (a) Series of isometric twitches building up in force to a constant tetanus state. [From Fung (1993)] (b) Isometric tension-length curve. [From Gordon et al. (1966)] (c) Velocity-force curve. [From Hill (1938)]

3. Fiber diameter increases with stress level, with both active and passive stress having similar effects (Stewart, 1972; Goldberg et al., 1975). Total tension seems to be the critical factor. Since isometric activation generates the highest tension, isometric exercise induces muscle hypertrophy very effectively (Goldberg et al., 1975). The hypertrophy is due to decreased protein breakdown and increased protein synthesis, with sarcomeres added in parallel (Goldberg et al., 1975; Goldspink, 1972; Spector et al., 1982).
4. For a given load, slow-twitch muscle fibers hypertrophy more than fast-twitch fibers (Stewart, 1972; Holly et al., 1980). Since slow fibers have smaller diameters, this behavior may be due to higher stress in these fibers.
5. Immobilized muscles atrophy. Muscles that are stretched and immobilized atrophy more slowly than those that are shortened and immobilized (Goldberg et al., 1975).
6. Hormones are necessary for stretch-induced growth *in vitro* (Vandeburgh et al., 1991).
7. Temporary damage occurs to muscle cells stretched *in vitro*, which may stimulate growth and remodeling (Vandeburgh et al., 1991).

The last observation is particularly interesting in light of the similar mechanism discussed for bone in the previous section.

### 6.2.3 Remodeling

Like bone, skeletal muscle microstructure and properties depend on the loading environment. Experimental investigations, for example, have shown the following:

1. Fibers orient in the direction of a continuous stretch *in vitro* (Vandeburgh, 1982).
2. The maximum developed tension of hypertrophied muscle increases, and the contraction time decreases (Goldberg et al., 1975).
3. Muscles immobilized in a lengthened configuration exhibit no change in passive elasticity, but the passive stiffness of muscles immobilized in a shortened position increases (Tabary et al., 1972). In addition, muscles immobilized in a shortened configuration suffer reduced tension-generating capacity, but the maximum intrinsic shortening velocity

changes little. Immobilization at neutral or lengthened positions has little effect on contractile properties (Simard et al., 1982).

4. When subjected to chronic low-frequency stimulation, fast-twitch muscle fibers transform into slow-twitch fibers (Salmons and Henriksson, 1981). Immobilization reverses this effect (Booth, 1982).

#### 6.2.4 Morphogenesis

In the embryo, muscle development begins with groups of mesenchymal cells called presumptive myoblasts proliferating and migrating to specific sites (Fischman, 1972). These mononucleated cells then elongate, transforming into **myoblasts**, which cease dividing and are capable of synthesizing contractile proteins, but they contain relatively few myofibrils. Next, the myoblasts align and fuse together to form multinucleated **myotubes**, which manufacture myofibrils arranged longitudinally around a central core of nuclei. Finally, the nuclei migrate to the periphery of the cells, and the myofibrils become distributed more evenly in the cytoplasm, as the myotubes transform into **myofibers**.

Several pieces of evidence suggest that biomechanical forces influence skeletal muscle morphogenesis. For instance, the muscles that develop earliest are generally those that elongate the most before birth (Stewart, 1972). In the young animal, moreover, denervated muscles grow at a reduced rate (Stewart, 1972). These findings suggest that passive muscle tension due to bone elongation is important in the embryo, while later development requires active tension. This conclusion is supported by the *in vitro* experiments of Vandeburgh (1982), who found that fiber alignment occurs optimally at a continuous stretch rate that is similar to the rate of bone elongation in the embryo.

## 7 CARDIOVASCULAR SYSTEM

### 7.1 The heart

#### 7.1.1 Structure and function

**The heart as a pump.** The mature heart of mammals and birds consists of four muscular chambers that pump blood through the circulatory system (Fig 42). Deoxygenated blood returns from the body through the vena cavae and fills the right atrium (RA), which contracts, sending the blood into the right ventricle (RV). The RV then contracts, forcing the blood into the pulmonary artery, which carries it to the lungs to pick up oxygen. Next, the oxygenated blood flows through the pulmonary vein into the left atrium (LA), which delivers it to the left ventricle (LV). Finally, the LV contracts, ejecting the blood into the aorta and out to the systemic circulation. A wave of depolarization coordinates all of this activity, and backflow is prevented by one-way valves between the chambers and blood vessels.

During the cardiac cycle, each chamber fills during a period of relaxation, or **diastole**, and ejects the blood during a period of active contraction, or **systole**. If pressure is plotted as a function of cavity volume, each chamber traverses a loop similar to that shown for the LV in Fig 43b. The legs of the loop represent diastolic filling (A-B), isovolumic contraction (B-C), ejection (C-D), and isovolumic relaxation (D-A). The portion of the loop between points B and D corresponds to systole, and the part between D and B corresponds to diastole, with B and D being end diastole and end systole, respectively. The isovolumic segments are due to the pressure needing to rise or fall sufficiently to force valves to open.

By experimentally altering the preload (end-diastolic volume) or the afterload (end-systolic pressure), various pressure-volume loops can be generated (Fig 43a). In the mature LV, the end-systolic corners of these loops (points D) fall essentially along a straight line called the end-systolic pressure-volume relation (ESPVR), whose slope increases with the contractility, i.e., the intrinsic contractile strength. In the puppy (Sagawa et al., 1988) and embryonic chicken heart (Taber et al., 1992), however, the ESPVR is curvilinear and concave downward. Using a series of experiments, Sagawa et al. (1988) showed that the total oxygen consumption per beat of the LV is proportional to the pressure-volume area (shaded area of Fig 43b). The area within the loop represents the stroke work, and the triangular area represents potential energy that is dissipated largely as heat. These energetics likely influence cardiac growth, since heart muscle, like skeletal muscle, responds to an increased workload by adding mass.

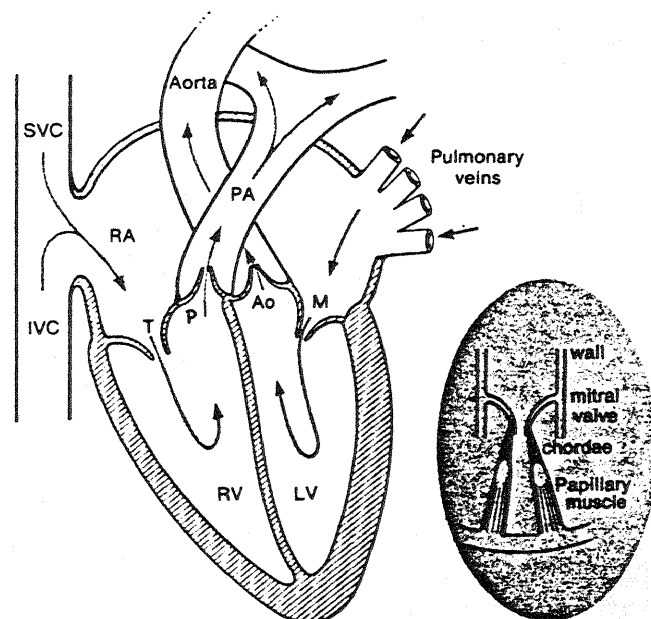


Fig 42. Schematic of the mature heart. SVC: superior vena cava; IVC: inferior vena cava; RA: right atrium; RV: right ventricle; LV: left ventricle; PA: pulmonary artery. The valves are T: tricuspid; P: pulmonary; Ao: aortic; M: mitral. [From Folkow and Neil (1971)]

**Heart muscle.** With a few important differences, the structure and function of heart muscle, or **myocardium**, are similar to those of skeletal muscle. Mechanically, both types of muscle exhibit similar force development during an isometric twitch, similar force-velocity behavior, and similar passive stress-strain curves. Cardiac muscle, however, cannot tetanize, and so the measured velocity corresponds to release at a specified time from the onset of stimulation.

The most significant ultrastructural difference is that, rather than being aligned, myocardial fibers branch, forming a syncytium (Fig 44a). Consequently, any depolarization wave spreads throughout the entire my-

ocardium, producing an "all-or-none" contraction.

Heart muscle contains a highly ordered interstitial collagen matrix (Fig 44b). Surrounding the entire muscle is a layer of collagen called the **epimysium**. Strands of epimysium called **perimysium** extend into the myocardium and bundle groups of fibers together with a weave pattern. These bundles are connected by perimysial strands, and the fibers inside the bundle are connected by struts of **endomysium**. The integrity of the collagen matrix is vital to normal cardiac function. For example, it helps prevent sarcomere overstretching, which could reduce contractile force (see Fig 41b).

Since the heart requires a continuous supply of energy, cardiac muscle fibers contain more mitochondria than do skeletal muscle fibers. Furthermore, myocardium contains more capillaries (about one per fiber in the adult). A final difference is that cardiac fibers contain only one or two nuclei, rather than many hundreds.

**Fiber architecture.** The left ventricle, which pumps blood through the body, generates the highest pressures in the heart [about 120 mmHg peak pressure in most mammals, regardless of size (Holt et al., 1962)]. Due to the corresponding large workload and energy requirement, most infarcts (heart attacks) occur in the LV, and

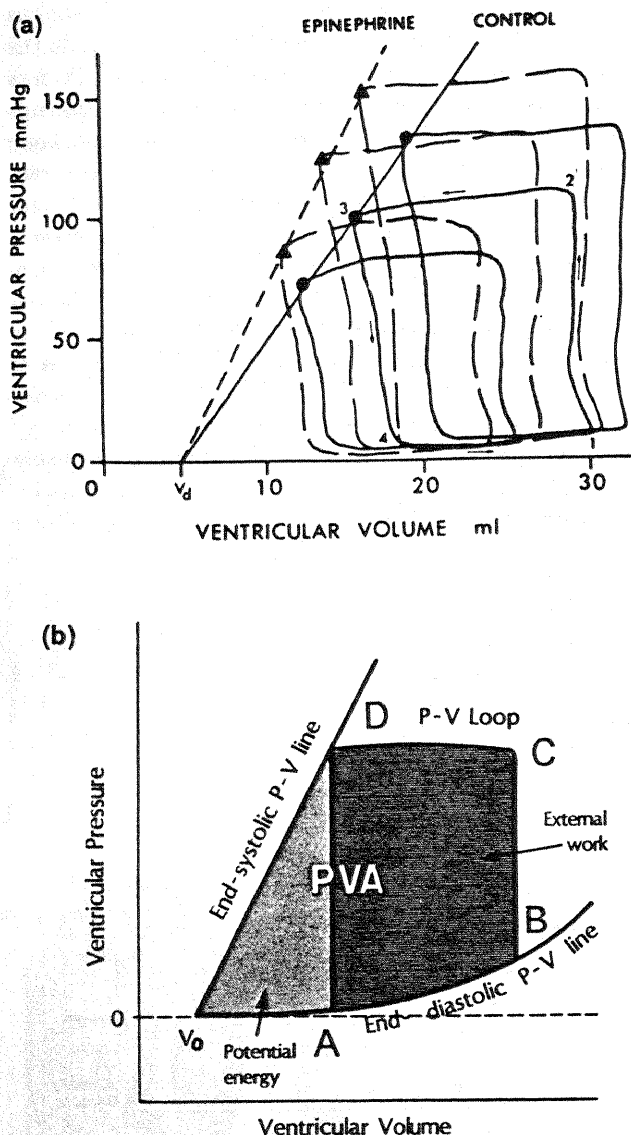


Fig 43. (a) Pressure-volume loops and end-systolic pressure-volume relation for normal LV and one with enhanced contractility. [From Suga et al. (1973), reproduced with permission. *Circulation Research*, copyright 1973 American Heart Association.] (b) Typical pressure-volume loop. Shaded pressure-volume area (PVA) represents total energy expenditure of ventricle per beat. [From Sagawa et al. (1988)]

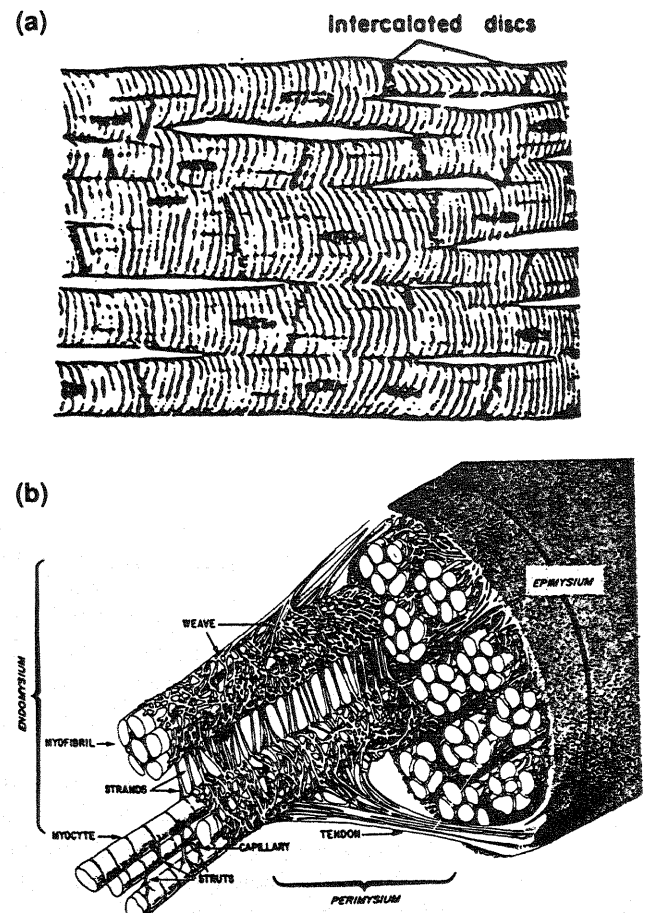


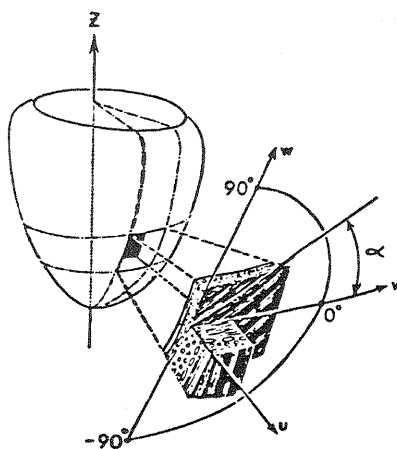
Fig 44. (a) Schematic of cardiac muscle fibers [From Guyton (1991)] (b) Schematic of collagen matrix of the myocardium. [From Weber et al. (1987)]



this chamber has received the most attention in the literature. Thus, we briefly describe its structure.

To a first approximation, the LV is a thick-walled ellipsoidal shell of revolution (Fig 45a), composed of myocardium between a thin outer membrane, or **epi-cardium**, and an inner membrane, or **endocardium**. Although myocardial fibers branch, there is a sense of direction (Fig 44a). The fibers wind around the ventricular cavity, and, relative to the circumferential direction, the fiber orientation changes continuously across the wall from about  $60^\circ$  at the endocardium to  $-60^\circ$  at the epicardium (Fig 45b) (Streeter, 1979). This anisotropic construction strongly influences the transmural distribution of wall stress (Tozeren, 1983; Taber, 1991; Bovendeerd et al., 1992).

(a)



(b)

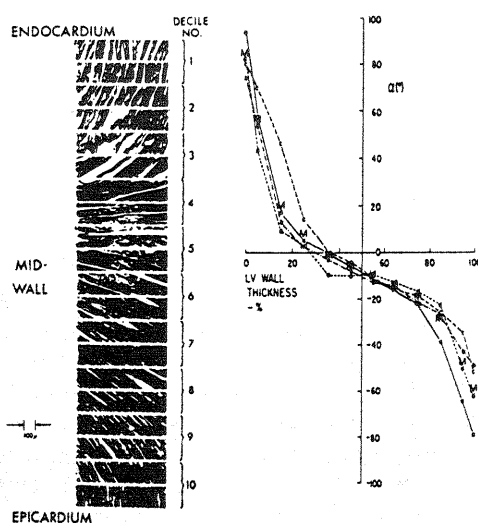


Fig 45. (a) Idealized geometry of left ventricle. (b) Variation of muscle fiber orientation through wall of dog left ventricle. [From Streeter et al. (1969), reproduced with permission. *Circulation Research*, copyright 1969 American Heart Association.]

### 7.1.2 Normal growth

Before and after birth, the heart grows to meet the increasing metabolic demands of the body. In the embryo, the heart grows by myocyte hyperplasia. Just before birth, cell growth begins to replace cell division, and by a few weeks after birth, hypertrophy becomes the primary mechanism for cardiac growth (Burton, 1972; Grossman, 1980). Interstitial cells such as fibroblasts, however, may continue to divide (Weber, 1989), and myocytes may replicate under certain pathological conditions (Kajstura et al., 1994). The ratio of normal heart weight to body weight depends on the species, being larger in animals that are more active (Poupa and Ostadal, 1969).

It long has been conjectured that wall stress affects the growth of the heart. Woods (1892) published the first stress analysis of the heart, modeling the ventricles as thin-walled membranes. Although the ventricles actually are thick-walled shells, membrane theory provides a useful approximation for the average transmural stresses. A normal force balance gives Laplace's law

$$p = t \left( \frac{\sigma_1}{R_1} + \frac{\sigma_2}{R_2} \right) \quad (57)$$

where  $p$  is the cavity pressure,  $t$  is the wall thickness,  $R_1$  and  $R_2$  are principal radii of curvature, and  $\sigma_1$  and  $\sigma_2$  are in-plane stresses. If the ventricular stresses are uniform ( $\sigma_1 = \sigma_2$ ), then the quantity  $C = t(1/R_1 + 1/R_2)$  should be constant in a given ventricle. Measuring the geometry at various points of human right and left ventricles, Woods (1892) found that  $C$  is indeed nearly constant.

Variations of Eq (57) have been used in conjunction with a wide range of experimental and clinical data to show that wall stress is likely a fundamental determinant of normal and abnormal cardiac growth. At birth, for example, the LV and RV have the same number of cells and are about the same size (Linzbach, 1976; Ferrans, 1984), consistent with the similar workloads of the two ventricles *in utero*. After birth, however, the LV pressure soon becomes much larger than that of the RV. If a nominal wall stress exists, then Eq (57) predicts that the LV wall thickness must be greater than the RV thickness, as is the case in the growing and adult animal.

Comparing the LVs of different species, Martin and Haines (1970) obtained more evidence supporting the importance of wall stress in cardiac growth. Although the weights of their studied hearts varied 767 times, the variation in  $C$  was only 22% [see also Ford (1976)]. Furthermore, the LV of the giraffe, which must pump blood against a very large pressure to reach the head, has a relatively thicker wall to keep the stress nearly the same as in other animals (Burton, 1972).

While these data offer strong support for wall stress as a growth-modulating factor, wall strain cannot be ruled out.<sup>4</sup> Pumping efficiency would be maximized if contraction begins with all sarcomeres at the optimal length of

<sup>4</sup>Since material properties are inhomogeneous in the heart, uni-

about  $2.2 \mu$ . This length could serve as a fixed reference length, overcoming the disadvantage of strain-modulated growth discussed in Sec 3.1.1.

Transmural sarcomere lengths (SL) can be altered by differential growth, i.e., through changes in residual strain in the *passive* LV (Omens and Fung, 1990). Recently, Rodriguez et al. (1993) obtained data to support the uniform SL hypothesis. Measuring SLs directly in the passive rat LV, they found that the transmural distribution is nearly uniform in the stress-free (cut) configuration, but the SL increases from endocardium to epicardium in the unloaded (intact) state. The authors postulated that the higher subendocardial strains that occur during diastolic filling would even out the SLs across the wall at end diastole.

### 7.1.3 Hypertrophy

Adaptive growth and remodeling of the heart due to abnormal loads are classified generally as "cardiac hypertrophy." Two types of hypertrophy commonly occur: concentric and eccentric. Usually associated with pressure overload due to hypertension (high blood pressure), **concentric hypertrophy** is characterized by an increased wall thickness with little change in cavity size (Fig 46). **Eccentric hypertrophy**, on the other hand, is usually associated with volume overload (increased end-diastolic volume), possibly due to a defective valve. To accommodate the greater blood volume, the ventricular cavity enlarges (Fig 46), and the wall thickness increases just enough to keep the ratio of radius to thickness approximately the same (Grossman, 1980).

In the short term, both types of hypertrophy represent successful adaptations of the heart to changing loads.

form wall stress does not necessarily imply uniform wall strain relative to the zero-stress configuration.

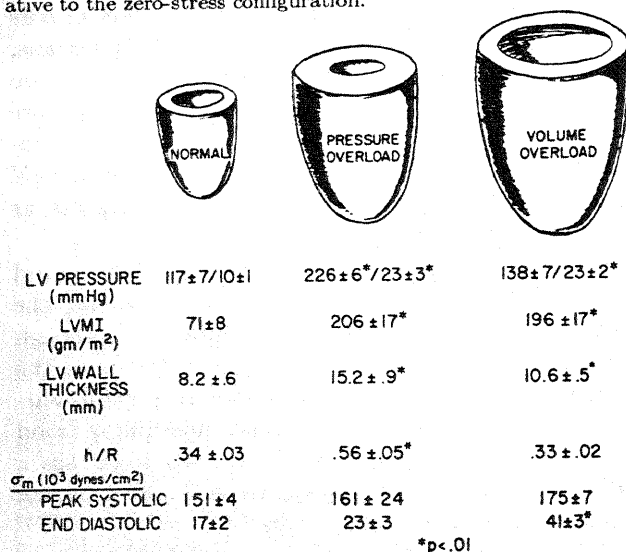


Fig 46. Characteristics of normal left ventricle compared to those from hearts subjected to chronic pressure or volume overloads. Note similarity of peak systolic pressures. [From Grossman (1980). Reprinted with permission from *American Journal of Medicine*.]

As long as the cardiac output (blood flow rate) meets the metabolic demands of the tissues, the response is termed **physiologic hypertrophy**, which is reversible (Weber et al., 1987). If an overload continues, however, **pathologic hypertrophy** may develop, which often leads to depressed cardiac performance and congestive heart failure (Grossman, 1980). It is important to note that chronic physiologic hypertrophy does not always become pathologic. Normal heart growth and hypertrophy due to exercise, for example, remain physiologic. [Normal growth is a form of eccentric hypertrophy as the blood volume increases in the growing animal (Ford, 1976; Grossman, 1980)]. Although the transition from physiologic to pathologic hypertrophy is not completely understood, some of the mechanisms involved are now becoming clear (see below).

The mechanics of cardiac hypertrophy have been studied extensively. Biomechanical models have been used to compute wall stress and material properties of the hypertrophied heart, but few models of the growth process have been proposed. Recently, Rodriguez et al. (1994) and Lin and Taber (1994) have used the methods of Sec 3.1.1 to examine how different types of hypertrophy can induce residual stress in mature and embryonic ventricles, respectively. Here, we focus on some of the fundamental biomechanical findings of experimental and clinical studies. More detail can be found in the reviews of Wikman-Coffelt et al. (1979), Grossman (1980), Mirsky and Pasipoularides (1980), Spann (1983), Weber et al. (1987), and Weber (1989).

**Growth.** In concentric hypertrophy, fibers increase in diameter through addition of sarcomeres in parallel, while in eccentric hypertrophy, fibers increase in length by adding sarcomeres in series. Some investigators have proposed that fiber slippage and rearrangement (Laks et al., 1974; Suwa, 1982; Weber et al., 1991) and interstitial cell hyperplasia (Weber, 1989) also contribute to wall thickness changes. Moreover, although mature myocytes normally do not divide, Linzbach (1976) suggested that fibers split longitudinally in cases of extreme hypertrophy, and Kajstura et al. (1994) found myocyte hyperplasia and loss in rats subjected to chronic ischemia (oxygen deficit).

As in normal heart growth, the available evidence indicates that wall stress likely modulates the type and degree of myocardial hypertrophy. For instance, when pressure overload causes abnormally high end-systolic stresses, the wall thickness increases according to Eq (57) to bring the stresses back to normal. On the other hand, volume overload (increasing  $R_1$  and  $R_2$ ) increases end-diastolic stresses, which also are brought down by a (more modest) thickness increase that keeps  $C = t(1/R_1 + 1/R_2)$  approximately constant [see Eq (57)]. In both cases, the adaptations allow the heart to meet the metabolic demands of the body while returning peak stresses to near normal levels (Grossman et al., 1975, 1983; Grossman, 1980). Thus, it appears that chamber

volume is controlled by end-diastolic pressure, and wall thickness by end-systolic pressure.

Recent biomechanical models of the LV predict that fiber stress is fairly uniform across the wall, with a relatively small peak occurring subendocardially, especially during systole (Tozeren, 1983; Taber, 1991; Bovendeerd et al., 1992). If myocardial growth is stress-modulated, then the inner layers would hypertrophy more due to pressure overload than the outer layers, consistent with the experimental data of Lund and Tomanek (1978). Moreover, if eccentric hypertrophy is controlled by the more uniform end-diastolic stresses, then the growth in this case would be nearly uniform. This prediction agrees with the volume-overload measurements of Omens and Covell (1991), who also found that the growth is essentially isotropic in planes parallel to the epicardium.

Although the case for stress-modulated growth in the heart appears strong, other factors remain candidates (see Sec 7.1.2). Zak (1984) discussed several other possibilities, including contractile activity (possibly energy-based), ATP depletion, stretch, humoral factors, hypoxia, and cell degradation.

**Remodeling.** During cardiac hypertrophy, the collagen matrix remodels. Due to chronic pressure overload, the collagen weaves and strands thicken (Ferrans, 1984; Weber, 1989). This fibrosis, however, does not occur in the hypertrophied hearts of athletes, which exhibit characteristics of both pressure and volume overload. Thus, interstitial fibrosis has been proposed as a primary factor delineating pathologic from physiologic hypertrophy (Weber et al., 1991).

To a lesser extent, the fiber architecture also remodels. Due to pressure overload, the fibers in the LV become slightly more longitudinally oriented near the epicardium and endocardium (Carew and Covell, 1979). Volume overload and exercise, however, have little effect.

Hypertrophic changes in material properties remain controversial (Mirsky et al., 1983), but some trends are becoming clear. First of all, hearts subjected to volume overloads maintain normal contractility (Cooper et al., 1973; Ross, 1974). Second, hearts subjected to severe pressure overloads suffer a depressed contractile state, including reduced force and velocity of contraction (Spann et al., 1967; Cooper et al., 1981). These features characterize pathologic hypertrophy, as opposed to the normal or augmented contractility of physiologic hypertrophy (Wikman-Coffelt et al., 1979). Finally, depending on the degree and duration of the overload, some studies find a normal passive muscle stiffness (Serizawa et al., 1982), while others find an increased stiffness (Peterson et al., 1978; Natarajan et al., 1979; Mirsky and Laks, 1980).

The effects of myocardial unloading also have been investigated. Due to unloading, heart muscle loses myofibrils and fiber alignment, becoming similar to neonatal myocardium (Thompson et al., 1984; Kent et al., 1985). In addition, the contractile force and velocity decrease

(Cooper and Tomanek, 1982; Thompson et al., 1984).

**Ischemia and infarction.** When myocardial oxygen demand exceeds supply, possibly due to a narrowed coronary artery, the muscle becomes **ischemic**. If the artery becomes completely blocked, a **myocardial infarction**, or "heart attack," can occur, resulting in a region of necrotic muscle (usually in the LV). Both conditions lead to remodeling of the myocardium.

During prolonged ischemia or immediately following an infarction, the collagen matrix degrades in the affected muscle (Zhao et al., 1987), and fiber slippage allows the ventricular wall to bulge outward locally during systole (Anversa et al., 1993; Grossman and Lorell, 1993). This bulging hampers the pumping performance of the heart, since part of the blood normally destined for the aorta is pumped into the bulge. To compensate, the undamaged portion of the ventricle hypertrophies eccentrically to increase end-diastolic volume (Anversa et al., 1993; Grossman and Lorell, 1993).

Within weeks of an infarction, fibrosis of the weakened area prevents the systolic bulging, improving cardiac performance. A large infarct, however, may remodel into a permanent bulge, or **aneurysm**, which usually leads to further complications. Unlike skeletal muscle, heart muscle is unable to repair itself following injury (Zak, 1973). Thus, the scar tissue is not replaced by new muscle, and so a heart suffering an infarction never recovers completely.

#### 7.1.4 Morphogenesis

**Primary cardiac development.** The heart is the first functioning organ in the embryo. Development of the heart begins with a pair of epithelial tubes forming on opposite sides of the early embryo (Clark and Van Mierop, 1989). These structures then merge and fuse along the ventral midline of the embryo (Fig 47a) to form a single cardiac tube composed of three layers: a relatively thin outer layer of myocardium, a middle layer of cardiac jelly, and an inner layer of endocardium (Fig 47b, left). The two-cell-thick myocardium contains the only contractile elements in the primitive ventricle; the **cardiac jelly (CJ)**, which is extracellular matrix material, makes up the bulk of the wall thickness; and the endocardium is an epithelium that lines the lumen of the tube.

Most research in cardiac development has used the embryonic chick heart as a model, since, except for the time scale, its development parallels that of the human heart. Since the rate of development depends to a certain extent on environmental factors such as temperature, Hamburger and Hamilton (1951) divided the 21-day incubation period of the chick embryo into 46 stages based on external characteristics of the developing embryo.

In the chick, contractions begin just after the primitive ventricle forms at stage 9 (1 day), which corresponds to about 17 days of human gestation. Effective blood flow, however, does not begin until stage 12 (2 days), with

endocardial cushions in the inflow and outflow regions of the ventricle preventing backflow. Soon after the onset of contraction, the morphogenetic process of **cardiac looping** begins, as the heart grows and deforms into a curved tube (Fig 48), with blood entering one end and pumped out the other.

Through the looping process, the ventricular wall remains relatively thin, and the metabolic needs of the myocardium are met entirely by diffusion from the lumen. Later, however, the wall grows too thick for this process to be sufficient. Thus, beginning at stage 17 (3 days) in the chick, the cardiac jelly is rapidly replaced by a network of myocardial trabeculae, which begin as endocardial ridges near the apex (bottom of the loop) with a prevailing circumferential orientation (Taber et al., 1993a). By stage 21 (4 days), the ventricular wall resembles a sponge with a thin outer sleeve of compact myocardium (Fig 47b, right). During these stages, direct blood flow through the trabecular spaces supplies nutrients to the myocardium. Trabeculation continues until stage 25 (4.5 days), when the myocardium begins to compact and the coronary circulation appears.

The interventricular septum eventually forms at the

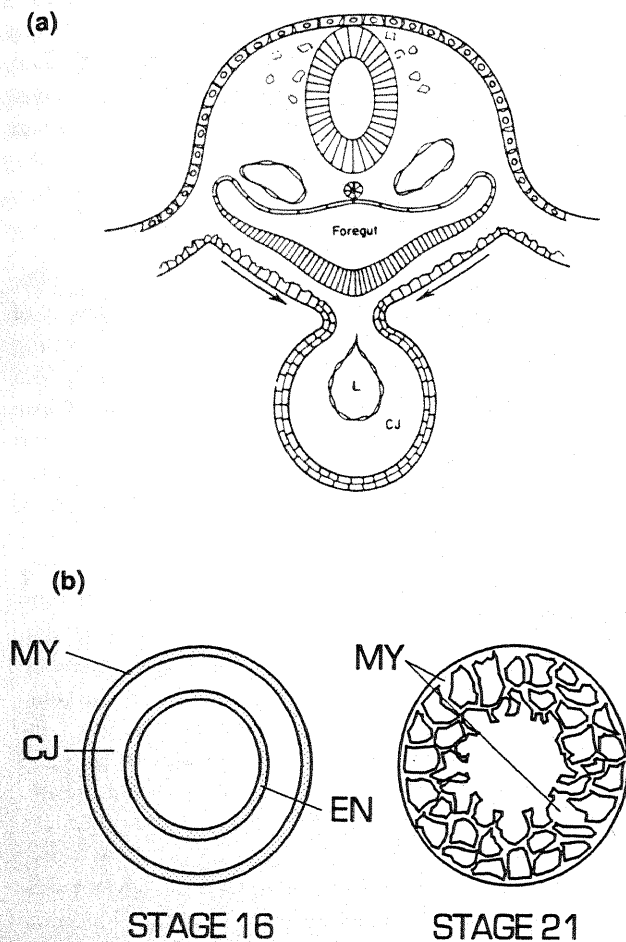


Fig 47. (a) Heart tube in early embryo. [From Manasek et al. (1972)] (b) Schematic of cross section of stage 16 and 21 embryonic chick heart. MY: myocardium; CJ: cardiac jelly; EN: endocardium; L: lumen of ventricle.

apex, dividing the tube into the left and right ventricles, and the atria form at the ends of the tube. Septation occurs between stages 21 (3.5 days) and 36 (10 days). Moreover, the endocardial cushions are molded into valves beginning at stage 34 (8 days).

Several investigators have described circumferentially arranged fibers over portions of the ventricle as early as stage 10, when looping begins (Nakamura et al., 1980; Manasek et al., 1984a; Itasaki et al., 1991; Shiraishi et al., 1992). Little is known, however, about how the fibers become aligned to form the highly ordered pattern of the mature LV (Fig 45b). Note that development of cardiac muscle is similar to that of skeletal muscle (Sec 6.2.4), except cardiac myoblasts do not fuse.

Although there are marked differences between the shapes of the embryonic and mature hearts, their physiologic characteristics are remarkably similar (Clark, 1989; Keller et al., 1990, 1991). The ventricular pressure-time curve and the pressure-volume loops in the embryo have the distinctive forms of those measured in the mature heart. The peak systolic pressure in the stage 16 embryonic chick heart is only about 1 mmHg, however, as compared to about 120 mmHg in the mature LV. Furthermore, like the mature heart, the embryonic heart can adjust its mass (by hyperplasia) in response to changes in load. In the chick, increasing ventricular pressure by banding the outflow tract increases ventricular mass without altering the process of ventricular septation (Clark et al., 1989). Thus, overloading the embryonic heart affects the rate of growth but not the rate of morphogenesis.

**Cardiac looping.** The process of looping is vital to normal cardiac morphogenesis; if it is abnormal, serious structural defects result. This process, therefore, has received much attention from investigators.

Cardiac looping involves biomechanical forces. Various

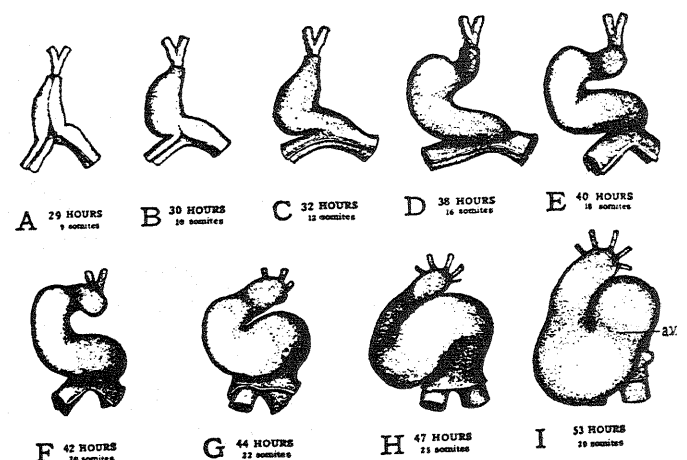


Fig 48. Schematic of the cardiac looping process in the chick embryo. [From Patten (1951) with permission of McGraw-Hill, Inc.]

hypotheses have been proposed for the looping mechanism, including:

1. *Constrained growth.* Patten (1922) suggested that the cardiac tube is forced to bend because its length grows faster than the space in which it is contained. In experiments, however, the heart loops when explanted and grown unconstrained in culture (Butler, 1952; Manning and McLachlan, 1990).
2. *Differential growth.* If cells along one side of the ventricle divide faster than cells along the opposite side, the tube will be forced to bend. However, Stalsberg (1969) found that the spatial variation in mitotic rate is not sufficient to cause looping. The similar mechanism of differential cell death also has been ruled out (Stalsberg, 1970).
3. *Cell shape change.* Using scanning electron microscopy, Manasek et al. (1972) observed that the myocytes of the inner curvature of the looped heart are tall radially and narrow longitudinally, while those at the outer curvature are flattened. Whether these shape changes are generated actively or passively is unknown. If the cells actively modify their shapes, this process could produce looping. However, on disrupting the microtubules of cardiac cells with colchicine, Icardo and Ojeda (1984) found that hearts still loop even though the cells round up, suggesting that the shape changes are passive.
4. *Cardiac jelly pressure with longitudinal constraint.* Manasek et al. (1984b) suggested that the dorsal mesocardium (DM), which forms a longitudinal ridge along the outside of the early tubular heart (Fig 49), acts as a stiffener, forcing the tube to bend as it inflates due to pressurization of the CJ. To sup-

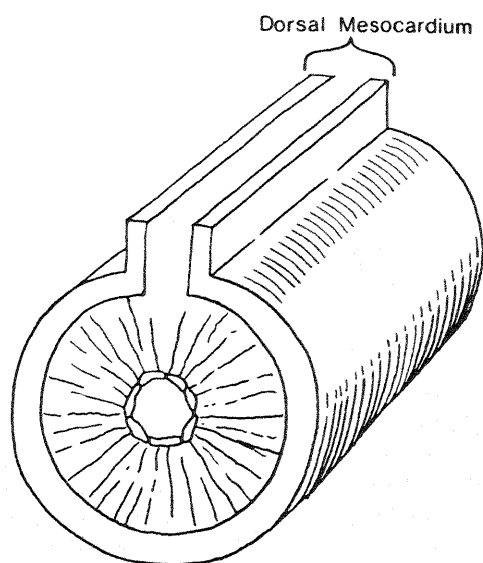


Fig 49. Schematic of cardiac tube with dorsal mesocardium. [From Manasek (1983)]

port their theory, Manasek et al. (1984a) measured the pressure in the CJ and found it to be about 0.5 mmHg. Moreover, they showed that a pressurized cylindrical latex membrane with a longitudinal stiffener and a system of relatively stiff spiral fibers bends and twists in a manner similar to that of the actual ventricle (Manasek et al., 1984b). Although these data indicate that CJ pressure is potentially a strong morphogenetic force, Baldwin and Solursh (1989) found that degrading the CJ with hyaluronidase does not prevent looping of hearts grown in culture.

Thus, none of the above hypotheses is consistent with all available experimental evidence, and so the mechanism of cardiac looping remains largely a mystery.

Any model for cardiac looping must account for the following experimental observations:

1. The heart loops when removed from the embryo and grown in culture with no loads (Butler, 1952; Manning and McLachlan, 1990).
2. Arresting myocardial contraction does not prevent looping (Manasek and Monroe, 1972).
3. Inhibiting contractile protein synthesis or myofibril assembly (cytodifferentiation) prevents looping (Manasek et al., 1978).
4. Globally disrupting actin filaments with cytochalasin B after differentiation prevents looping. Local application of the chemical to the left side of the caudal part of the ventricle results in (normal) looping to the right, but application to the right side results in looping to the left (Itasaki et al., 1991).
5. Disrupting microtubules does not prevent looping (Icardo and Ojeda, 1984).
6. Dissolving the cardiac jelly does not prevent looping (Baldwin and Solursh, 1989).
7. Growth is relatively uniform over the ventricle during looping (Stalsberg, 1969).
8. The DM is located along the inner curvature of the looped ventricle (Butler, 1952).
9. The myocardium of the inner curvature of the looped ventricle thickens, while that of the outer curvature thins (Manasek et al., 1972).
10. The actin filaments in the looped ventricle are oriented circumferentially near the inner curvature and randomly near the outer curvature (Itasaki et al., 1989).

Although it seems clear that looping involves mechanical forces, few biomechanical models have been proposed for this process. Recently, Taber et al. (1995) proposed



two models. The first model is based on the hypothesis that an initial tension in or near the DM drives the bending as the cardiac tube pulls away from the embryo. To relieve the bending stresses in the tube, the myocytes change shape passively, and then they deform actively to continue the process to completion of a full loop. In the second model, contraction of the circumferentially arranged actin microfilaments produces circumferential compression and longitudinal expansion (due to incompressibility) of the myocytes. The DM locally constrains the longitudinal deformation, forcing the tube to bend. In both cases, the DM occupies the inner curvature of the bent tube. A bending analysis of beams composed of two layers representing the DM and the ventricular myocardium showed that the models are consistent with most of the known data listed above. These potential looping mechanisms, however, must be tested experimentally.

## 7.2 Arteries

### 7.2.1 Structure and function

Arteries conduct blood from the heart to the tissues and peripheral organs. The LV pumps blood into the **aorta**, and the RV pumps blood into the **pulmonary artery**. These main conduits branch into smaller and smaller vessels, and the relatively narrow **arterioles** actively alter their diameters to regulate blood flow. At the smallest end of the spectrum are the **capillaries**, where gas exchange takes place. Veins then carry the blood back to the heart.

Arteries are viscoelastic tubes composed of three layers: the intima, media, and adventitia (Fung, 1993). The inner layer is the **intima**, which consists primarily of an endothelium and a basement membrane. The **media**, the middle layer, contains concentric layers of spiraling smooth muscle cells tied together by collagen and elastin. And the **adventitia** is a membrane of connective tissue on the outside. The material properties of various arteries have been studied fairly extensively (Fung, 1993).

### 7.2.2 Residual stress and strain

Vaishnav and Vossoughi (1983; 1987) and Fung (1984) first demonstrated the existence of residual stress in arteries. As discussed in Sec 3.1, they did this by cutting unloaded arteries and observing the resulting deformation. First, they cut the vessel perpendicular to the longitudinal axis to obtain a short cylinder virtually free of longitudinal residual stress. Then, after a radial transmural cut to relieve circumferential stresses, the cross section opened immediately into a sector, giving the first-approximation "zero stress" configuration (Fig 50). The deformation required to restore the unloaded section prior to the radial cut defines the "residual strain."

To explore whether a single transmural cut is sufficient to relieve the residual stresses, Fung and Liu (1989) made more transmural cuts and found little additional

deformation. They, therefore, concluded that one cut is enough. Recently, however, Vossoughi et al. (1993) cut along the midline of the open sector, and the inside segment opened even more, while the outside segment closed substantially. These results indicate that the initial residual strain is greater than previously thought and that the deformation following a radial cut is more complex than simple bending of a curved beam.

For an artery modeled as a thick-walled, incompressible, homogeneous tube subjected to an internal blood pressure, finite elasticity theory predicts large stress concentrations in the inner layers if the unloaded configuration is assumed to be stress-free (Fig 51a) (Chuong and Fung, 1983). This behavior is due to the large strains that decrease from intima to adventitia coupled with the highly nonlinear arterial constitutive relations. Realizing that an efficient load-bearing structure would exhibit more uniform stresses, Vaishnav and Vossoughi (1983; 1987) and Fung (1984; 1991) hypothesized that one function of residual stress is to reduce these stress concentrations. Since the circumferential residual strains in a section that opens when cut are compressive in the inner layers and tensile in the outer layers, these residual strains tend to make the transmural strain distribution

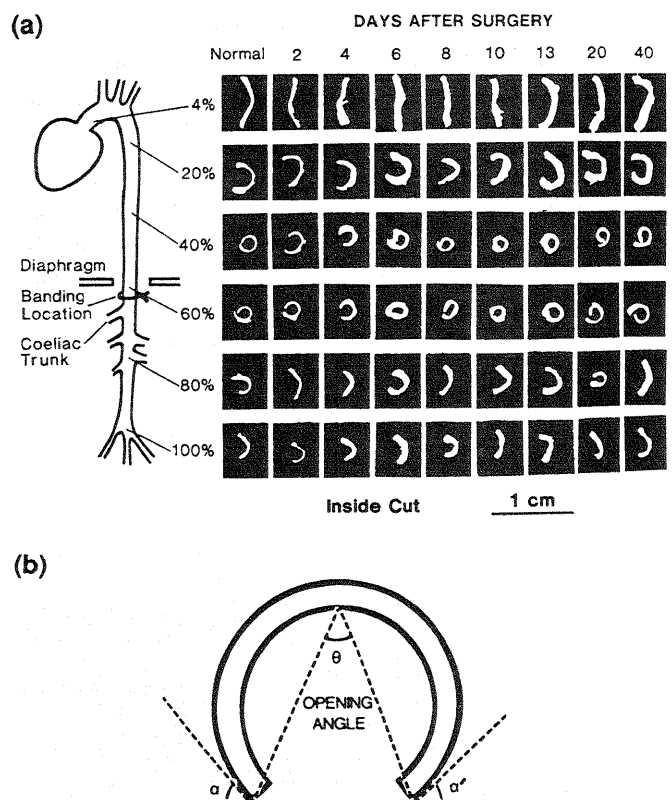


Fig 50. (a) Cross sections of rat aorta following a radial cut at different times after banding. The effect of banding is to increase arterial pressure proximal to the band and decrease it distally. (b) Schematic of arterial cross section in zero-stress configuration showing the opening angle  $\theta$ . [From Fung and Liu (1989), reproduced with permission. *Circulation Research*, copyright 1989 American Heart Association.]



in the loaded artery more uniform. Including residual stress in their model, Chuong and Fung (1986b; 1986a) found a large decrease in the stress gradient across the wall of the loaded artery (Fig 51b).

Much of the recent work of Fung and coinvestigators has involved studies of residual strain in the cardiovascular system. To characterize the magnitude of residual circumferential strain, they use an opening angle  $\theta$  (Fig 50b). These researchers have found that  $\theta$  depends on the location in the vascular system (Fig 50a) (Liu and Fung, 1988; Fung and Liu, 1991, 1992), the circumferential location of the radial cut (Liu and Fung, 1988), and the species (Han and Fung, 1991a). The largest opening angles, which can be more than  $360^\circ$ , generally occur in regions of large curvature, such as the aortic arch and the pulmonary artery trunk (Liu and Fung, 1988; Fung

and Liu, 1991). Moreover, altering the contracture state of the smooth muscle has little effect on  $\theta$ , indicating that the source of the residual stress is the connective tissue (Liu and Fung, 1988; Fung and Liu, 1991; Han and Fung, 1991a). These authors also pointed out that since the smooth muscle is distributed fairly symmetrically about the neutral surface, it would be expected to have little influence on bending of the cut section.

The residual strains in arteries, compressive on the inside and tensile on the outside, can be produced by differential growth, with the inner layers growing faster than the outer layers. This view is consistent with the concept of stress-induced growth, since the inner layers are more highly stressed than the outer layers (Fung, 1990, 1991) (see Fig 51).

Stress-induced growth also offers an explanation for the increased residual strain found in regions of large curvature. As Fung and Liu (1989; 1991) pointed out, the stresses in a pressurized curved tube vary around the circumference, with the peak wall stress occurring at the inner curvature and increasing with the degree of curvature. This asymmetry has two consequences. First, the opening angle would depend on the circumferential position of the cut. Second, additional growth due to the large stresses would induce a larger opening angle. Both of these features have been found experimentally (Liu and Fung, 1988; Fung and Liu, 1991). Further evidence for stress-induced growth in arteries is discussed below.

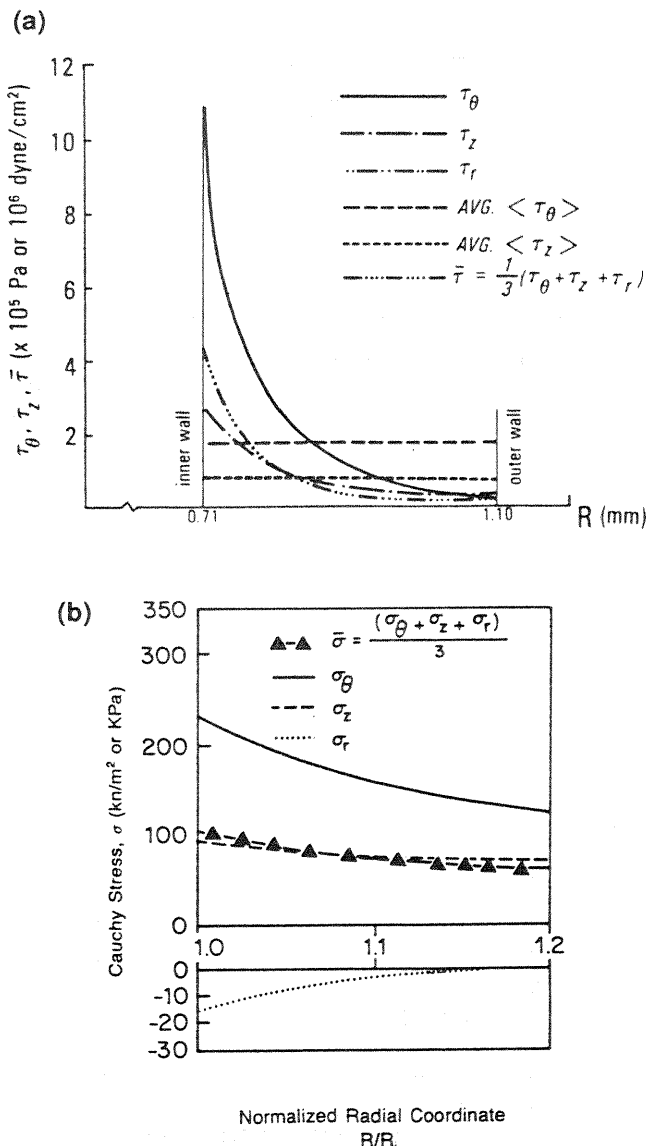


Fig 51. Computed stress distributions in artery with internal pressure of 120 mmHg: (a) without and (b) with residual strain included. [From Chuong and Fung (1983; 1986b)]

### 7.2.3 Hypertrophy

Blood flowing through an artery exerts primarily two types of stresses on the wall: pressure and shear. The directly applied pressure on the intima also induces circumferential stretching of the artery as it expands. This section considers the response of the vessel to pressure loads, with shear discussed in the following section.

Hypertension long has been associated with cardiovascular disease. It is generally agreed that hypertension induces arterial walls to thicken with little change in lumen diameter (Wiener et al., 1977; Matsumoto and Hayashi, 1994), but the mechanism of the thickening remains controversial. In particular, *in vivo* studies disagree on whether the response is due primarily to hypertrophy or to hyperplasia of the smooth muscle in the media. Bevan (1976), Bevan et al. (1976), and Owens and Reidy (1985) found mostly hyperplasia, Olivetti et al. (1980) found mostly hypertrophy, and Wiener et al. (1977) found both. As in the studies of cardiac hypertrophy (Sec 7.1.3), these conflicting results are likely due to the differences in the vessel type, the cause of the overloading, and the duration and magnitude of the hypertension.

When the loading on an artery changes, the medial smooth muscle remodels. Using aortic medial cells cultured on elastic sheets, Leung et al. (1976) and Dartsch et al. (1986) examined the response to cyclic stretch. Leung et al. (1976) found an increased collagen content with no increase in mitotic rate, while Dartsch et

al. (1986) focused on changes in cellular orientation. In the latter study, the cells remained oriented randomly when stretched at an amplitude of 2%. For 5% and 10% stretch, however, the cells aligned about  $50^\circ$ – $70^\circ$  and  $70^\circ$ – $90^\circ$ , respectively, relative to the direction of stretch. These orientations are similar to those generally found relative to the circumferential (stretch) direction in the middle and inner layers of the media, respectively, consistent with the fact that hoop strain increases from the outside to the inside of the wall. Recent data suggest that the remodeling that accompanies hypertrophy in the aorta keeps circumferential stress-strain relations near normal (Vaishnav et al., 1990; Matsumoto and Hayashi, 1994).

If arterial growth is stress-modulated, then changes in loading conditions should alter residual stress, with changes in residual strain reflecting nonuniform growth across the wall. Following experimentally induced hypertension, Fung and Liu (1989) and Liu and Fung (1989) measured the opening angle as a function of time and position along the aorta, and Fung and Liu (1991) did the same in the pulmonary artery. In these experiments, the blood pressure and wall thickness increased nearly monotonically to equilibrium states (see Fig 52a for the carotid artery). The opening angle, however, first increased rapidly to a peak and then dropped more slowly toward an asymptotic value (Fig 52b). In the rat pulmonary artery, Fung and Liu (1991) correlated the initial increase in  $\theta$  with intimal swelling and thickening and the subsequent decrease in  $\theta$  with a thickening adventitia. This remodeling occurs within a period of hours or days, rather than the months that bones take.

Theoretically, the increased residual strains in hypertension counteract an increased stress concentration due to the higher pressure. To further investigate the possibility of stress-regulated growth, Liu and Fung (1989) computed the mean hoop stress, which followed a time-course similar to that of the opening angle (Fig 52c). Of significance is that the wall stress at growth equilibrium was nearly the same as the original stress. These results are consistent with those obtained by Matsumoto and Hayashi (1994), suggesting that arterial hypertrophy is a response to abnormally high wall stress.

#### 7.2.4 Atherogenesis

Atherosclerosis is a disease of arteries that features a narrowing of the vascular lumen. The consequent impediment to blood flow can cause myocardial or cerebral ischemia and, if severe enough, myocardial infarction or stroke. Growth is an important factor in the disease process, since the formation of occlusive lesions requires proliferation of smooth muscle cells that migrate from the media into the intima (Ross, 1990).

The trigger for the formation of atherosclerotic lesions is not known. Several features, however, suggest that fluid mechanical effects play a role in atherogenesis, including (1) the local nature of the disease; (2) geometry-

dependent risk factors, such as vessel branching architecture; and (3) the high incidence of lesions in regions of low shear (Nerem, 1992). Most studies of flow effects have focused on the vascular endothelium, since this layer experiences direct hemodynamic loads. Moreover, most investigators have considered only the shear stress  $\tau$  at the blood-endothelial interface. Only recently have the stresses within the cells themselves and the forces transmitted to the media been examined (Fung and Liu, 1993).

This section reviews some of the main findings of fluid mechanical studies. Other important factors, such as biochemistry, have been discussed by Ross (1990) and Nerem (1992).

There is considerable evidence that arteries respond to the shear imposed by blood flow (Nerem, 1992, 1993). In fact, the entire arterial tree may be designed for a single optimal shear stress, except possibly near sharp

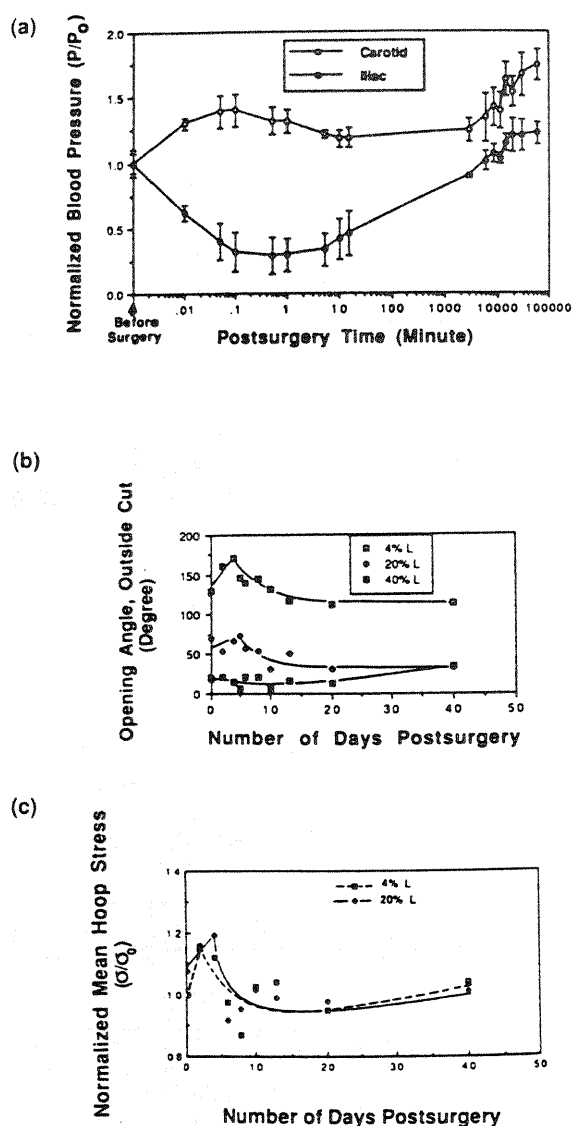


Fig 52. Changes in mechanical parameters with time following banding in the rat aorta. (a) Blood pressure. (b) Opening angle. (c) Mean hoop stress. [From Liu and Fung (1989)]

turns and bifurcations, where higher values of  $\tau$  can occur. For instance, estimating the shear stress in large arteries, arterioles, and capillaries, Kamiya and Togawa (1980) found that  $\tau$  falls within the relatively narrow range of 10–22 dyn/cm<sup>2</sup> throughout the arterial system. In addition, these researchers studied the response of the canine carotid artery to chronic alterations in flow rate. For flow below normal and up to four times the normal rate, the artery adjusted its diameter through growth or atrophy (over 6–8 months) to bring  $\tau$  back to near normal levels (Fig 53). The vessel, however, did not adapt to larger flow rates.

Many investigators feel that the endothelium is largely responsible for regulating flow-dependent adaptation of arteries. Thus, several *in vitro* studies have examined growth and remodeling of endothelial cells exposed to various flow environments (Nerem, 1992, 1993). As for growth, laminar flow, whether steady or oscillating, induces no increase in cell division rate for  $\tau$  as large as 15 dyn/cm<sup>2</sup> (Dewey et al., 1981; Davies et al., 1986). In fact, Levesque et al. (1990) found that the mitotic rate actually *decreases* as  $\tau$  increases (Fig 54), and pulsatile flow enhances this effect.

Remodeling is observed consistently in vascular endothelial cells exposed to flow. When  $\tau$  is greater than a critical value (about 5 dyn/cm<sup>2</sup>), the cells elongate and align in the direction of flow (Fig 55a) (Nerem et al., 1981; Dewey et al., 1981; Levesque and Nerem, 1985; Levesque et al., 1986; Ives et al., 1986; Helmlinger et al., 1991). Moreover, the cellular orientations follow the complex flow patterns near branches (Nerem et al., 1981; Levesque et al., 1986), and the magnitude of the elongation increases with  $\tau$  (Levesque and Nerem, 1985; Levesque et al., 1986) and depends on the nature of the flow (Helmlinger et al., 1991). Recall that stretched endothelial cells

align perpendicular to the direction of stretch (Sec 4.5), which also corresponds to orientation along the flow direction in an artery. Thus, the effects of fluid shear and wall stretch reinforce each other, yielding a geometry that likely reduces drag on the flow of blood (Ives et al., 1986).

The available evidence suggests that epithelial alignment is an active process, rather than a passive deformation due to the shear stress. Cells exposed to flow, for example, elongate *before* they reorient (Levesque and Nerem, 1985). The following experimental findings implicate actin microfilaments in this process:

1. Stress fibers (aligned microfilaments) form in the cells and align with the direction of flow (Fig 55b) (Dewey et al., 1981; Wong et al., 1983; White et al., 1983; White and Fujiwara, 1986; Franke et al., 1984).
2. Arterial stress fibers are thicker in hypertensive than in normotensive rats (White et al., 1983).
3. Stress fibers are more numerous in regions of high shear (White and Fujiwara, 1986).
4. Elongated cells are stiffer, presumably due to cytoskeletal reorganization (Sato et al., 1987).
5. Cell proliferation slows as the cells adapt to the flow (Fig 54), possibly because the actin needed for contractile ring formation is being used for shape change instead (Levesque et al., 1990).
6. Cytochalasin B, which disrupts actin, retards the elongation (Ookawa et al., 1992) and promotes cell loss from the endothelium (Wechezak et al., 1989).

These data indicate that cellular elongation and alignment are active adaptations to maintain the structural

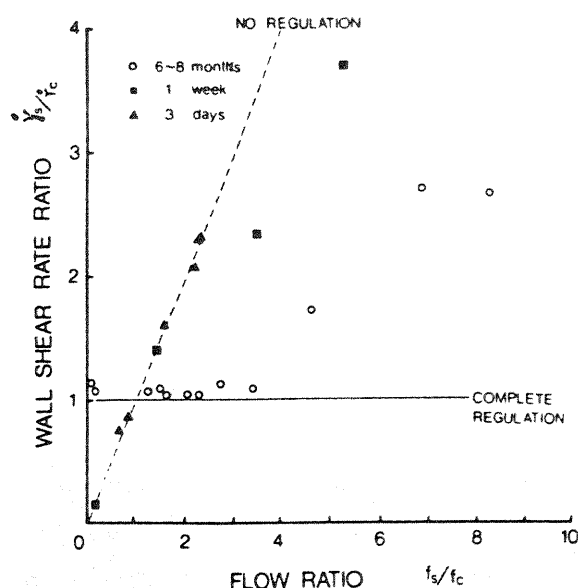


Fig 53. Adaptation of artery to chronic changes in flow rate. The shear strain rate returns to near normal levels for flow rates up to about four times normal. [From Kamiya and Togawa (1980)]

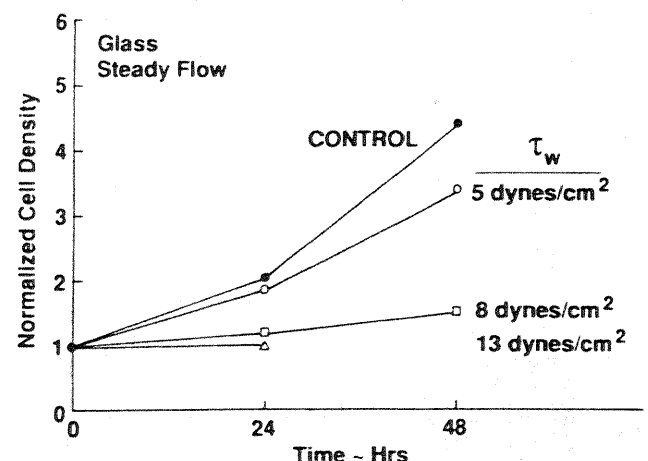


Fig 54. Effect of shear stress on hyperplasia due to flow over bovine aortic endothelium. [Reprinted from Levesque MJ, Nerem RM, and Sprague EA (1990), Vascular endothelial cell proliferation in culture and the influence of flow, *Biomaterials* 11, 702–707, copyright 1990, with kind permission from Elsevier Science Ltd, The Boulevard, Langford Lane, Kidlington OX5 1GB, UK.]

integrity and adhesion of the cells in the face of potentially damaging shear stresses. In this way, the cytoskeletal reorganization may help protect the arterial endothelium from injury (Franke et al., 1984), which has been suggested as a possible stimulus for atherogenesis. This idea, however, seems at odds with the observation that lesions form most often in regions of low shear (Nerem, 1992). Thus, much remains to be learned about atherogenesis.

### 7.2.5 Morphogenesis

The developing circulatory system transports nutrients and oxygen to the embryo. Blood vessels form in two ways (Fig 56) (Risau, 1991). In **vasculogenesis**, mesenchymal cells aggregate into **angiogenic clusters**. These clusters then hollow out to form tubes, with the inner cells of each tube flattening into an endothelial lining and the outer cells becoming smooth muscle. Cells remaining in the lumen differentiate into embryonic blood cells. In **angiogenesis**, new vessels sprout from pre-existing vessels. While vasculogenesis apparently is restricted to embryonic development, angiogenesis can oc-

cur throughout life (Risau, 1991). In the embryo, the growing vessels eventually merge, forming a capillary network that drains into two viteline veins leading to the heart (Gilbert, 1991).

Waxman (1981) presented a biomechanical model of a growing blood vessel. His model is a cylindrical elastic shell with fixed ends, embedded in a viscous fluid that represents the surrounding tissue. The analysis is based on thin shell theory, with orthotropic growth included by a specified uniform growth pressure. In addition to a solid arterial wall, the author examined the case of a wall composed of two thin layers separated by a fluid, i.e., an "inflated shell." Due to the restricted motion of the ends, longitudinal growth induces buckling, and Waxman discussed several possible modes that are observed *in vivo* (Fig 57). A buckling analysis of the varicose mode (Fig 57b) revealed that the dominant (dimensionless) wave number is

$$k \cong \begin{cases} (12/h^2)^{1/4} & \text{for solid shells} \\ (4/h^2)^{1/4} & \text{for inflated shells} \end{cases} \quad (58)$$

where  $h$  is the nondimensional wall thickness. Comparing this prediction with experimental measurements indicated that the inflated shell is a more realistic representation of the blood vessel.

## 8 FUTURE RESEARCH DIRECTIONS

Although the mechanisms of growth, remodeling, and morphogenesis have received considerable attention for many years, several aspects of these processes remain poorly understood. Theoretical models help sort out the effects of the various factors involved, especially since

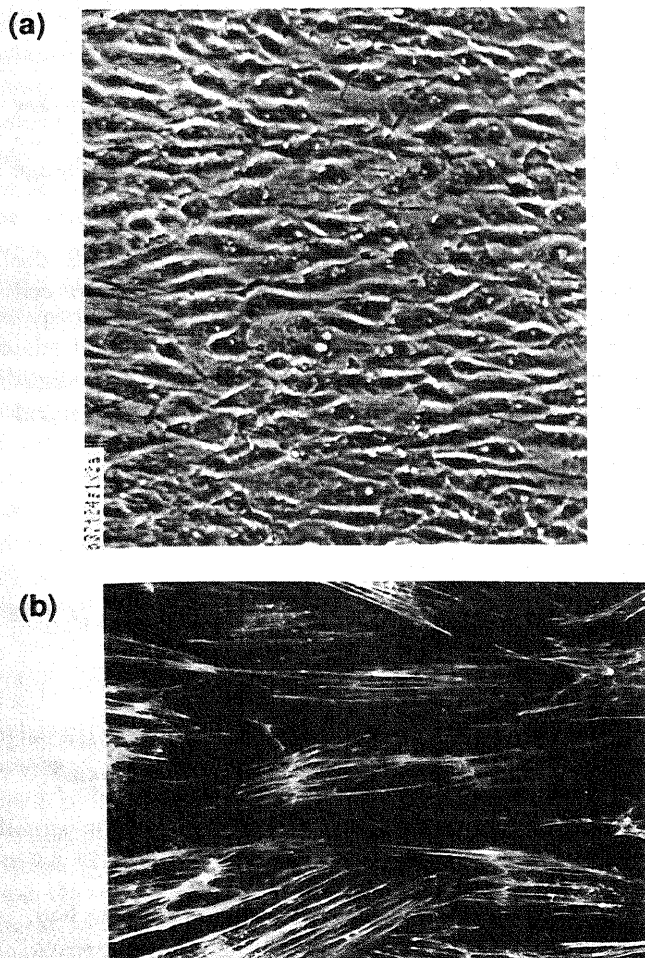


Fig 55. (a) Micrographs of bovine aortic endothelial cells subjected to steady flow from left to right for 24 hours. (b) Actin microfilaments in cells subjected to steady flow from left to right. [From Helmlinger et al. (1991)]

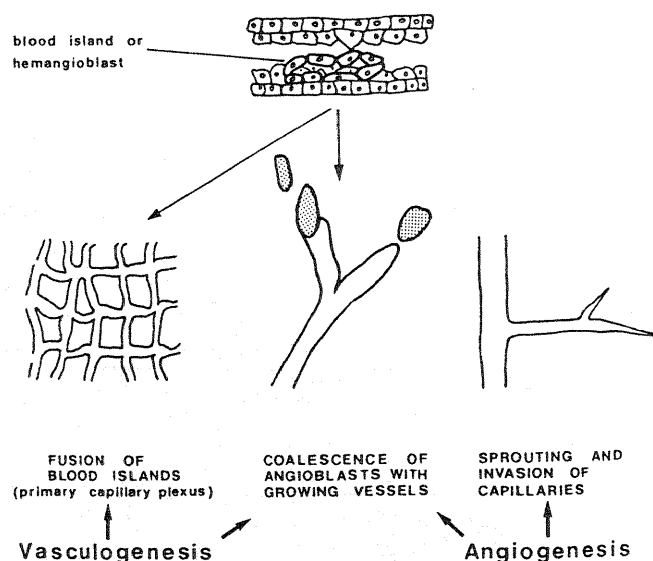


Fig 56. Two types of blood vessel formation in the embryo. [From Risau (1991), reproduced with permission, S Karger AG, Basel.]

some quantities, such as stress, cannot be measured directly. Models, however, require careful experimental verification, and so a combined theoretical/experimental approach is necessary to gain a full understanding of these subjects. To date, with the possible exception of bone, research in this field has been dominated largely by experimental studies, of which this review only scratches the surface. Although the length of this article might indicate otherwise, modeling of these processes is still in its infancy.

In spite of its relatively brief history, biomechanical modeling of growth, remodeling, and morphogenesis has achieved some notable successes. The theories for functional adaptation of bones are excellent examples of the power and utility of theoretical models. In less than 20 years, models for bone growth and remodeling have evolved to a quite advanced state, and they already are being used to help design implants. It is remarkable that such a simple growth/remodeling law, i.e., a growth/remodeling rate linearly proportional to strain, can predict the behavior of such complex biomechanical processes. On the other hand,  $E = mc^2$  also is a remarkably simple formula. Thus, simplicity seems to underlie much of nature's complexity [or *vice versa*, see Cohen and Stewart (1994)].

Models also have provided insight into the biomechanics of cell movement, cell division, pattern formation, and epithelial morphogenesis. These models, however, generally have not yet been validated through carefully controlled experiments. In addition, the mechanics of organogenesis has received little attention.

Cardiovascular disease is the leading cause of death in the United States. Engineers have contributed to experimental and clinical investigations of the problem, especially studies of cardiac hypertrophy, myocardial infarction, and atherosclerosis. Modeling of adaptive mechanisms in the cardiovascular system, however, is just beginning and is a lucrative topic for future research.

One problem facing biomechanical models in general is the relative lack of reliable information on material properties. This problem is especially acute in studies of growth, remodeling, and morphogenesis, since these

properties can change with time. Little is known about their temporal evolution, even in bone. Collecting these data will be crucial to the future success of modeling efforts.

Several vital questions remain largely unresolved concerning the mechanics of growth, remodeling, and morphogenesis. Among these are the following:

1. How do genetic and epigenetic factors interact?
2. What biomechanical factors modulate these processes?
3. What biomechanical principle(s) governs functional adaptation?

As discussed in this review, answers to each of these questions have been proposed. The available data support some of the answers to a certain extent, but many controversies remain, e.g., stress-modulated versus strain-modulated growth. One focus of future work should be to test these theories rigorously through carefully designed experiments that yield *quantitative* results.

We conclude with a final remark. Although it would be intellectually satisfying to find a law for functional adaptation that is valid for all biological tissues in all organisms from embryo to adult, a universal law may not exist. The responses of cells, tissues, and organs to their biomechanical environment may be as varied as their forms and functions. Unlocking the secrets of nature is not always as straightforward as one would like.

## ACKNOWLEDGMENTS

This research was supported by an NIH Specialized Center of Research (SCOR) in Pediatric Cardiovascular Diseases (P50 HL51498) at the University of Rochester and by NIH grant R01 HL46367. The author thanks Charlene Taber for her editorial assistance.

## 9 REFERENCES

- Abercrombie M, Heaysman JEM, and Pegrum SM (1970). The locomotion of fibroblasts in culture, *Exp Cell Res* **62**, 389-398.
- Akkas N (1980a). Letter to the editor, *J Biomech* **13**, 459-460.
- Akkas N (1980b). On the biomechanics of cytokinesis in animal cells, *J Biomech* **13**, 977-988.
- Akkas N (1981). A viscoelastic model for cytokinesis in animal cells, *J Biomech* **14**, 621-631.
- Akkas N (1987). A mechanician's view of the biomechanics of cytokinesis, in *Biomechanics of Cell Division*, N Akkas, Ed, Plenum Press, New York, 347-371.
- Alberch P (1980). Ontogenesis and morphological diversification, *Am Zool* **20**, 653-667.
- Alberch P (1982). Developmental constraints in evolutionary processes, in *Evolution and Development*, JT Bonner, Ed, Springer-Verlag, New York, 313-332.
- Alt W (1990). Mathematical models and analyzing methods for the lamellipodial activity of leukocytes, in *Biomechanics of Active Movement and Deformation of Cells*, N Akkas, Ed, Springer-Verlag, Berlin, 403-422.

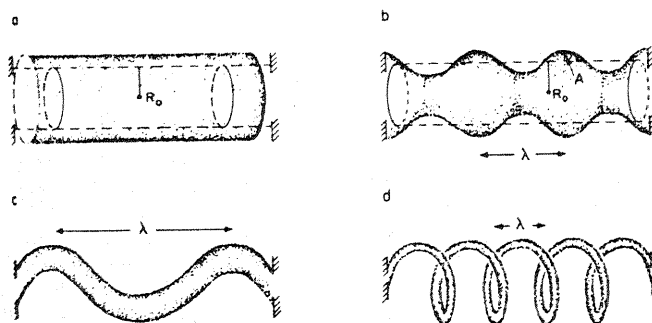


Fig 57. Modes of growth for blood vessel with fixed ends. [From Waxman (1981)]



- Anversa P, Olivetti G, Meggs LG, Sonnenblick EH, and Capasso JM (1993). Cardiac anatomy and ventricular loading after myocardial infarction, *Circulation* **87** (Suppl. 7), VII-22-VII-27.
- Ascenzi A (1993). Biomechanics and Galileo Galilei, *J Biomech* **26**, 95-100.
- Baldwin HS and Solursh M (1989). Degradation of hyaluronic acid does not prevent looping of the mammalian heart in situ, *Dev Biol* **136**, 555-559.
- Bard JBL and Ross ASA (1982). The morphogenesis of the ciliary body of the avian eye. I. Lateral cell detachment facilitates epithelial folding, *Dev Biol* **92**, 73-86.
- Bassett CAL (1965). Electrical effects in bone, *Sci Am* **213**(4), 18-25.
- Beaupre GS, Orr TE, and Carter DR (1990a). An approach for time-dependent bone modeling and remodeling—Application: a preliminary remodeling simulation, *J Orthop Res* **8**, 662-670.
- Beaupre GS, Orr TE, and Carter DR (1990b). An approach for time-dependent bone modeling and remodeling—Theoretical development, *J Orthop Res* **8**, 651-661.
- Bekesy GV (1960). *Experiments in Hearing*, McGraw Hill, New York.
- Belintsev BN, Belousov LV, and Zarsky AG (1987). Model of pattern formation in epithelial morphogenesis, *J Theor Biol* **129**, 369-394.
- Belousov LV, Dorfman JG, and Cherdantzev VG (1975). Mechanical stresses and morphological patterns in amphibian embryos, *J Embryol Exp Morph* **34**, 559-574.
- Belousov LV (1980). The role of tensile fields and contact cell polarization in the morphogenesis of amphibian axial rudiments, *Roux's Arch Dev Biol* **188**, 1-7.
- Belousov LV, Lakirev AV, and Naumidi II (1988). The role of external tensions in differentiation of xenopus laevis embryonic tissues, *Cell Diff Dev* **25**, 165-176.
- Belousov LV and Lakirev AV (1991). Generative rules for the morphogenesis of epithelial tubes, *J Theor Biol* **152**, 455-468.
- Bevan RD (1976). An autoradiographic and pathological study of cellular proliferation in rabbit arteries correlated with an increase in arterial pressure, *Blood Vessels* **13**, 100-128.
- Bevan RD, Van Marthens E, and Bevan JA (1976). Hyperplasia of vascular smooth muscle in experimental hypertension in the rabbit, *Circ Res* **38** (Suppl. 2), II-58-II-62.
- Blenman PR, Carter DR, and Beaupre GS (1989). Role of mechanical loading in the progressive ossification of a fracture callus, *J Orthop Res* **7**, 398-407.
- Booth FW (1982). Effect of limb immobilization on skeletal muscle, *J Appl Physiol* **52**, 1113-1118.
- Bouvier M (1989). The biology and composition of bone, in *Bone Biomechanics*, SC Cowin, Ed, CRC Press, Boca Raton, FL, 1-13.
- Bovendeerd PHM, Arts T, Huyghe JM, van Campen DH, and Reneman RS (1992). Dependence of local left ventricular wall mechanics on myocardial fiber orientation: a model study, *J Biomech* **25**, 1129-1140.
- Brodland GW and Clausi DA (1994). Embryonic tissue morphogenesis modelled by FEM, *J Biomech Eng* **116**, 146-155.
- Brown TD, Pedersen DR, Gray ML, Brand RA, and Rubin CT (1990). Toward an identification of mechanical parameters initiating periosteal remodeling: a combined experimental and analytic approach, *J Biomech* **23**, 893-905.
- Buchacek K (1990). Nonequilibrium bone remodelling: changes of mass density and of the axes of anisotropy, *Int J Eng Sci* **28**, 1039-1044.
- Buck RC (1980). Reorientation response of cells to repeated stretch and recoil of the substratum, *Exp Cell Res* **127**, 470-474.
- Burger EH, Klein-Nulend J, and Veldhuijzen JP (1991). Modulation of osteogenesis in fetal bone rudiments by mechanical stress in vitro, *J Biomech* **24** (Suppl. 1), 101-109.
- Burnside B (1973). Microtubules and microfilaments in amphibian neurulation, *Am Zool* **13**, 989-1006.
- Burr DB, Martin RB, Schaffler MB, and Radin EL (1985). Bone remodeling in response to in vivo fatigue microdamage, *J Biomech* **18**, 189-200.
- Burrage K (1981). Are stress fibers contractile? *Nature* **294**, 691-692.
- Burton RR (1972). Heart growth and size in homeotherms, in *Regulation of Organ and Tissue Growth*, RJ Goss, Ed, Academic Press, New York, 101-125.
- Butler JK (1952). An experimental analysis of cardiac loop formation in the chick, MS Thesis, University of Texas.
- Carew TE and Covell JW (1979). Fiber orientation in hypertrophied canine left ventricle, *Am J Physiol* **236**, H487-H493.
- Carter DR (1982). The relationship between in vivo strains and cortical bone remodeling, *CRC Crit Rev Biomed Eng* **8**, 1-28.
- Carter DR (1984). Mechanical loading histories and cortical bone remodeling, *Calcif Tissue Int* **36**, S19-S24.
- Carter DR (1987). Mechanical loading history and skeletal biology, *J Biomech* **20**, 1095-1109.
- Carter DR, Fyhrie DP, and Whalen RT (1987a). Trabecular bone density and loading history: regulation of connective tissue biology by mechanical energy, *J Biomech* **20**, 785-794.
- Carter DR, Orr TE, Fyhrie DP, and Schurman DJ (1987b). Influences of mechanical stress on prenatal and postnatal skeletal development, *Clin Orthop* **219**, 237-250.
- Carter DR, Blenman PR, and Beaupre GS (1988). Correlations between mechanical stress history and tissue differentiation in initial fracture healing, *J Orthop Res* **6**, 736-748.
- Carter DR, Orr TE, and Fyhrie DP (1989). Relationships between loading history and femoral cancellous bone architecture, *J Biomech* **22**, 231-244.
- Carter DR, Wong M, and Orr TE (1991). Musculoskeletal ontogeny, phylogeny, and functional adaptation, *J Biomech* **24**, 3-16.
- Carter DR and Wong M (1988). The role of mechanical loading histories in the development of diarthrodial joints, *J Orthop Res* **6**, 804-816.
- Chamay A and Tschantz P (1972). Mechanical influences in bone remodeling. experimental research on Wolff's law, *J Biomech* **5**, 173-180.
- Chen WT (1981). Surface changes during retraction-induced spreading of fibroblasts, *J Cell Sci* **49**, 1-13.
- Chuong CJ and Fung YC (1983). Three-dimensional stress distribution in arteries, *J Biomech Eng* **105**, 268-274.
- Chuong CJ and Fung YC (1986a). Residual stress in arteries, in *Frontiers in Biomechanics*, GW Schmid-Schonbein, SL-Y Woo, and BW Zweifach, Eds, Springer, New York, 117-129.
- Chuong CJ and Fung YC (1986b). On residual stresses in arteries, *J Biomech Eng* **108**, 189-192.
- Clark EB (1989). Growth, morphogenesis, and function: the dynamics of cardiac development, in *Fetal, Neonatal, and Infant Heart Disease*, JH Moller, W Neal, and J Lock, Eds, Appleton-Century-Crofts, New York, 1-17.
- Clark EB, Hu N, Frommelt P, Vandekieft GK, Dummett JL, and Tomanek RJ (1989). Effect of increased pressure on ventricular growth in the stage 21 chick embryo, *Am J Physiol* **257**, H55-H61.
- Clark EB and Van Mierop LHS (1989). Development of the cardiovascular system, in *Heart Disease in Infants, Children, and Adolescents*, FH Adams, GC Emmanouilides, and TA Riemen-schneider, Eds, Williams and Wilkins, Baltimore, 2-15.
- Clausi DA and Brodland GW (1993). Mechanical evaluation of the theories of neurulation using computer simulations, *Development* **118**, 1013-1023.
- Cohen J and Stewart I (1994). *The Collapse of Chaos*, Viking, New York.
- Cooper G, Puga FJ, Zujko KJ, Harrison CE, and Coleman HN (1973). Normal myocardial function and energetics in volume-overload hypertrophy in the cat, *Circ Res* **32**, 140-148.



- Cooper G, Tomanek RJ, Ehrhardt JC, and Marcus ML (1981). Chronic progressive pressure overload of the cat right ventricle, *Circ Res* **48**, 488-497.
- Cooper G and Tomanek RJ (1982). Load regulation of the structure, composition, and function of mammalian myocardium, *Circ Res* **50**, 788-798.
- Coulombre AJ (1956). The role of intraocular pressure in the development of the chick eye, *J Exp Zool* **133**, 211-225.
- Coulombre AJ and Coulombre JL (1958). The role of intraocular pressure in the development of the chick eye. IV. Corneal curvature, *Arch Ophthalmol* **59**, 502-506.
- Cowin SC (1981). Continuum models of the adaptation of bone to stress, in *Mechanical Properties of Bone*, SC Cowin, Ed, ASME, New York, 193-210.
- Cowin SC (1983). The mechanical and stress adaptive properties of bone, *Ann Biomed Eng* **11**, 263-295.
- Cowin SC (1984). Mechanical modeling of the stress adaptation process in bone, *Calcif Tissue Int* **36**, S98-S103.
- Cowin SC, Hart RT, Balser JR, and Kohn DH (1985). Functional adaptation in long bones: establishing in vivo values for surface remodeling rate coefficients, *J Biomech* **18**, 665-684.
- Cowin SC (1986). Wolff's law of trabecular architecture at remodeling equilibrium, *J Biomech Eng* **108**, 83-88.
- Cowin SC (1987). Bone remodeling of diaphyseal surfaces by torsional loads: theoretical predictions, *J Biomech* **20**, 1111-1120.
- Cowin SC (1990). Structural adaptation of bones, *Appl Mech Rev* **43**, S126-S133.
- Cowin SC, Moss-Salentijn L, and Moss ML (1991). Candidates for the mechanosensory system in bone, *J Biomech Eng* **113**, 191-197.
- Cowin SC, Sadegh AM, and Luo GM (1992). An evolutionary Wolff's law for trabecular architecture, *J Biomech Eng* **114**, 129-136.
- Cowin SC (1993). Bone stress adaptation models, *J Biomech Eng* **115**, 528-533.
- Cowin SC, Arramon YP, Luo GM, and Sadegh AM (1993). Chaos in the discrete-time algorithm for bone-density remodeling rate equations, *J Biomech* **26**, 1077-1089.
- Cowin SC, Luo GM, Sadegh AM, and Harrigan TP (1994). On the sufficiency conditions for the stability of bone remodeling equilibrium, *J Biomech* **183**-186.
- Cowin SC and Firozbakhsh K (1981). Bone remodeling of diaphyseal surfaces under constant load: theoretical predictions, *J Biomech* **14**, 471-484.
- Cowin SC and Hegedus DH (1976). Bone remodeling I: Theory of adaptive elasticity, *J Elasticity* **6**, 313-326.
- Cowin SC and Van Buskirk WC (1978). Internal bone remodeling induced by a medullary pin, *J Biomech* **11**, 269-275.
- Cowin SC and Van Buskirk WC (1979). Surface bone remodeling induced by a medullary pin, *J Biomech* **12**, 269-276.
- Cox RW and Peacock MA (1978). The velocity field of growing ear cartilage, *J Anat* **126**, 555-566.
- Cox RW and Peacock MA (1979). The growth of elastic cartilage, *J Anat* **128**, 207-213.
- Currey JD (1968). The adaptation of bones to stress, *J Theor Biol* **20**, 91-106.
- Currey JD (1984). *The Mechanical Adaptations of Bones*, Princeton University Press, Princeton, NJ.
- Curtis ASG and Seehar GM (1978). The control of cell division by tension or diffusion, *Nature* **274**, 52-53.
- Dartsch PC, Hammerle H, and Betz E (1986). Orientation of cultured arterial smooth muscle cells growing on cyclically stretched substrates, *Acta Anat* **125**, 108-113.
- Dartsch PC and Betz E (1989). Response of cultured endothelial cells to mechanical stimulation, *Basic Res Cardiol* **84**, 268-281.
- Davies PF, Remuzzi A, Gordon EJ, Dewey CF, and Gimbrone MA (1986). Turbulent fluid shear stress induces vascular endothelial cell turnover in vitro, *Proc Natl Acad Sci USA* **83**, 2114-2117.
- Dembo M (1989). Mechanics and control of the cytoskeleton in amoeba proteus, *Biophys J* **55**, 1053-1080.
- Dembo M and Harris AK (1981). Motion of particles adhering to the leading lamella of crawling cells, *J Cell Biol* **91**, 528-536.
- Demiray H (1983). Electro-mechanical remodelling of bones, *Int J Eng Sci* **21**, 1117-1126.
- Desmond ME and Jacobson AG (1977). Embryonic brain enlargement requires cerebrospinal fluid pressure, *Dev Biol* **57**, 188-198.
- Dewey CF, Bussolari SR, Gimbrone MA, and Davies PF (1981). The dynamic response of vascular endothelial cells to fluid shear stress, *J Biomech Eng* **103**, 177-185.
- Edelman GM (1988). *Topobiology: An Introduction to Molecular Embryology*, Basic Books, New York.
- Ettensohn CA (1985). Mechanisms of epithelial invagination, *Q Rev Biol* **60**, 289-307.
- Evans E and Dembo M (1990). Physical model for phagocyte motility: local growth of a contractile network from a passive body, in *Biomechanics of Active Movement and Deformation of Cells*, N Akkas, Ed, Springer-Verlag, Berlin, 185-214.
- Ferrans VJ (1984). Cardiac hypertrophy: morphological aspects, in *Growth of the Heart in Health and Disease*, R Zak, Ed, Raven Press, New York, 187-239.
- Firozbakhsh K and Aleyaasin M (1989). The effect of stress concentration on bone remodeling: theoretical predictions, *J Biomech Eng* **111**, 355-360.
- Firozbakhsh K and Cowin SC (1980). Devolution of inhomogeneities in bone structure—Predictions of adaptive elasticity theory, *J Biomech Eng* **102**, 287-293.
- Firozbakhsh K and Cowin SC (1981). An analytical model of Pauwels' functional adaptation mechanism in bone, *J Biomech Eng* **103**, 246-252.
- Fischman DA (1972). Development of striated muscle, in *The Structure and Function of Muscle*, GH Bourne, Ed, Academic Press, New York, 75-148.
- Folkman J and Moscona A (1978). Role of cell shape in growth control, *Nature* **273**, 345-349.
- Folkow B and Neil E (1971). *Circulation*, Oxford University Press, New York.
- Ford LE (1976). Heart size, *Circ Res* **39**, 297-303.
- Frankel RP, Grafe M, Schnittler H, Seiffge D, Mittermayer C, and Drenckhan D (1984). Induction of human vascular endothelial stress fibers by fluid shear stress, *Nature* **307**, 648-649.
- Fristrom D (1988). The cellular basis of epithelial morphogenesis: a review, *Tissue & Cell* **20**, 645-690.
- Frost HM (1964). *The Laws of Bone Structure*, Charles C. Thomas, Springfield, IL.
- Frost HM (1988). Structural adaptations to mechanical usage. A proposed "three-way rule" for bone modeling, *Vet Comp Orthop Traum* **1**, 7-17.
- Fung YC (1984). *Biodynamics: Circulation*, Springer, New York.
- Fung YC (1990). *Biomechanics: Motion, Flow, Stress, and Growth*, Springer, New York.
- Fung YC (1991). What are the residual stresses doing in our blood vessels? *Ann Biomed Eng* **19**, 237-249.
- Fung YC (1993). *Biomechanics: Mechanical Properties of Living Tissues*, 2nd Ed., Springer, New York.
- Fung YC and Liu SQ (1989). Change of residual strains in arteries due to hypertrophy caused by aortic constriction, *Circ Res* **65**, 1340-1349.
- Fung YC and Liu SQ (1991). Changes of zero-stress state of rat pulmonary arteries in hypoxic hypertension, *J Appl Physiol* **70**, 2455-2470.
- Fung YC and Liu SQ (1992). Strain distribution in small blood vessels with zero-stress state taken into consideration, *Am J Physiol* **262**, H544-H552.
- Fung YC and Liu SQ (1993). Elementary mechanics of the endothelium of blood vessels, *J Biomech Eng* **115**, 1-12.

- Fyhrie DP and Carter DR (1986). A unifying principle relating stress to trabecular bone morphology, *J Orthop Res* **4**, 304-317.
- Fyhrie DP and Carter DR (1990). Femoral head apparent density distribution predicted from bone stresses, *J Biomech* **23**, 1-10.
- Gierer A (1977). Physical aspects of tissue evagination and biological form, *Q Rev Biophys* **10**, 529-593.
- Gilbert JA, Weinhold PS, Banes AJ, Link GW, and Jones GL (1994). Strain profiles for circular cell culture plates containing flexible surfaces employed to mechanically deform cells in vitro, *J Biomech* **27**, 1169-1177.
- Gilbert SF (1991). *Developmental Biology*, 3rd Ed., Sinauer Associates, Sunderland, MA.
- Gjelsvik A (1973a). Bone remodeling and piezoelectricity—I, *J Biomech* **6**, 69-77.
- Gjelsvik A (1973b). Bone remodeling and piezoelectricity—II, *J Biomech* **6**, 187-193.
- Goldberg AL, Etlinger JD, Goldspink DF, and Jablecki C (1975). Mechanism of work-induced hypertrophy of skeletal muscle, *Med Sci Sports Exerc* **7**, 248-261.
- Goldin GV (1980). Towards a mechanism for morphogenesis in epithelio-mesenchymal organs, *Q Rev Biol* **55**, 251-265.
- Goldspink G (1972). Postembryonic growth and differentiation of striated muscle, in *The Structure and Function of Muscle*, GH Bourne, Ed, Academic Press, New York, 179-236.
- Goldstein SA, Matthews LS, Kuhn JL, and Hollister SJ (1991). Trabecular bone remodeling: an experimental model, *J Biomech* **24** (Suppl. 1), 135-150.
- Gordon AM, Huxley AF, and Julian FJ (1966). The variation in isometric tension with sarcomere length in vertebrate muscle fibers, *J Physiol* **184**, 170-192.
- Gordon R and Brodland GW (1987). The cytoskeletal mechanics of brain morphogenesis. Cell state splitters cause primary neural induction, *Cell Biophys* **11**, 177-238.
- Goss RJ (1966). Hypertrophy versus hyperplasia, *Science* **153**, 1615-1620.
- Gould SJ (1982). Change in developmental timing as a mechanism of macroevolution, in *Evolution and Development*, JT Bonner, Ed, Springer-Verlag, New York, 333-346.
- Green AE and Adkins JE (1970). *Large Elastic Deformations*, 2nd Ed., Oxford University Press, London.
- Green AE and Zerna W (1968). *Theoretical Elasticity*, 2nd Ed., Oxford University Press, London.
- Greenspan HP (1977a). On the dynamics of cell cleavage, *J Theor Biol* **65**, 79-99.
- Greenspan HP (1977b). On the deformation of a viscous droplet caused by variable surface tension, *Stud Appl Math* **57**, 45-58.
- Greenspan HP (1978). On fluid-mechanical simulations of cell division and movement, *J Theor Biol* **70**, 125-134.
- Gross D and Williams WS (1982). Streaming potential and the electromechanical response of physiologically moist bone, *J Biomech* **15**, 277-295.
- Grossman W, Jones D, and McLaurin LP (1975). Wall stress and patterns of hypertrophy in the human left ventricle, *J Clin Invest* **56**, 56-64.
- Grossman W (1980). Cardiac hypertrophy: useful adaptation or pathologic process? *Am J Med* **69**, 576-584.
- Grossman W, Carabello BA, Gunther S, and Fifer MA (1983). Ventricular wall stress and the development of cardiac hypertrophy and failure, in *Perspectives in Cardiovascular Research, Vol. 7, Myocardial Hypertrophy and Failure*, NR Alpert, Ed, Raven Press, New York, 1-18.
- Grossman W and Lorell BH (1993). Hemodynamic aspects of left ventricular remodeling after myocardial infarction, *Circulation* **87** (Suppl. 7), VII-28-VII-30.
- Guccione JM, McCulloch AD, and Waldman LK (1991). Passive material properties of intact ventricular myocardium determined from a cylindrical model, *J Biomech Eng* **113**, 42-55.
- Guyton AC (1991). *Textbook of Medical Physiology*, 8th Ed., W.B. Saunders, Philadelphia.
- Guzeisu N and Saha S (1984). Electro-mechanical behavior of wet bone—Part I: Theory, *J Biomech Eng* **106**, 249-261.
- Hamburger V and Hamilton HL (1951). A series of normal stages in the development of the chick embryo, *J Morphol* **88**, 49-92.
- Han HC and Fung YC (1991a). Species dependence of the zero-stress state of aorta: pig versus rat, *J Biomech Eng* **113**, 446-451.
- Han HC and Fung YC (1991b). Residual strains in porcine and canine trachea, *J Biomech* **24**, 307-315.
- Hardin JD and Cheng LY (1986). The mechanisms and mechanics of archenteron elongation during sea urchin gastrulation, *Dev Biol* **115**, 490-501.
- Harrigan TP and Hamilton JJ (1992). An analytical and numerical study of the stability of bone remodelling theories: dependence on microstructural stimulus, *J Biomech* **25**, 477-488.
- Harrigan TP and Hamilton JJ (1994). Bone remodeling and structural optimization, *J Biomech* **27**, 323-328.
- Harrigan TP and Mann RW (1984). Characterization of microstructural anisotropy in orthotropic materials using a second rank tensor, *J Mater Sci* **19**, 761-767.
- Harris AK, Wild P, and Stopak D (1980). Silicone rubber substrata: a new wrinkle in the study of cell locomotion, *Science* **208**, 177-179.
- Harris AK, Stopak D, and Wild P (1981). Fibroblast traction as a mechanism for collagen morphogenesis, *Nature* **290**, 249-251.
- Harris AK (1984). Tissue culture cells on deformable substrata: biomechanical implications, *J Biomech Eng* **106**, 19-24.
- Harris AK, Stopak D, and Warner P (1984). Generation of spatially periodic patterns by a mechanical instability: a mechanical alternative to the Turing model, *J Embryol Exp Morph* **80**, 1-20.
- Harris AK (1990). Protrusive activity of the cell surface and the movements of tissue cells, in *Biomechanics of Active Movement and Deformation of Cells*, N Akkas, Ed, Springer-Verlag, Berlin, 249-294.
- Harrison LG (1987). What is the status of reaction-diffusion theory thirty-four years after Turing? *J Theor Biol* **125**, 369-384.
- Hart RT, Davy DT, and Heiple KG (1984a). A computational method for stress analysis of adaptive elastic materials with a view toward applications in strain-induced bone remodeling, *J Biomech Eng* **106**, 342-350.
- Hart RT, Davy DT, and Heiple KG (1984b). Mathematical modeling and numerical solutions for functionally dependent bone remodeling, *Calcif Tissue Int* **36**, S104-S109.
- Hart RT (1989). Computational techniques for bone remodeling, in *Bone Mechanics*, SC Cowin, Ed, CRC Press, Boca Raton, FL, 279-304.
- Hart RT (1990). A theoretical study of the influence of bone maturation rate on surface remodeling predictions: idealized models, *J Biomech* **23**, 241-257.
- Hart RT and Davy DT (1989). Theories of bone modeling and remodeling, in *Bone Mechanics*, SC Cowin, Ed, CRC Press, Boca Raton, FL, 253-277.
- Hay ED and Svoboda KK (1989). Extracellular matrix interaction with the cytoskeleton, in *Cell Shape: Determinants, Regulation, and Regulatory Role*, WD Stein and F Bronner, Eds, Academic Press, San Diego, 147-172.
- Hayes WC and Snyder B (1981). Toward a quantitative formulation of Wolff's law in trabecular bone, in *Mechanical Properties of Bone*, SC Cowin, Ed, ASME, New York, 43-68.
- Hegedus DH and Cowin SC (1976). Bone remodeling II: Small strain adaptive elasticity, *J Elasticity* **6**, 337-352.
- Helmlinger G, Geiger RV, Schreck S, and Nerem RM (1991). Effects of pulsatile flow on cultured vascular endothelial cell morphology, *J Biomech Eng* **113**, 123-131.
- Hill AV (1938). The heat of shortening and the dynamic constants of muscle, *Proc Roy Soc London* **B126**, 136-195.

- Hiramoto Y (1968). The mechanics and mechanism of cleavage in the sea-urchin egg, *Symp Soc Exp Biol* **22**, 311-327.
- Holly RG, Barnett JG, Ashmore CR, Taylor RG, and Mole PA (1980). Stretch-induced growth in chicken wing muscles: a new model of stretch hypertrophy, *Am J Physiol* **238**, C62-C71.
- Holt JP, Rhode EA, Peoples SA, and Kines H (1962). Left ventricular function in mammals of greatly different size, *Circ Res* **10**, 798-806.
- Hsu FH (1968). The influences of mechanical loads on the form of a growing elastic body, *J Biomech* **1**, 303-311.
- Huiskes R, Weinans H, Grootenboer HJ, Dalstra M, Fudala B, and Slooff TJ (1987). Adaptive bone-remodeling theory applied to prosthetic-design analysis, *J Biomech* **20**, 1135-1150.
- Huiskes R and Hollister SJ (1993). From structure to process, from organ to cell: recent developments of FE-analysis in orthopaedic biomechanics, *J Biomech Eng* **115**, 520-527.
- Icardo JM and Ojeda JL (1984). Effects of colchicine on the formation and looping of the tubular heart of the embryonic chick, *Acta Anat* **119**, 1-9.
- Itasaki N, Nakamura H, and Yasuda M (1989). Changes in the arrangement of actin bundles during heart looping in the chick embryo, *Anat Embryol* **180**, 413-420.
- Itasaki N, Nakamura H, Sumida H, and Yasuda M (1991). Actin bundles on the right side in the caudal part of the heart tube play a role in dextro-looping in the embryonic chick heart, *Anat Embryol* **183**, 29-39.
- Ives CL, Eskin SG, and McIntire LV (1986). Mechanical effects on endothelial cell morphology: in vitro assessment, *In Vitro Cell Dev Biol* **22**, 500-507.
- Jacobson AG (1980). Computer modeling of morphogenesis, *Am Zool* **20**, 669-677.
- Jacobson AG, Oster GF, Odell GM, and Cheng LY (1986). Neuration and the cortical tractor model for epithelial folding, *J Embryol Exp Morph* **96**, 19-49.
- Jacobson AG and Gordon R (1976). Changes in the shape of the developing vertebrate nervous system analyzed experimentally, mathematically, and by computer simulation, *J Exp Zool* **197**, 191-246.
- Kajstura J, Zhang X, Reiss K, Szoke E, Li P, Lagrasta C, Cheng W, Darzynkiewicz Z, Olivetti G, and Anversa P (1994). Myocyte cellular hyperplasia and myocyte cellular hypertrophy contribute to chronic ventricular remodeling in coronary artery narrowing-induced cardiomyopathy in rats, *Circ Res* **74**, 383-400.
- Kamiya A and Togawa T (1980). Adaptive regulation of wall shear stress to flow change in the canine carotid artery, *Am J Physiol* **239**, H14-H21.
- Keller BB, Hu N, and Clark EB (1990). Correlation of ventricular area, perimeter, and conotruncal diameter with ventricular mass and function in the chick embryo from stages 12 to 24, *Circ Res* **66**, 109-114.
- Keller BB, Hu N, Serrino PJ, and Clark EB (1991). Ventricular pressure-area loop characteristics in the stage 16-24 chick embryo, *Circ Res* **68**, 226-231.
- Kent RL, Uboh CE, Thompson EW, Gordon SS, Marino TA, Hooper JK, and Cooper G (1985). Biochemical and structural correlates in unloaded and reloaded cat myocardium, *J Mol Cell Cardiol* **17**, 153-165.
- Klein-Nulend J, Veldhuijzen JP, and Burger EH (1986). Increased calcification of growth plate as a result of compressive force in vitro, *Arth Rheum* **29**, 1002-1009.
- Koch JC (1917). The laws of bone architecture, *Am J Anat* **21**, 177-298.
- Kolega J (1986). Effects of mechanical tension on protrusive activity and microfilament and intermediate filament organization in an epidermal epithelium moving in culture, *J Cell Biol* **102**, 1400-1411.
- Kummer BKF (1972). Biomechanics of bone: mechanical properties, functional structure, functional adaptation, in *Biomechanics: Its Foundations and Objectives*, YC Fung, N Perrone, and M Anliker, Eds, Prentice-Hall, Englewood Cliffs, NJ, 237-271.
- Laks MM, Morady F, Garner D, and Swan HJC (1974). Temporal changes in canine right ventricular volume, mass, cell size, and sarcomere length after banding the pulmonary artery, *Cardiovasc Res* **8**, 106-111.
- Lanyon LE, Goodship AE, Pye CJ, and MacFie JH (1982). Mechanically adaptive bone remodeling, *J Biomech* **15**, 141-154.
- Lanyon LE (1984). Functional strain as a determinant for bone remodeling, *Calcif Tissue Int* **36**, S56-S61.
- Lanyon LE (1987). Functional strain in bone tissue as an objective and controlling stimulus for adaptive bone remodeling, *J Biomech* **20**, 1083-1093.
- Lanyon LE and Rubin CT (1984). Static vs dynamic loads as an influence on bone remodeling, *J Biomech* **17**, 897-905.
- Leung DYM, Glagov S, and Mathews MB (1976). Cyclic stretching stimulates synthesis of matrix components by arterial smooth muscle cells in vitro, *Science* **191**, 475-477.
- Levesque MJ, Liepsch D, Moravec S, and Nerem RM (1986). Correlation of endothelial cell shape and wall shear stress in a stenosed dog aorta, *Arteriosclerosis* **6**, 220-229.
- Levesque MJ, Nerem RM, and Sprague EA (1990). Vascular endothelial cell proliferation in culture and the influence of flow, *Biomaterials* **11**, 702-707.
- Levesque MJ and Nerem RM (1985). The elongation and orientation of cultured endothelial cells in response to shear stress, *J Biomech Eng* **107**, 341-347.
- Lewis WH (1947). Mechanics of invagination, *Anat Rec* **97**, 139-156.
- Lin IE and Taber LA (1995). A model for stress-induced growth in the developing heart, *J Biomech Eng* (in press).
- Linzbach AJ (1976). Hypertrophy, hyperplasia, and structural dilatation of the human heart, *Adv Cardiol* **18**, 1-14.
- Liu SQ and Fung YC (1988). Zero-stress states of arteries, *J Biomech Eng* **110**, 82-84.
- Liu SQ and Fung YC (1989). Relationship between hypertension, hypertrophy, and opening angle of zero-stress state of arteries following aortic constriction, *J Biomech Eng* **111**, 325-335.
- Lund DD and Tomanek RJ (1978). Myocardial morphology in spontaneously hypertensive and aortic-constricted rats, *Am J Anat* **152**, 141-152.
- Maini PK and Solursh M (1991). Cellular mechanisms of pattern formation in the developing limb, *Int Rev Cytol* **129**, 91-133.
- Manasek FJ, Burnside MB, and Waterman RE (1972). Myocardial cell shape changes as a mechanism of embryonic heart looping, *Dev Biol* **29**, 349-371.
- Manasek FJ, Kulikowski RR, and Fitzpatrick L (1978). Cytodifferentiation: a causal antecedent of looping? *Birth Defects* **14**, 161-178.
- Manasek FJ (1983). Control of early embryonic heart morphogenesis: a hypothesis, in *Development of the Vascular System*, Pitman, London.
- Manasek FJ, Isobe Y, Shimada Y, and Hopkins W (1984a). The embryonic myocardial cytoskeleton, interstitial pressure, and the control of morphogenesis, in *Congenital Heart Disease: Causes and Processes*, JJ Nora and A Takao, Eds, Futura Publishing, Mount Kisco, NY, 359-376.
- Manasek FJ, Kulikowski RR, Nakamura A, Nguyenphuc Q, and Lactis JW (1984b). Early heart development: a new model of cardiac morphogenesis, in *Growth of the Heart in Health and Disease*, R Zak, Ed, Raven Press, New York, 105-130.
- Manasek FJ and Monroe RG (1972). Early cardiac morphogenesis is independent of function, *Dev Biol* **27**, 584-588.
- Manning A and McLachlan JC (1990). Looping of chick embryo hearts in vitro, *J Anat* **168**, 257-263.

- Martin RB and Burr DB (1982). A hypothetical mechanism for the stimulation of osteonal remodelling by fatigue damage, *J Biomech* **15**, 137-139.
- Martin RR and Haines H (1970). Application of Laplace's law to mammalian hearts, *Comp Biochem Physiol* **34**, 959-962.
- Matsumoto T and Hayashi K (1994). Mechanical and dimensional adaptation of rat aorta to hypertension, *J Biomech Eng* **116**, 278-283.
- McMahon TA (1973). Size and shape in biology, *Science* **179**, 1201-1204.
- McMahon TA (1984). *Muscles, Reflexes, and Locomotion*, Princeton University Press, Princeton, NJ.
- Meade JB (1989). The adaptation of bone to mechanical stress: experimentation and current concepts, in *Bone Mechanics*, SC Cowin, Ed, CRC Press, Boca Raton, FL, 211-251.
- Mirsky I, Pfeffer JM, and Pfeffer MA (1983). Mechanical properties of normal and hypertrophied myocardium: is there a relationship between diastolic and systolic function? in *Perspectives in Cardiovascular Research, Vol. 7, Myocardial Hypertrophy and Failure*, NR Alpert, Ed, Raven Press, New York, 39-55.
- Mirsky I and Laks MM (1980). Time course of changes in the mechanical properties of the canine right and left ventricles during hypertrophy caused by pressure overload, *Circ Res* **46**, 530-542.
- Mirsky I and Pasipoularides A (1980). Elastic properties of normal and hypertrophied cardiac muscle, *Fed Proc* **39**, 156-161.
- Mitchison JM and Swann MM (1955). The mechanical properties of the cell surface: III. The sea-urchin egg from fertilization to cleavage, *J Exp Biol* **32**, 734-750.
- Mittenthal JE (1987). The shaping of cell sheets: an application of mechanics in developmental biology, in *Biomechanics of Cell Division*, N Akkas, Ed, Plenum, New York, 327-346.
- Mittenthal JE (1989). Physical aspects of the organization of development, in *Complex Systems, SFI Studies in the Sciences of Complexity*, D Stein, Ed, Addison-Wesley Longman, New York, 226-274.
- Mittenthal JE and Mazo RM (1983). A model for shape generation by strain and cell-cell adhesion in the epithelium of an arthropod leg segment, *J Theor Biol* **100**, 443-483.
- Mow VC, Kuei SC, Lai WM, and Armstrong CG (1980). Biphasic creep and stress relaxation of articular cartilage in compression: theory and experiments, *J Biomech Eng* **102**, 73-84.
- Mullender MG, Huiskes R, and Weinans H (1994). A physiological approach to the simulation of bone remodeling as a self-organizational control process, *J Biomech* **27**, 1389-1394.
- Murray JD (1982). Parameter space for Turing instability in reaction-diffusion mechanisms: a comparison of models, *J Theor Biol* **98**, 143-163.
- Murray JD (1989). *Mathematical Biology*, Springer-Verlag, Berlin.
- Murray JD and Oster GF (1984). Cell traction models for generating pattern and form in morphogenesis, *J Math Biol* **19**, 265-280.
- Nakamura A, Kulikowski RR, Lacktis JW, and Manasek FJ (1980). Heart looping: a regulated response to deforming forces, in *Etiology and Morphogenesis of Congenital Heart Disease*, R van Praagh and A Takao, Eds, Futura Publishing, Mount Kisco, NY, 81-98.
- Natarajan G, Bove AA, Coulson RL, Carey RA, and Spann JF (1979). Increased passive stiffness of short-term pressure-overload hypertrophied myocardium in cat, *Am J Physiol* **237**, H676-H680.
- Nerem RM, Levesque MJ, and Cornhill JF (1981). Vascular endothelial morphology as an indicator of the pattern of blood flow, *J Biomech Eng* **103**, 172-176.
- Nerem RM (1990). Active motion and deformation in vascular endothelial cells exposed to flow, in *Biomechanics of Active Movement and Deformation of Cells*, N Akkas, Ed, Springer-Verlag, Berlin, 461-469.
- Nerem RM (1992). Vascular fluid mechanics, the arterial wall, and atherosclerosis, *J Biomech Eng* **114**, 274-282.
- Nerem RM (1993). Hemodynamics and the vascular endothelium, *J Biomech Eng* **115**, 510-514.
- O'Connor JA, Lanyon LE, and MacFie H (1982). The influence of strain rate on adaptive bone remodelling, *J Biomech* **15**, 767-781.
- Odell GM, Oster G, Alberch P, and Burnside B (1981). The mechanical basis of morphogenesis. I. Epithelial folding and invagination, *Dev Biol* **85**, 446-462.
- Odell GM and Frisch HL (1975). A continuum theory of the mechanics of amoeboid pseudopodium extension, *J Theor Biol* **50**, 59-86.
- Olivetti G, Anversa P, Melissari M, and Loud AV (1980). Morphometry of medial hypertrophy in the rat thoracic aorta, *Lab Invest* **42**, 559-565.
- Omens JH and Covell JW (1991). Transmural distribution of myocardial tissue growth induced by volume-overload hypertrophy in the dog, *Circulation* **84**, 1235-1245.
- Omens JH and Fung YC (1990). Residual strain in rat left ventricle, *Circ Res* **66**, 37-45.
- Ookawa K, Sato M, and Ohshima N (1992). Changes in the microstructure of cultured porcine aortic endothelial cells in the early stage after applying a fluid-imposed shear stress, *J Biomech* **25**, 1321-1328.
- Oster G and Alberch P (1982). Evolution and bifurcation of developmental programs, *Evolution* **36**, 444-459.
- Oster GF, Perelson AS, and Tilney LG (1982). A mechanical model for elongation of the acrosomal process in thyone sperm, *J Math Biol* **15**, 259-265.
- Oster GF, Murray JD, and Harris AK (1983). Mechanical aspects of mesenchymal morphogenesis, *J Embryol Exp Morph* **78**, 83-125.
- Oster GF (1984). On the crawling of cells, *J Embryol Exp Morph* **83** (Suppl.), 329-364.
- Oster GF, Murray JD, and Maini PK (1985). A model for chondrogenic condensations in the developing limb: the role of extracellular matrix and cell tractions, *J Embryol Exp Morph* **89**, 93-112.
- Oster GF and Murray JD (1989). Pattern formation models and developmental constraints, *J Exp Zool* **251**, 186-202.
- Oster GF and Perelson AS (1987). The physics of cell motility, *J Cell Sci* **8** (Suppl.), 35-54.
- Owens GK and Reidy MA (1985). Hyperplastic growth response of vascular smooth muscle cells following induction of acute hypertension in rats by aortic coarctation, *Circ Res* **57**, 695-705.
- Patten BM (1922). The formation of the cardiac loop in the chick, *Am J Anat* **30**, 373-397.
- Patten BM (1951). *Early Embryology of the Chick*, 4th Ed., McGraw-Hill, New York.
- Pauwels F (1980). *Biomechanics of the Locomotor Apparatus*, Springer-Verlag, Berlin.
- Perelson AS, Maini PK, Murray JD, Hyman JM, and Oster GF (1986). Nonlinear pattern formation in a mechanical model for morphogenesis, *J Math Biol* **24**, 525-541.
- Peterson KL, Tsuji J, Johnson A, DiDonna J, and LeWinter M (1978). Diastolic left ventricular pressure-volume and stress-strain relations in patients with valvular aortic stenosis and left ventricular hypertrophy, *Circulation* **58**, 77-89.
- Phillips CA and Petrofsky JS (1983). The force-velocity relationship in skeletal muscle, in *Mechanics of Skeletal and Cardiac Muscle*, CA Phillips and JS Petrofsky, Eds, Charles C. Thomas, Springfield, IL, 19-58.
- Phillips HM and Davis GS (1978). Liquid-tissue mechanics in amphibian gastrulation: germ-layer assembly in rana pipiens, *Am Zool* **18**, 81-93.
- Poupa O and Ostadal B (1969). Experimental cardiomegalies and "cardiomegalies" in free-living animals, *Ann New York Acad Sci* **156**, 445-468.
- Prendergast PJ and Taylor D (1994). Prediction of bone adaptation using damage accumulation, *J Biomech* **27**, 1067-1076.

- Pujara P and Lardner TJ (1979). A model for cell division, *J Biomech* **12**, 293-299.
- Rappaport R (1990). Cytokinesis in animal cells, in *Biomechanics of Active Movement and Deformation of Cells*, N Akkas, Ed, Springer-Verlag, Berlin, 1-34.
- Rhinelander FW (1972). *The Biochemistry and Physiology of Bone*, 2nd Ed., Academic Press, New York.
- Risau W (1991). Vasculogenesis, angiogenesis, and endothelial cell differentiation during embryonic development, in *The Development of the Vascular System*, RN Feinberg, GK Sherer, and R Auerbach, Eds, Karger, Basel, 58-68.
- Rodriguez EK, Omens JH, Waldman LK, and McCulloch AD (1993). Effect of residual stress on transmural sarcomere length distributions in rat left ventricle, *Am J Physiol* **264**, H1048-H1056.
- Rodriguez EK, Hoger A, and McCulloch AD (1994). Stress-dependent finite growth in soft elastic tissues, *J Biomech* **27**, 455-467.
- Roesler H (1981). Some historical remarks on the theory of cancellous bone structure (Wolff's law), in *Biomechanics of Bone*, SC Cowin, Ed, ASME, New York, 27-42.
- Ross J (1974). Adaptations of the left ventricle to chronic volume overload, *Circ Res* **34/35 (Suppl. 2)**, II-64-II-70.
- Ross R (1990). Mechanisms of atherosclerosis—A review, *Adv Nephrol* **19**, 79-86.
- Sachs F (1986). Biophysics of mechanoreception, *Membr Biochem* **6**, 173-195.
- Sadegh AM, Luo GM, and Cowin SC (1993). Bone ingrowth: an application of the boundary element method to bone remodeling at the implant interface, *J Biomech* **26**, 167-182.
- Sagawa K, Maughan L, Suga H, and Sunagawa K (1988). *Cardiac Contraction and the Pressure-Volume Relationship*, Oxford University Press, New York.
- Salmons S and Henriksson J (1981). The adaptive response of skeletal muscle to increased use, *Muscle & Nerve* **4**, 94-105.
- Salzstein RA, Pollack SR, Mak AFT, and Petrov N (1987). Electromechanical potentials in cortical bone—I. A continuum approach, *J Biomech* **20**, 261-270.
- Sato M, Levesque MJ, and Nerem RM (1987). Micropipette aspiration of cultured bovine aortic endothelial cells exposed to shear stress, *Arteriosclerosis* **7**, 276-286.
- Schmid-Schonbein GW and Skalak R (1984). Continuum mechanical model of leukocytes during protopod formation, *J Biomech Eng* **106**, 10-18.
- Schoenwolf GC, Folsom D, and Moe A (1988). A reexamination of the role of microfilaments in neurulation in the chick embryo, *Anat Rec* **220**, 87-102.
- Schroeder TE (1987). The origin and action of the contractile ring, in *Biomechanics of Cell Division*, N Akkas, Ed, Plenum Press, New York, 209-230.
- Serizawa T, Mirsky I, Carabello BA, and Grossman W (1982). Diastolic myocardial stiffness in gradually developing left ventricular hypertrophy in dog, *Am J Physiol* **242**, H633-H637.
- Shiraishi I, Takamatsu T, Minamikawa T, and Fujita S (1992). 3-d observation of actin filaments during cardiac myofibrinogenesis in chick embryo using a confocal laser scanning microscope, *Anat Embryol* **185**, 401-408.
- Shirinsky VP, Antonov AS, Birukov KG, Sobolevsky AV, Romanov YA, Kabaeva NV, Antonova GN, and Smirnov VN (1989). Mechano-chemical control of human endothelium orientation and size, *J Cell Biol* **109**, 331-339.
- Silk WK and Erickson RO (1979). Kinematics of plant growth, *J Theor Biol* **76**, 481-501.
- Simard CP, Spector SA, and Edgerton VR (1982). Contractile properties of rat hind limb muscles immobilized at different lengths, *Exp Neurol* **77**, 467-482.
- Simon SI and Schmid-Schonbein GW (1990). Kinematics of cytoplasmic deformation in neutrophils during active motion, *J Biomech Eng* **112**, 303-310.
- Skalak R, Tozeren A, Zarda RP, and Chien S (1973). Strain energy function of red blood cell membranes, *Biophys J* **13**, 245-264.
- Skalak R (1981). Growth as a finite displacement field, in *Proceedings of the IUTAM Symposium on Finite Elasticity*, DE Carlson and RT Shield, Eds, Martinus Nijhoff Publishers, The Hague, 347-355.
- Skalak R, Dasgupta G, Moss M, Otten E, Dullemeijer P, and Vilmann H (1982). Analytical description of growth, *J Theor Biol* **94**, 555-577.
- Skalak R, Dong C, and Zhu C (1990). Passive deformations and active motions of leukocytes, *J Biomech Eng* **112**, 295-302.
- Skalak R and Zhu C (1990). Thermodynamics and mechanics of active cell motions, in *Biomechanics of Active Movement and Deformation of Cells*, N Akkas, Ed, Springer-Verlag, Berlin, 155-183.
- Spann JF, Buccino RA, Sonnenblick EH, and Braunwald E (1967). Contractile state of cardiac muscle obtained from cats with experimentally produced ventricular hypertrophy and heart failure, *Circ Res* **21**, 341-354.
- Spann JF (1983). Contractile and pump function of the pressure-overloaded heart, in *Perspectives in Cardiovascular Research, Vol. 7, Myocardial Hypertrophy and Failure*, NR Alpert, Ed, Raven Press, New York, 19-38.
- Spector SA, Simard CP, Fournier M, Sternlicht E, and Edgerton VR (1982). Architectural alterations of rat hind-limb skeletal muscles immobilized at different lengths, *Exp Neurol* **76**, 94-110.
- Stalsberg H (1969). Regional mitotic activity in the precardiac mesoderm and differentiating heart tube in the chick embryo, *Dev Biol* **20**, 18-45.
- Stalsberg H (1970). Mechanism of dextral looping of the embryonic heart, *Am J Cardiol* **25**, 265-271.
- Stewart DM (1972). The role of tension in muscle growth, in *Regulation of Organ and Tissue Growth*, RJ Goss, Ed, Academic Press, New York, 77-100.
- Stopak D and Harris AK (1982). Connective tissue morphogenesis by fibroblast traction, *Dev Biol* **90**, 383-398.
- Streeter DD, Spotnitz HM, Patel DJ, Ross J, and Sonnenblick EH (1969). Fiber orientation in the canine left ventricle during diastole and systole, *Circ Res* **24**, 339-347.
- Streeter DD (1979). Gross morphology and fiber geometry of the heart, in *Handbook of Physiology, Section 2: The Cardiovascular System, Volume I: The Heart*, RM Berne, N Sperelakis, and SR Geiger, Eds, American Physiological Society, Bethesda, MD, 61-112.
- Suga H, Sagawa K, and Shoukas AA (1973). Load independence of the instantaneous pressure-volume ratio of the canine left ventricle and effects of epinephrine and heart rate on the ratio, *Circ Res* **32**, 314-322.
- Sumpio BE, Banas AJ, Levin LG, and Johnson G (1987). Mechanical stress stimulates aortic endothelial cells to proliferate, *J Vasc Surg* **6**, 252-256.
- Suwa N (1982). Myocardial structure of hypertrophied hearts, *Jap Circ J* **46**, 995-1000.
- Tabary JC, Tabary C, Tardieu C, Tardieu G, and Goldspink G (1972). Physiological and structural changes in the cat's soleus muscle due to immobilization at different lengths by plaster casts, *J Physiol* **224**, 231-244.
- Taber LA (1991). On a nonlinear theory for muscle shells: II. Application to the active left ventricle, *J Biomech Eng* **113**, 63-71.
- Taber LA, Keller BB, and Clark EB (1992). Cardiac mechanics in the stage-16 chick embryo, *J Biomech Eng* **114**, 427-434.
- Taber LA, Hu N, Pexieder T, Clark EB, and Keller BB (1993a). Residual strain in the ventricle of the stage 16-24 chick embryo, *Circ Res* **72**, 455-462.
- Taber LA, Lin IE, and Clark EB (1995). Mechanics of cardiac looping, *Dev Dynamics* **203**, 42-50.
- Takamizawa K and Matsuda T (1990). Kinematics for bodies undergoing residual stress and its applications to the left ventricle, *J Appl Mech* **57**, 312-329.



- Tanaka M and Adachi T (1994). Preliminary study on mechanical bone remodeling permitting residual stress, *JSME Int J* **37**, 87-95.
- Terracio L, Tingstrom A, Peters WH, and Borg TK (1990). A potential role for mechanical stimulation in cardiac development, *Ann New York Acad Sci* **588**, 48-60.
- Thompson DW (1942). *On Growth and Form*, 2nd Ed., Cambridge University Press, Cambridge.
- Thompson EW, Marino TA, Uboh CE, Kent RL, and Cooper G (1984). Atrophy reversal and cardiocyte redifferentiation in reloaded cat myocardium, *Circ Res* **54**, 367-377.
- Tozeren A (1983). Static analysis of the left ventricle, *J Biomech Eng* **105**, 39-46.
- Tozeren A and Skalak R (1988). Interaction of stress and growth in a fibrous tissue, *J Theor Biol* **130**, 337-350.
- Treharne RW (1981). Review of Wolff's law and its proposed means of operation, *Orthop Rev* **10**, 35-47.
- Trinkaus JP (1984). *Cells into Organs: The Forces That Shape the Embryo*, 2nd Ed., Prentice-Hall, Englewood Cliffs, NJ.
- Turing AM (1952). The chemical basis of morphogenesis, *Phil Trans Roy Soc London* **B237**, 37-72.
- Vaishnav RN and Vossoughi J (1983). Estimation of residual strains in aortic segments, in *Recent Developments in Biomedical Engineering*, CW Hall, Ed, New York, Pergamon Press, 330-333.
- Vaishnav RN and Vossoughi J (1987). Residual stress and strain in aortic segments, *J Biomech* **20**, 235-239.
- Vaishnav RN, Vossoughi J, Patel DJ, Cothran LN, Coleman BR, and Ison-Franklin EL (1990). Effect of hypertension on elasticity and geometry of aortic tissue from dogs, *J Biomech Eng* **112**, 70-74.
- Van Rietbergen B, Huiskes R, Weinans H, Sumner DR, Turner TM, and Galante JO (1993). The mechanism of bone remodeling and resorption around press-fitted THA stems, *J Biomech* **26**, 369-382.
- Vandenberg HH (1982). Dynamic mechanical orientation of skeletal myofibers in vitro, *Dev Biol* **93**, 438-443.
- Vandenberg HH, Hatfaludy S, Karlisch P, and Shansky J (1991). Mechanically induced alterations in cultured skeletal muscle growth, *J Biomech* **24** (Suppl. 1), 91-99.
- Vaughan RB and Trinkaus JP (1966). Movements of epithelial cell sheets in vitro, *J Cell Sci* **1**, 407-413.
- Vossoughi J, Hedjazi Z, and Borris FS (1993). Intimal residual stress and strain in large arteries, in *Proc. Summer Bioengineering Conference*, NA Langrana, MH Friedman, and ES Grood, Eds, New York, ASME, 434-437.
- Wainwright SA, Biggs WD, Currey JD, and Gosline JM (1976). *Mechanical Design in Organisms*, Wiley, New York.
- Watson PA (1991). Function follows form: generation of intracellular signals by cell deformation, *FASEB J* **5**, 2013-2019.
- Waxman AM (1981). A continuum approach to blood vessel growth: axisymmetric elastic structures, *J Theor Biol* **91**, 273-301.
- Weber KT, Clark WA, Janicki JS, and Shroff SG (1987). Physiologic versus pathologic hypertrophy and the pressure-overloaded myocardium, *J Cardiovasc Pharmacol* **10** (Suppl. 6), S37-S49.
- Weber KT (1989). Cardiac interstitium in health and disease: the fibrillar collagen network, *J Am Coll Cardiol* **13**, 1637-1652.
- Weber KT, Brilla CG, and Janicki JS (1991). Myocardial remodeling and pathologic hypertrophy, *Hosp Prac* 73-80.
- Wechezak AR, Wight TN, Viggers RF, and Sauvage LR (1989). Endothelial adherence under shear stress is dependent upon microfilament reorganization, *J Cell Physiol* **139**, 136-146.
- Weinans H, Huiskes R, and Grootenboer HJ (1992). The behavior of adaptive bone-remodeling simulation models, *J Biomech* **25**, 1425-1441.
- Weinbaum S, Cowin SC, and Zeng Y (1994). A model for the excitation of osteocytes by mechanical loading-induced bone fluid shear stresses, *J Biomech* **27**, 339-360.
- Weliky M, Minsuk S, Keller R, and Oster G (1991). Notochord morphogenesis in xenopus laevis: simulation of cell behavior underlying tissue convergence and extension, *Development* **113**, 1231-1244.
- Weliky M and Oster G (1990). The mechanical basis of cell rearrangement: I. Epithelial morphogenesis during fundulus epiboly, *Development* **109**, 373-386.
- Wessells NK, Spooner BS, Ash JF, Bradley MO, Luduena MA, Taylor EL, Wrenn JT, and Yamada KM (1971). Microfilaments in cellular and developmental processes, *Science* **171**, 135-143.
- Whalen RT, Carter DR, and Steele CR (1988). Influence of physical activity on the regulation of bone density, *J Biomech* **21**, 825-837.
- White GE, Gimbrone MA, and Fujiwara K (1983). Factors influencing the expression of stress fibers in vascular endothelial cells in situ, *J Cell Biol* **97**, 416-424.
- White GE and Fujiwara K (1986). Expression and intracellular distribution of stress fibers in aortic endothelium, *J Cell Biol* **103**, 63-70.
- White JG and Borisy GG (1983). On the mechanisms of cytokinesis in animal cells, *J Theor Biol* **101**, 289-316.
- Wiener J, Loud AV, Giacomelli F, and Anversa P (1977). Morphometric analysis of hypertension-induced hypertrophy of rat thoracic aorta, *Am J Pathol* **88**, 619-634.
- Wikman-Coffelt J, Parmley WW, and Mason DT (1979). The cardiac hypertrophy process: analyses of factors determining pathological vs. physiological development, *Circ Res* **45**, 697-707.
- Williams PE and Goldspink G (1971). Longitudinal growth of striated muscle fibres, *J Cell Sci* **9**, 751-767.
- Wilson BF and Archer RR (1979). Tree design: some biological solutions to mechanical problems, *BioScience* **29**, 293-298.
- Wolff J (1986). *The Law of Bone Remodeling*, Springer, Berlin.
- Wolpert L (1969). Positional information and the spatial pattern of cellular differentiation, *J Theor Biol* **25**, 1-47.
- Wolpert L (1978). Pattern formation in biological development, *Sci Am* **239**, 154-164.
- Wong AJ, Pollard TD, and Herman IM (1983). Actin filament stress fibers in vascular endothelial cells in vivo, *Science* **219**, 867-869.
- Wong M and Carter DR (1988). Mechanical stress and morphogenetic endochondral ossification of the sternum, *J Bone Joint Surg* **70-A**, 992-1000.
- Wong M and Carter DR (1990a). Theoretical stress analysis of organ culture osteogenesis, *Bone* **11**, 127-131.
- Wong M and Carter DR (1990b). A theoretical model of endochondral ossification and bone architectural construction in long bone ontogeny, *Anat Embryol* **181**, 523-532.
- Woo SL-Y (1981). The relationships of changes in stress levels on long bone remodeling, in *Biomechanics of Bone*, SC Cowin, Ed, ASME, New York, 107-129.
- Xie JP, Liu SQ, Yang RF, and Fung YC (1991). The zero-stress state of rat veins and vena cava, *J Biomech Eng* **113**, 36-41.
- Yang M, Taber LA, and Clark EB (1994). A nonlinear poroelastic model for the trabecular embryonic heart, *J Biomech Eng* **116**, 213-223.
- Yoneda M and Dan K (1972). Tension at the surface of the dividing sea-urchin egg, *J Exp Biol* **57**, 575-587.
- Zak R (1973). Cell proliferation during cardiac growth, *Am J Cardiol* **31**, 211-219.
- Zak R (1984). Factors controlling cardiac growth, in *Growth of the Heart in Health and Disease*, R Zak, Ed, Raven Press, New York, 165-185.
- Zhao M, Zhang H, Robinson TF, Factor SM, Sonnenblick EH, and Eng C (1987). Profound structural alterations of the extracellular collagen matrix in postischemic dysfunctional ("stunned") but viable myocardium, *J Am Coll Cardiol* **10**, 1322-1334.



- Zhu C, Skalak R, and Schmid-Schonbein GW (1989). One-dimensional steady continuum model of retraction of pseudopod in leukocytes, *J Biomech Eng* **111**, 69-77.
- Zhu C and Skalak R (1988). A continuum model of protrusion of pseudopod in leukocytes, *Biophys J* **54**, 1115-1137.
- Zinemanas D and Nir A (1987). Fluid mechanical simulations of cell furrowing due to anisotropic surface forces, in *Biomechanics of Cell Division*, N Akkas, Ed, Plenum Press, New York, 281-305.
- Zinemanas D and Nir A (1988). On the viscous deformation of biological cells under anisotropic surface tension, *J Fluid Mech* **193**, 217-241.
- Zinemanas D and Nir A (1990). Surface viscoelastic effects in cell cleavage, *J Biomech* **23**, 417-424.
- Zinemanas D and Nir A (1992). A fluid-mechanical model of deformation during embryo exogastrulation, *J Biomech* **25**, 341-346.



**Larry A Taber** is Professor of Mechanical Engineering and of Pediatrics at the University of Rochester. In 1970, he received a Bachelor of Aerospace Engineering with highest honors from the Georgia Institute of Technology. He then attended Stanford University, earning a MS (1975) and PhD (1979) in Aeronautics and Astronautics. In 1978, he joined the Biomedical Science Department at the General Motors Research Laboratories, where he studied the biomechanics of crash injury. In 1982, he moved to Rochester. His research interests include topics in both applied mechanics and biomechanics, with numerous articles published on the mechanics of hearing, bone vibration, large deformation of the eyeball, nonlinear shell theory, poroelastic plate and shell theory, cardiac mechanics, and the mechanics of heart development. This research has been supported by the National Science Foundation and the National Institutes of Health. For his work in heart development, Professor Taber received a National Research Service Award (1989) and a James A Shannon Director's Award (1991) from the National Institutes of Health.